Investigations related to the generation of reaction products in the target of Accelerator Driven Systems for nuclear waste incineration

Véronique Baylac-Domengetroy

Institut für Reaktorsicherheit
Projekt NUKLEAR

Investigations related to the generation of reaction products in the target of Accelerator Driven Systems for nuclear waste incineration

Diplomarbeit zum Erwerb des Diploms Physiker
Fakultät für Physik der Universität Karlsruhe (TH)

Stage de fin d'études présenté pour obtenir le diplôme d'ingénieur physicien ENSPG
Ecole Nationale Supérieure de Physique de Grenoble

Véronique Baylac-Domengetroy

Abstract

For many years, many countries have been considering Accelerator Transmutation of Waste (ATW) as a solution for processing the nuclear waste as well as a mean of generating power with a subcritical system. Several research groups are now working on this topic all over the world and this has already led to the proposal of Accelerator Driven Systems (ADS) concepts. The main objective of these systems is the incineration of long-lived isotopes from the spent fuel of actual and future reactors.

At the Institute for Reactor Safety (IRS) of the Research Center of Karlsruhe, some of the actual activities are focussed on the near future developments of ADS. In this scope, IRS is participating within the 5th *European Community Framework Program* to MEGAPIE, MUSE and XADS projects. Development and experimental qualification of theoretical tools for core design and safety evaluations of accelerator driven sub-critical systems are important current topics investigated at IRS.

In particular, for the analysis of accelerator driven systems (ADS), the coupling of a proton source with a sub-critical reactor system may be investigated with the current version of MCNPX, a code developed at LANL and for which IRS is beta-tester. The present work was done in the scope of this Beta-Testing activity. We analysed the applied theoretical models for investigations of spallation physics as well as their application in the code MCNPX. We validated our application of MCNPX by making comparisons with available benchmark results and with experimental data for neutron yields per proton, for thin target cross-section measurements and for a thick target activation experiment. We also calculated several parameters related to important reaction products for the MEGAPIE project.

Résumé

Depuis quelques années, plusieurs pays considèrent ce que l'on appelle "Accelerator Transmutation of Wate" (ATW) comme une solution pour traiter les déchets nucléaires ainsi que comme un moyen de produire de l'énergie avec un système sous-critique. De nombreux groupes de recherche travaillent actuellement sur ce sujet et des concepts de systèmes sous-critiques commandés par accélérateurs (Accelerator Driven System, ADS) ont déjà été proposés. Le but essentiel de ces systèmes est de bruler les isotopes à longue vie issus des combustibles usés des réacteurs actuels ou à venir.

A l'Institut de Sécurité des Réacteurs (IRS) du Centre de Recherches de Karlsruhe (FZK), certains des travaux menés actuellement sont axés sur le développement, dans un futur proche, de systèmes sous-critiques commandés par accélérateurs. Dans cette optique, l'IRS participe aux projets MEGAPIE, MUSE et XADS dans le cadre du " 5th *European Community Framework Programm"*. Le développement et la validation expérimentale de moyens théoriques, utilisés pour la conception du coeur et les calculs de sûreté concernant les systèmes sous-critiques commandés par accélérateurs, sont des sujets actuellement traités à l'IRS.

En particulier, pour l'analyse des systèmes sous-critiques commandés par accélérateurs, on pourra étudier le couplage entre une source de protons et un système sous-critique grace à MCNPX, un code développé à LANL (Los Alamos National Laboratory) et pour lequel l'IRS est *"Beta-Tester"*. Le présent travail a été réalisé dans le cadre du *"Beta-Testing"* de MCNPX. Nous avons analysé les modèles théoriques utilisés pour l'étude de la spallation ainsi que leur application dans le code MCNPX. Nous avons validé notre utilisation de MCNPX en faisant des comparaisons avec des résultats de Benchmarks et avec des données expérimantales concernant les taux de production de neutrons par proton, des mesures de sections-efficaces dans des cibles minces et des mesures d'activité dans des cibles épaisses. Nous avons aussi calculé plusieurs grandeurs caractéristiques pour certains isotopes importants dans le cadre du projet MEGAPIE.

iv

Zusammenfassung

Seit einigen Jahren wird die sogenannte "Accelerator Transmutation of Waste (ATW)" als eine mögliche Lösung für die Behandlung und die Wiederverwertung der nuklearen Abfälle sowie als eine Möglichkeit Energie mit einem unterkritischen System zu erzeugen betrachtet. Hauptziel von ATW ist die Verminderung der Gefahr der langfristigen Lagerung von nuklearem Brennstoff.

Am Institut für Reaktorsicherheit des Forschungszemtrums Karlsruhe konzentrieren sich einige der zur Zeit ausgeführten Arbeiten auf die kurzfristige Entwicklung von Beschleuniger-getriebenen Systemen. In diesem Sinne, nimmt IRS an den MEGAPIE, MUSE und XADS Projekten im Rahmen des " 5th *European Community Framework Programm"* teil. Die Entwicklung und die Validierung der theoretischen Mittel zum Kern Design und Sicherheitsberechnungen für Beschleuniger-getriebene Systeme sind wichtige Themen, die zur Zeit am IRS untersucht werden.

Insbesondere, für die Analyse der Beschleuniger-getriebenen Systeme, soll die Kopplung zwischen einer Protonenquelle und einem unterkritischen System mit MCNPX untersucht werden. IRS ist *"Beta-Tester"* von MCNPX, ein Monte Carlo Code, der im LANL (Los Alamos National Laboratory) entwickelt worden ist. Diese Arbeit wurde im Rahmen des *"Beta-Testing"* von MCNPX gemacht. Die im MCNPX angewandten theoretischen Modelle wurden analysiert. Wir haben unsere Anwendung von MCNPX durch Vergleiche mit Benchmark Ergebnissen und experimentellen Daten für Neutronenausbeute, für Wirkungsquerschnitts-Messungen in "Thin targets" sowie für Aktivitätsmessungen in "Thick targets" validiert. Wir haben auch verschiedene Grössen für bestimmte wichtige Isotope für das MEGAPIE Projekt berechnet.

Acknowledgments

A scientific work never results from the efforts of only one person. This was especially the case for my work. I therefore want to thank cordially Dr. C. Broeders for his patience, his kindness and his permanent availability. Working with him has been very pleasant and instructive.

Many thanks also to the colleagues of the Institute for Reactor Safety for having welcomed me so friendly. Special thanks to L. Sharp, M. Zimmermann, D. Stephany for their help and advice for solving administrative problems, and to the colleagues of the department (B. Merk, R. Dagan, V. Sanchez...) who have always been very kind with me and never forgot to come and call me for lunch.

I am also very grateful to the persons who kindly answered to my many E-mails and helped me very much for my work : L. Waters and E. Pitcher from L.A.N.L, F. Atchinson from PSI, I. Broeders from FZK.

I also want to thank here Prof. Dr. K.-H. Kampert for allowing me making this research work at FZK, as well as Dr. V. Heinzel for accepting being referee of my work. Many thanks to Prof. Dr. D. G. Cacuci, director of the IRS and to Dr. D. Struwe, head of "Plant safety and System simulation" department for allowing me making my diploma thesis in their institute, resp. department. I do not want to forget Prof. Dr. Engelhardt who has made important efforts since many years for developing exchange programs between Karlsruhe and European Universities. It was really a great opportunity for me to take part in the double diploma program between Grenoble and Karlsruhe.

Contents

List of Figures

List of Tables

Chapter 0

Introduction

For many years, many countries have been considering Accelerator Transmutation of Waste (ATW) as a solution for processing the nuclear waste as well for generating power with a subcritical system. Several research groups are working on this topic all over the world now. Their efforts to go forward are quite important as indicated by the increasing number of meetings or publications about that subject during the last years [2, 3]. The Accelerator Driven Transmutation of Waste is a technological approach of nuclear waste treatment which aims at reducing the long term hazards of the spent nuclear fuel disposal. This technology uses three basic components [1] as shown in fig. 1:

- An accelerator (linear or cyclotron) for delivering a proton beam with megawatts of beam power : protons with an energy between 250 MeV and $\simeq$ 2 GeV are needed.

- A sub-critical nuclear assembly made of the spallation target and the so-called blanket with fissile material for multiplication of neutrons. In this assembly, the proton beam is first converted into an intense neutron flux thanks to the spallation reactions occuring in the target. Then, these high energy neutrons insure the transmutation of the fissile isotopes and the long-lived fission products of the blanket into short-lived radioisotopes and stable nuclei.

- A chemical process for treating nuclear waste in order to isolate transuranics and long-lived radioisotopes. Spent nuclear fuel recycling is a prerequisite for ATW.

As accelerator-driven subcritical reactors are planned to be used in the scope of ATW, one of the decisive advantages of this technology is the expected absence of energetic reactivity accidents such as Chernobyl, provided if sufficient subcriticality is ensured. ATW is also interesting because it could offer a supplement to current fuel cycles using MOX and a support for fast reactors. It could help converting thermal reactors from U^{235}/Pu^{239} fuel cycles to Th^{232}/U^{233} cycles. This would also be helpful in the waste repository field [1, 44] because it would allow the separation of the most hazardous materials i.e. the plutonium, the minor actinides (neptunium, americium, curium) and some long-lived fission products from the waste. It would also allow to convert them into short-lived or stable products. More informations and explanations can be found on the webpage of LANL (Los Alamos National Laboratory) dedicated to ATW [12], in which an interesting "Transmutation of Waste Overview Tour" is proposed.
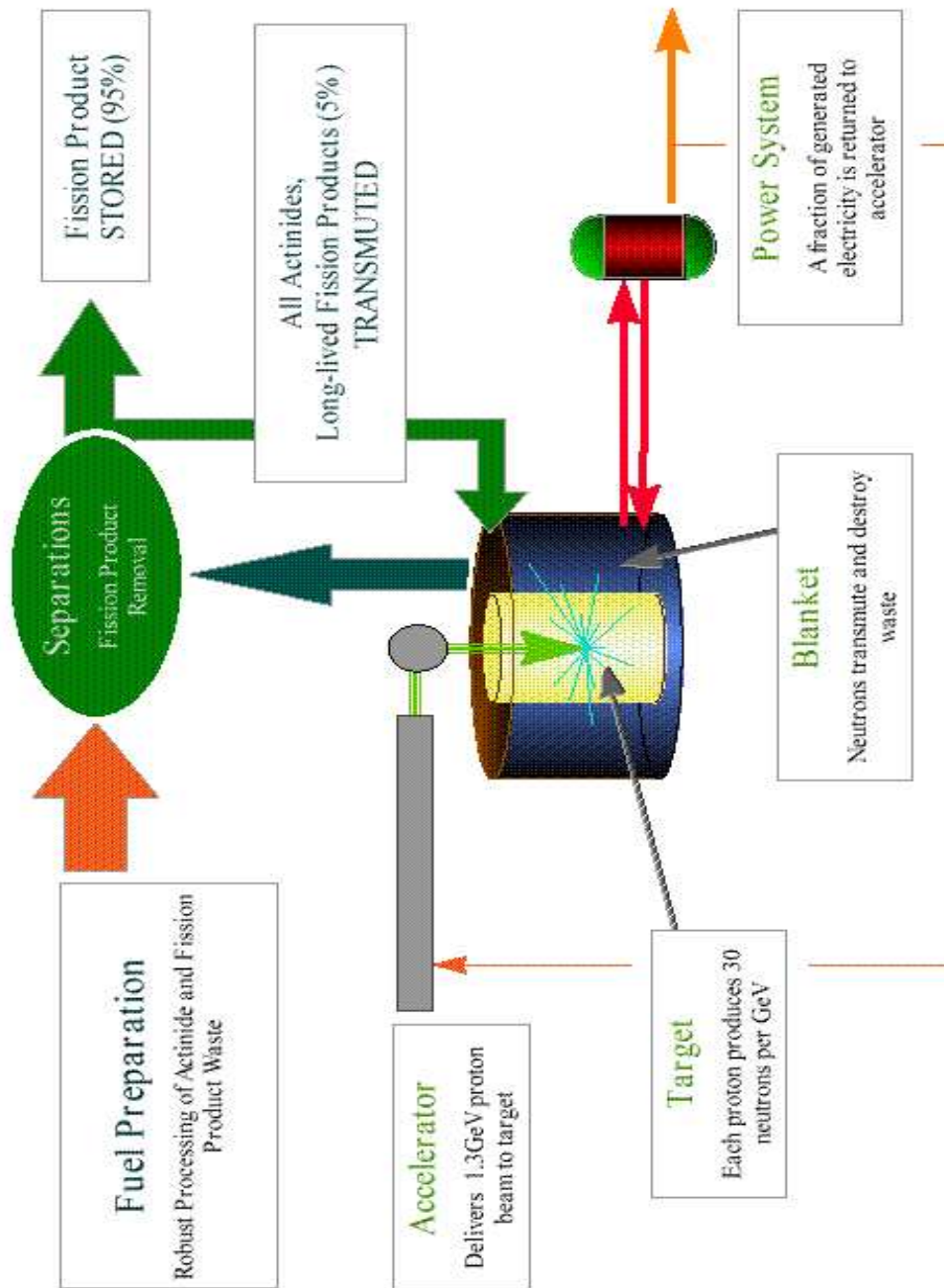
Figure 1: *Example of a general layout of ATW components* [48].

High current accelerators are under development in the world so that intense neutron sources will be available soon. For the moment, the improvement of the beam stability is the main issue. The target technology and the chemical process technology are also fields of great technological challenges. Scientific teams working on ATW in the world agree that molten lead or lead-bismuth eutectic (LBE) are good candidates for the spallation source. Such a source would offer major advantages [1]. Heat removal would be facilitated by the circulation of molten lead. In contrast to sodium, the coolant traditionally used for fast reactors, neither lead nor LBE are reactive to air and moisture. On one hand, there would be certain operating advantages in using LBE [45] because its melting point is 123 °C whereas the one of lead is 327 °C. LBE has also already been succesfully used as a reactor coolant in russian submarines. On the other hand, LBE has the disadvantage of forming polonium 210, a short-lived alpha emitter with $T_{1/2} = 138$ days, produced by the irradiation of bismuth by neutrons. Nevertheless most of the countries involved in ATW development favor LBE for being used in the spallation target.

The efforts of the research teams working on ATW led to the proposal of Roadmaps in Europe as well as in the USA. In Europe, the first ADS (Accelerator Driven System) concept was proposed by C. Rubbia [1, 10, 11]. Shortly after Rubbia, several other groups have proposed other innovative concepts [48]. In the USA, the first proposal was made by C.D. Bowman in the scope of the ADTT (Accelerator Driven Transmutation Technology) project [8, 9]. Since then, other groups have also proposed possible solutions in the scope of the AAA (Advanced Accelerator Applications) project [12].

In the present work, we focussed on the generation of spallation products in the target of Accelerator Driven Systems. As a matter of fact, the irradiation of the target of an Accelerator Driven System leads directly to spallation reactions which create many reaction products. Among these products, the most important are the neutrons which can be used afterwards to induce the fission of the nuclear fuel which has to be incinerated. The other spallation products are more or less considered as "parasitic" and may have consequences for the neutron balance, the materials properties, the final disposal, etc.
After being produced, the neutrons induce other interactions in the target where transmutations and a slowing down of the neutrons to the low energies are going on.
During the spallation many isotopes are created, they are called residual nuclei. They can be either similar to the target nucleus (remnant nuclei of spallation for example) or not when they have been created by evaporation (case of the light nuclei). Nevertheless most of them are radioactive and this can modify (especially increase) the activity of the target which would then be dangerous to handle for maintenance. This may also require special disposal of waste if the isotopes which are produced have a long half-life. Usually during operation high neutron fluxes exist in the spallation target. This high neutron fluxes also lead to transitions of the target inventory by neutron induced reaction. Especially for LBE target materials the buildup of ^{210}Po from ^{209}Bi is an important issue to be considered in order to assess the polonium contamination in the target.
The production of the "parasitic" products needs to be analysed in order to estimate its consequences, such as its influence on the lifetime of the target or its influence on the radioactivity of the target at the end of the working time. Two work areas shall be investigated :

- The description of the interactions between the proton beam and the target material.

- The description of the modifications occuring in the target due to the irradiation with the proton beam and the nuclear decays themselves.

Aim of the present work was therefore :

- The preparation of MCNPX. The Institute for Reactor Safety (IRS) of the Research Center in Karlsruhe participates in the international testing of the code and is MCNPX-Beta-Tester [4, 5].

- The validation of our application of MCNPX.

- Calculations related to MEGAPIE, a project for developing a spallation target for experimental use in the SINQ facility at PSI Villingen, Switzerland.

Chapter 1

Physical Models

1.1 The spallation reaction

Although spallation reactions have been studied since the end of the fourties [7], the reaction itself is not precisely known and described yet [6]. Nevertheless, since a few years, scientists have been more and more interested in spallation because of its huge application field (from fundamental research to the generation of electronuclear energy) [7]. For instance spallation reactions have a major importance for the development of intense neutron sources which could be used for hybrid reactors devoted to energy production or nuclear waste incineration, for spallation sources devoted to material structure analyses or irradiation studies and for tritium production units [6, 13].

1.1.1 General description of a spallation reaction

Spallation is a nuclear reaction in which a relativistic light particle (neutron, proton,..) hits a heavy nucleus. The energy of the incoming particle usually varies between a few hundreds of MeV and a few GeV per nucleon. Spallation is usually considered as a two-step reaction [17]: in the first step the target nucleus is heated, then comes the de-excitation of the target in the second step (see fig.1.1 taken from [34]).

1.1.2 The intra nuclear cascade

One can consider that the first step of the reaction consists in individual collisions between the nucleons [17]. As a matter of fact, the reduced wavelength $\frac{\lambda}{2\pi}$ of a few hundreds of MeV incoming nucleon is about 10^{-14} cm. Thus $\frac{\lambda_{nucleon}}{2\pi}$ is smaller than the distance between nucleons, usually about 1 fermi $= 10^{-13}$ cm, so the incoming nucleon "sees" the substructure of the nucleus i.e. a bundle of nucleons.
The interaction leads to the ejection of some of the nucleons and to the excitation of the residual nucleus which will cool itself afterwards. The typical duration of the intra nuclear cascade is 10^{-22} sec.
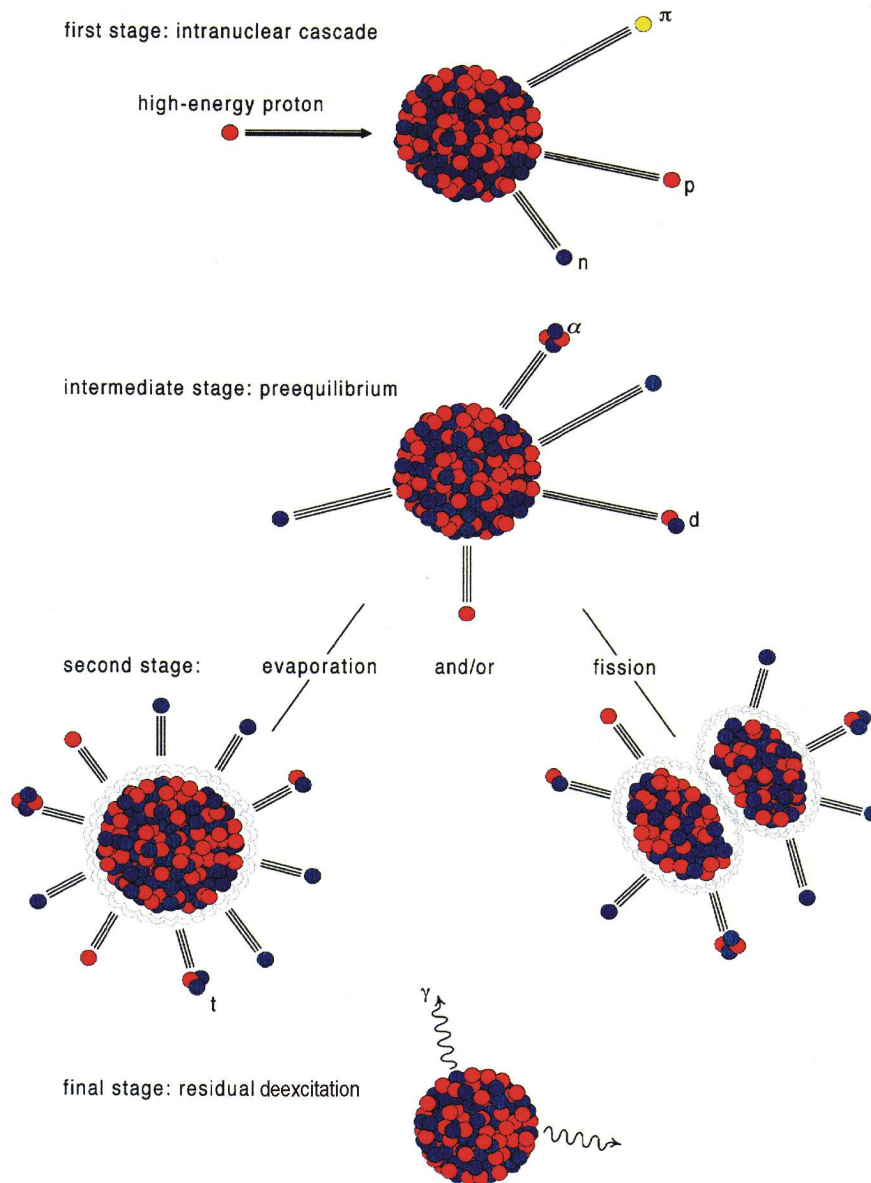
Figure 1.1: *Spallation mechanism [34].*

1.1.3 The de-excitation modes

When the intra nuclear cascade is finished and the last nucleon has been ejected, the nucleus is being left in an excited state. Then the de-excitation of the residual nucleus can proceed in two main ways : evaporation and fission. The typical duration of the de-excitation process is 10^{-16} sec.

The evaporation is the dedicated de-excitation mode for non fissile or hardly fissile nuclei which have been excited above the energy required for the separation of one neutron. In this case, the excited nucleus emits nucleons or light nuclei such as D, T, He^3, α, Li, Be.

Fission is the second important de-excitation channel. During the fission process, the nucleus changes its shape to reach firstly the so called *saddle point* at which the fission is due to occur then a second point, *the scission point*, at which the nucleus is cut into two fragments with differents masses.

During de-excitation, emission of photons is also possible. The nucleus emits particles until its energy of excitation goes below the binding energy of the last nucleon. At this state, about 8 MeV are remaining. They will be evacuated out of the nucleus by gamma radiation.

The ending of gamma emission does not mean that the de-excitation process is at the end. As a matter of fact, the resulting nucleus after gamma decay is often a radio-isotope. This radio-isotope will decay until the corresponding stable nucleus is reached.

1.1.4 The spallation products

Here we will focus on proton induced reactions. The example below (fig.1.2) shows a code calculated residual nuclei production in a lead target irradiated on its axis with a proton beam. One can cut this graphic into four major zones :

- residual nuclei of mass close to the target mass : they are coming directly from the spallation process.

- residual nuclei of mass $A \simeq 100$: they are resulting from fission processes.

- light residual nuclei : they are ejected from the nucleus during the intra nuclear cascade and they are also results of the evaporation of the remnant nucleus.

- residuals of mass between light fragments and fission products : one can infer [13] that they are created by the splitting of the remnant nucleus or by successive evaporation-like reactions, but nothing is really settled yet.
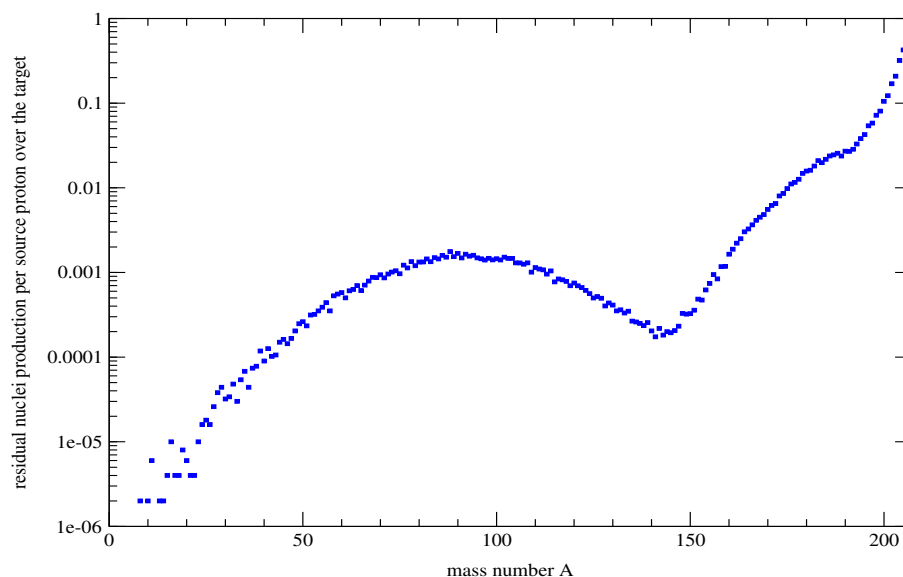
Figure 1.2: *Residual nuclei production in a lead target by an 800 MeV proton beam.*

From a more general point of view, Hüfner proposed in 1985 to classify the different types of interaction encountered in nucleus-nucleus reactions as a function of two parameters (see [6]) : the number of residual nuclei and the mass of the heaviest fragment compared to the mass of the "mother-nucleus". He obtained the very simplified classification as shown in fig.1.3.
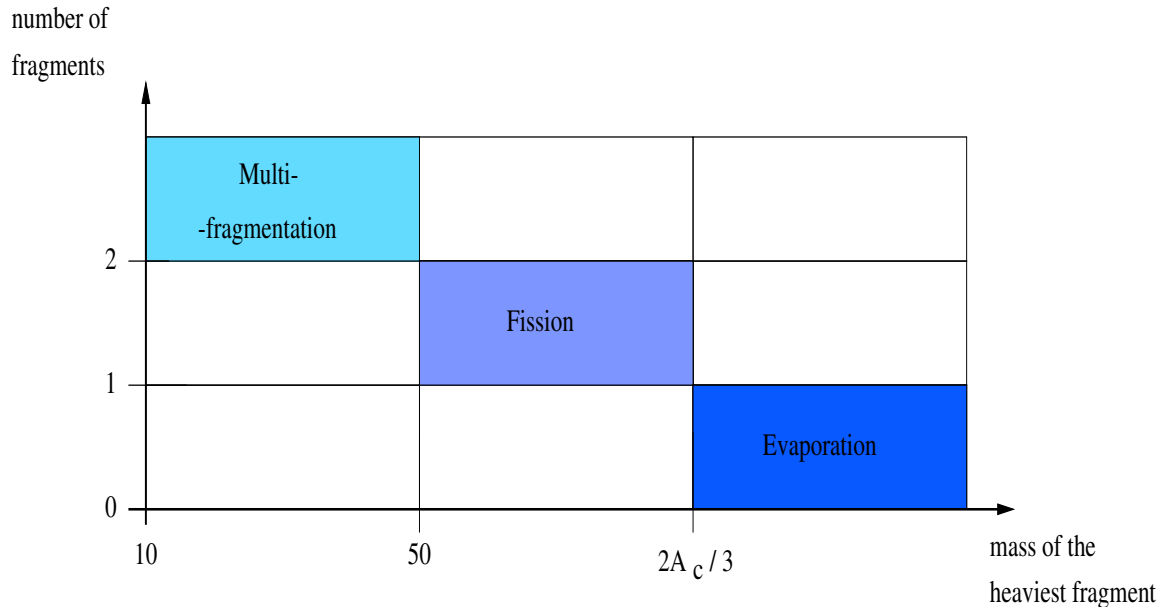
Figure 1.3: *Hüfners classification of the reaction products (see [6]).*

1.2   The Intra Nuclear Cascade, INC

1.2.1   The INC model

The INC model, first proposed by Serber [17], is used to describe the interaction between high energy hadrons (pions, protons, anti-protons...) or light nuclei with a target nucleus. The nucleus is considered under a statistical point of view. When the nucleus is at rest, it is regarded as a degenerated Fermi gas at zero temperature. All the particles which are scattered or produced during the cascade are treated in the field of the classical mechanics, they are defined by their velocity and their position. Every scattering which would lead to an already occupied energy level is forbidden because the nucleons are fermions. As a matter of fact, only one fermion can be in a given state according to the Pauli exclusion principle.
There are two main approaches to describe the intra nuclear cascades (see fig.1.4). In the first approach (Bertini approach, [18, 20]), the incoming particle hits the target material (target nuclei) which is regarded as a continuous medium. The particles have a specific mean free path $\lambda = (\rho\sigma)^{-1}$ in this medium (i.e inside a target nucleus). After each path, the particle scatters on a nucleon with which it exchanges energy. In the second approach (Cugnon approach, [23, 24]), the incoming particle is propagating freely in the target material (i.e inside a target nucleus) until it is at its minimum distance of approach from a nucleon d_{min}. The particle is scattered if $d_{min} \leq \sqrt{\frac{\sigma_{tot}}{\pi}}$.
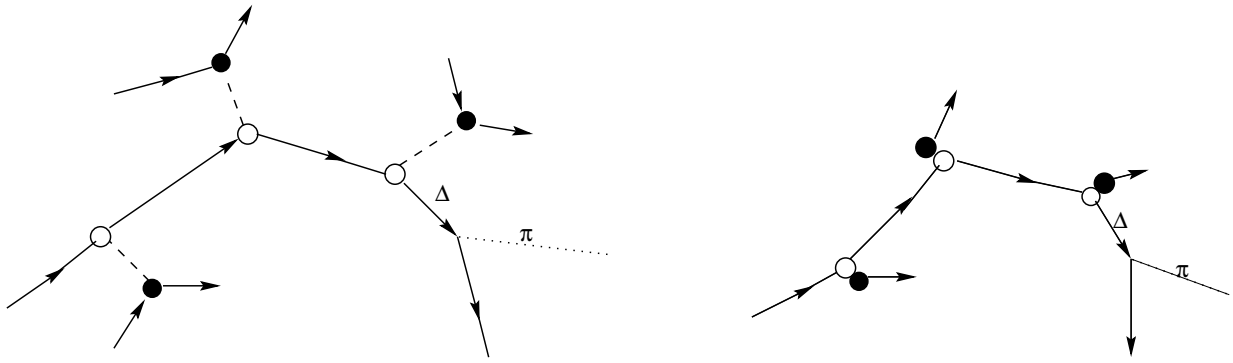
Figure 1.4: *The two approaches of the INC model [13] : left Cugnon approach, right Bertini approach. These two models describe how an incoming nucleon interacts with the nucleons inside of the target nucleus. The incoming nucleon is represented by a white circle, the nucleons of the target nucleus are represented by black circles. Note that pions and delta particles may be produced during the cascade (we noted them π and Δ).*

1.2.2 Simulation of the INC

The INC is often simulated by using the Monte Carlo calculation method. The Monte Carlo method has two major advantages : firstly it is quite easy to do the programming of the code, secondly Monte Carlo calculations give a quite good representation of the physical phenomena if the physical informations (for example nuclear cross section libraries) included in the code are well determined. The quality of the result given by the code depends on the statistical method (number of simulated particles or reactions) which is used, thus the computing time limits the use of such a calculation method.

The calculations of this work were done with MCNPX, a coupling of two already existing codes, LAHET and MCNP. Versions 2.2.3, 2.2.6 and 2.4.j of the code were used. Three INC models are available in running these MCNPX versions, the Bertini, ISABEL and CEM packages. The Bertini model is incorporated into MCNPX through the LAHET implementation of the HETC Monte Carlo code developed at Oak Ridge National Laboratory. In this model, based on the work of Bertini [18, 19], the nuclear density is represented by three density steps. The most recent version of the Bertini-like cascade has been developed by Yariv and Fränkel [20, 21] and has led to the ISABEL model available in MCNPX. This model was derived from the VEGAS INC code [22]. The ISABEL model allows neutron, proton, deuteron, hydrogen, helium, antiprotons, .. as projectiles and the nuclear density is represented by 16 steps. A third INC model, CEM, was available in the three MCNPX versions we used. CEM is an INC model which was developed in Dubna, Russia. By lack of informations about this model, we will not explain more about it, nevertheless more details about the models used in MCNPX can be found in table 2.3 in section 2.3.

Presently two major types of INC models are existing. They correspond to two different approaches of the nucleus. The first approach was developed in the sixties by Bertini (base for Bertini and ISABEL models in MCNPX), the second was developed in the eighties by Cugnon (base of the INCL code [26]). These two approaches will be discussed and presented hereafter in sections 1.2.3 and 1.2.4.

1.2.3   The Bertini cascade

Before 1963, INC calculations had been done by several groups, i.e. by the group of Metroplis et al. [15, 16]. Their work was based on a nuclear model in which the nucleon density within the nucleus was supposed to be constant. The results of their work showed that the model was quite good for many problems but that there were still non negligible discrepancies between experiments and calculations. Bertini therefore began to investigate those discrepancies by using an improved nuclear model. In 1963 he proposed a new model for calculations of intra nuclaer cascades [18]. Bertini describes the nucleus according to three concentric spherical zones. These zones are characterised by a given nuclear density and a given nuclear potential. The radius of each zone is determined by the distance at which the charge distribution function reaches given fractions of the central density. In the standard configuration, these fractions were 0.9, 0.2 and 0.01 [18].

The proton density in each region is set equal to the average value of the charge distribution in the considered region. The ratio between proton and neutron densities is considered to be the same for all regions and is set equal to the proton to neutron ratio in the nucleus [18, 6]. In other words :

$$\frac{\rho_{n_i}}{\rho_{p_i}} = \frac{\rho_n}{\rho_p} = \frac{N}{Z} = const. \tag{1.1}$$

with ρ_{n_i} the local density of neutrons in the zone number i and ρ_{p_i} the local density of protons in the zone number i.

After the model of Bertini, new Bertini-based models were developed. For instance, the model of Chen [22], with seven density steps, which led to the VEGAS code, and afterwards the model of Yariv and Fränkel which led to the ISABEL cascade [20, 21].

For all these Bertini-based models the above condition 1.1 is used. The Pauli exclusion principle is treated in such a way that the only kept nucleons for the calculations, are the nucleons produced in the target material with an energy larger than the Fermi energy associated to a given density zone.

The mean free path of the nucleons is given by :

$$\lambda_i = \frac{A}{\rho \times (Z \times \sigma_{ip} + (A - Z) \times \sigma_{in})} \tag{1.2}$$

where i stands for n or p. σ_{ip} is the cross section for the neutron-proton, or proton-proton interaction .

The nucleons are going straight as long as there is no nuclear reaction and as long as their path stays in the same zone of density. As a nucleon enters a zone of new density, it encounters a new nuclear potential. Thus the kinetic energy of a nucleon changes as the nucleon enters a new density zone. It increases or decreases according to the type of potential encountered in the considered zone.

A minimum energy is defined below which Bertini considers that a nucleon can not induce a nuclear reaction any more. The Bertini cascade is stopped when all the nucleons have an energy (*kinetic* + *potential* + *mass*) lower than this cut off energy or when they have been

ejected out of the nucleus. Important is then that the stopping criterium for the Bertini cascade is *the Bertini cut off energy*.

A schematic representation of a nucleon entering a zone of new density is given in fig. 1.5:
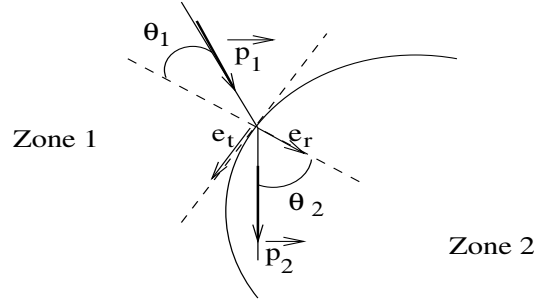
Figure 1.5: *Nucleon entering a zone of new density.*

Let us consider the plane $P = (\vec{p}_1, \vec{p}_2)$ and lets define $\vec{e}_r$ (respectively $\vec{e}_t$), the vectors belonging to P and being normal (respectively tangential) to the surface of the zone of new density. Let us use $p_{i\parallel} = \vec{p}_i.\vec{e}_t$ and $p_{i\perp} = \vec{p}_i.\vec{e}_r$, where i stands for 1 or 2.
For invariance reasons, one can write the boundary conditions for the momentum of a nucleon entering a new zone, just as one does it in electromagnetism :

$$p_{1\parallel} - p_{2\parallel} = 0 \quad \text{and} \quad p_{1\perp} - p_{2\perp} \neq 0 \tag{1.3}$$

assuming the invariance of the norm of the 4-momentum $P_\mu = \begin{pmatrix} E \\ \vec{p} \end{pmatrix}$, one has $E_1^2 - \vec{p}_1^2 = E_2^2 - \vec{p}_2^2$ (using units such that $c = 1$), so that one can then write these conditions as :

$$p_{1\parallel} - p_{2\parallel} = 0 \quad \text{and} \quad E_1^2 - p_{1\perp}^2 = E_2^2 - p_{2\perp}^2 \tag{1.4}$$

The nucleon can be either transmitted or reflected. One has :

$$\sin\theta_1 = \frac{p_{1\parallel}}{\|p_1\|} \quad \text{and} \quad \sin\theta_2 = \frac{p_{2\parallel}}{\|p_2\|} \tag{1.5}$$

and with the equation 1.3 follows :

$$\sin\theta_2 = \frac{\|p_1\|}{\|p_2\|}.\sin\theta_1 \tag{1.6}$$

One can then define a critical angle for which total reflexion of the nucleon occurs. Total reflexion means that $\theta_2 = \frac{\pi}{2}$. Thus we have $p_{1\perp}^2 = E_1^2 - E_2^2$ and as $\cos\theta_{TR} = \frac{p_{1\perp}}{\|p_1\|}$ we get finally :

$$\cos\theta_{TR} = \frac{\sqrt{E_1^2 - E_2^2}}{\|p_1\|} \tag{1.7}$$

Let us estimate now the probability that a projectile nucleon interacts with a nucleon of the nucleus.

Let us firstly consider the interaction between a beam of identical particles, characterised by density ρ_1 and momentum $\vec{p}_1$, with a second beam of particles characterised by density ρ_2 and momentum $\vec{p}_2$. Chen showed in his work [22] that the Lorentz invariant probability of interaction between the two beams (see fig. 1.6) is defined by :

$$W_{12} = v_{12}.\sigma_{12}.\rho_1.\rho_2 \tag{1.8}$$

where v_{12} is the relative velocity of the two beams and σ_{12} the cross section for the interaction between one particle of beam 1 with momentum $\vec{p}_1$ and one particle of beam 2 with $\vec{p}_2$.
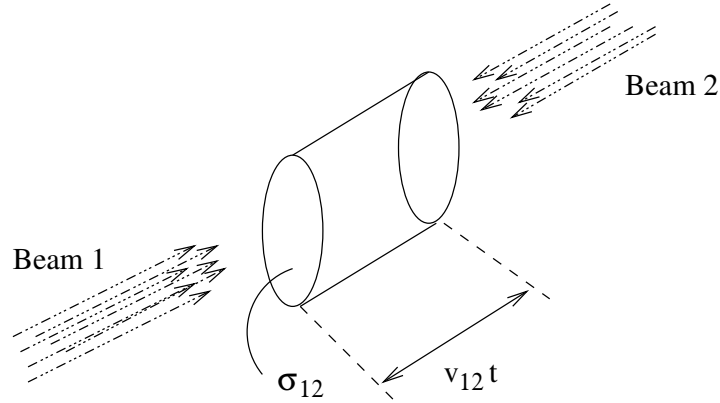
Figure 1.6: *Interaction of two beams of particles. In beam 1, the particles are characterised by density ρ_1 and momentum $\vec{p}_1$. In beam 2, particles are characterised by density ρ_2 and momentum $\vec{p}_2$. σ_{12} is the cross section for the interaction between one particle of beam 1 with momentum $\vec{p}_1$ and one particle of beam 2 with momentum $\vec{p}_2$. (v_{12} t) is equal to the distance crossed during time t at velocity v_{12}.*

Let us imagine now that the second beam is composed of particles with a continuous momentum distribution. In this case W_{12} becomes :

$$W_{12} = \rho_1 . \int_{\vec{p}_2} v_{12}(\vec{p}_2).\sigma_{12}(\vec{p}_2).\frac{\partial \rho_2(\vec{p}_2)}{\partial \vec{p}_2}.d\vec{p}_2 \tag{1.9}$$

With this model, if beam 1 represents the projectile beam and beam 2 represents the target, then the momentum distribution 2 is in fact the momentum distribution in the target nucleus. The number of particles of beam 1 going through a unit-surface S (S=1) during time t is $n_1 = \rho_1.v_1.S.t$. For one single bombarding nucleon we get then :

$$\omega_{12} = \frac{W_{12}}{\rho_1.v_1} = \frac{1}{v_1}.\int_{\vec{p}_2} v_{12}.\sigma_{12}.\frac{\partial \rho_2(\vec{p}_2)}{\partial \vec{p}_2}.d\vec{p}_2 = \frac{1}{\lambda_1} \tag{1.10}$$

where v_1 is the laboratory velocity of the bombarding particle and λ_1 is the mean free path of the nucleon in the target nucleus.

Then the probability that a projectile nucleon interacts between x and $x + dx$ is :

$$dP(x) = \omega_{12} e^{-\omega_{12}.x} dx \qquad (1.11)$$

and then the probability of collision in interval x is :

$$P(x) = 1 - e^{-\omega_{12}.x} \qquad (1.12)$$

P(x) is the probability that a projectile particle interacts with a nucleon of the target after having crossed the distance x in the nucleus.

Note that σ_{12} depends on the energy and thus depends on v_{12}. Usually, it is not possible to write a closed form of σ_{12} as a function. ω_{12} has therefore to be evaluated by numerical integration. For this approximation one considers that :

$$\int_{\vec{p}_2} v_{12}.\sigma_{12}.\frac{\partial \rho_2(\vec{p}_2)}{\partial \vec{p}_2}.d\vec{p}_2 = \sum_i v_{12}.\sigma_{12}.\frac{\partial \rho_2(\vec{p}_2)}{\partial \vec{p}_2}.\Delta\vec{p}_{2,i} \qquad (1.13)$$

After the intra nulear cascade, a nucleus is produced in an excited state. Its excitation energy is given by :

$$E^* = \sum_{particle=0}^{N_{part}} (\varepsilon_{part} - \varepsilon_{F_j}) + \sum_{hole=0}^{N_{hole}} (\varepsilon_{hole} - \varepsilon_{F_j}) \qquad (1.14)$$

The first term is the summation of the kinetic energy of the particles produced by the cascade compared to the Fermi energy of the medium in which the particles are (j index). The second term is the total energy of the holes which have been created in the distribution of the particles, once more compared to the local Fermi energy.

1.2.4 The Cugnon cascade

The Cugnon approach of the INC is completely different from the Bertini approach [13, 25]. Cugnon describes the nucleus as a sphere over which the nuclear density is a constant (it should be here mentioned that in a recent paper [26] Cugnon takes into account the radial dependence of the nuclear density). The radius of this sphere is :

$$R = 1.2 \times A^{1/3} \qquad (1.15)$$

The nucleus is not considered as a continuous medium but as a bundle of individual nucleons moving in a given potential. When a nucleon hits the target surface, it can be transmitted (reflection inside the target) or it can escape from it (total reflexion). For a constant spherical potential V_0, the probability of transmission is taken as a generalisation of the probability for a step potential and is given by the following formula :

$$T = \frac{4p\left(p^2 - 2mV_0 + V_0^2\right)^{1/2}}{\left[p + \left(p^2 - 2mV_0 + V_0^2\right)^{1/2}\right]^2} \tag{1.16}$$

where p is the momentum of the incident nucleon.

When a nucleon enters inside the nucleus, it is then regarded as a part of the nucleus and is therefore described just as the other nucleons of the nucleus. A consequence of such a description of the nucleus is that the criterium for interaction between the nucleons is now the distance between them. Scattering happens when two nucleons are closer to each other than a minimal distance d_{min}, depending on the total interaction cross section. There can be elastic or inelastic scattering. The expression of d_{min} is given by :

$$d_{min} = \sqrt{\frac{\sigma_{tot}}{\pi}} \tag{1.17}$$

The final momenta of the particles are estimated in agreement with the conservation laws [26] and the experimental cross sections. When inelastic scattering occurs pions are created and delta particles are excited according to the following reactions :

$$NN \rightleftharpoons N\Delta \quad \Delta \rightleftharpoons \pi N \tag{1.18}$$

The final channels are chosen at random according to the total cross sections.
Let us give an expression for the excitation energy of the produced nucleus. One can write the conservation of the energy as :

$$E_0 = E^* + E_{recoil} + S + E_{ej} + E_\pi \tag{1.19}$$

E_0 is the energy of the incoming particle, E^* is the excitation energy of the remnant nucleus, E_{recoil} is the recoil energy of the target nucleus, S is the separation energy of the particles which can be ejected from the nucleus, E_{ej} is the energy of the ejectiles, E_π is the energy of the emitted pions.
Cugnon explains in [26] that E_{recoil} is allways very small compared to the other terms of this equation. Thus we can simplify the upper equation and write the conservation of the energy as :

$$E_0 = E^* + S + \sum_{p=0}^{N_{ej}} \varepsilon_{ej,p} + \sum_{q=0}^{N_\pi} \varepsilon_{\pi,q} \tag{1.20}$$

As already said, S is the separation energy. It is the minimum energy required to remove all ejectiles and pions from the ground state of the target nucleus.
One can write it as $S = (A_{remnant} - A_{target})(V_0 - E_F)$ where V_0 is the nuclear potential and E_F is the Fermi energy so that one gets the excitation energy of the remnant nucleus :

$$E^* = T_0 - S - \sum_{j=0}^{N_{ej}} T_j - \sum_{k=0}^{N_\pi} \varepsilon_k \tag{1.21}$$

Important is that the stopping criterium for the Cugnon cascade is *the Cugnon cut off time*. The stopping time t_{stop} is the time at which the intranuclear cascade is stopped and gives way to evaporation. During the reaction, the excitation energy begins to grow rapidly and reaches a maximum (fig. 1.7). After a few fm/c it decreases rapidly with the ejection of cascade particles. After a longer time, about 25 fm/c in the given example, the decrease of the energy is smoother, there proceeds the evaporation.
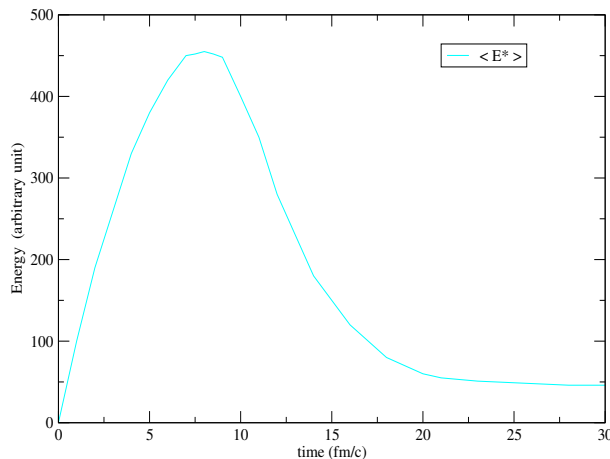
Figure 1.7: *Typical shape of the time evolution of the excitation energy of the remnant nucleus for a reaction like 1 GeV p + nucleus. Figure inspired from [6].*

Cugnon explains in [26] how t_{stop} is chosen, for instance in the example of fig. 1.7 it would be set to $25\,fm/c$. In the last version of the Cugnon INC model (INCL4), t_{stop} is set equal to $t_{stop} = t_0 \left(\frac{A_T}{208}\right)^{0.16}$ with $t_0 = 70\,fm/c$. At t_{stop}, the state of the nucleus is "frozen" and informations about the remnant nucleus such as its excitation energy, its spin, its charge number, its mass number are stored.

1.3 The de-excitation

1.3.1 The evaporation

There are several evaporation models. Here we will focuss on one of the first models, the Weisskopf - Ewing model [28, 29]. K.-H. Schmidt, from GSI Darmstadt, Germany, has recently developed an evaporation model which we will briefly present at the end of this chapter.

Let us begin with the Weisskopf-Ewing model. Let us consider an excited nucleus A, which emits a particle x, the remnant nucleus being called B. The reaction is then :

$$A \rightleftharpoons x + B \tag{1.22}$$

The total energy of the system is conserved, thus :

$$E_A = E_B + S_x + \varepsilon_x \tag{1.23}$$

with S_x the separation energy of x in the nucleus A, ε_x the kinetic energy of x, E_A and E_B the energy of the excited nucleus A and of the remnant nucleus B.

It is to be noticed that the use of the statistical model implies that there must be a large number of excited levels for the remnant nucleus B, so that there are many possibilities for the reaction to happen. As there must be several excited states of B with an excitation energy less than $E_A - \varepsilon_x$, we can assume that E_A should be much larger than ε_x, and also of course smaller than the binding energy of the nucleus.

Let us consider now the compound nucleus $(B + x)$. It is enclosed in the volume V, the velocity of x is called v, and $\sigma(E_A, \varepsilon_x)$ is the cross-section for x at energy ε_x colliding with B and producing A at energy E_A.

We call ω_x the probability per time unit that particle x, with an energy between ε_x and $\varepsilon_x + d\varepsilon_x$, is captured in nucleus B and creates nucleus A with energy between E_A and $E_A + dE_A$. We have (see also fig. 1.8) :

$$\omega_x = \frac{1}{t} \frac{\sigma(E_A, \varepsilon_x) v t}{V} \tag{1.24}$$

with v being the velocity of particle x.

As $v = \frac{p_x}{m_x}$, p_x being the momentum of particle x, one can write this as :

$$\omega_x = \frac{1}{t} \frac{\sigma(E_A, \varepsilon_x) p_x t}{m_x V} \tag{1.25}$$

incoming
particle

σ v . t
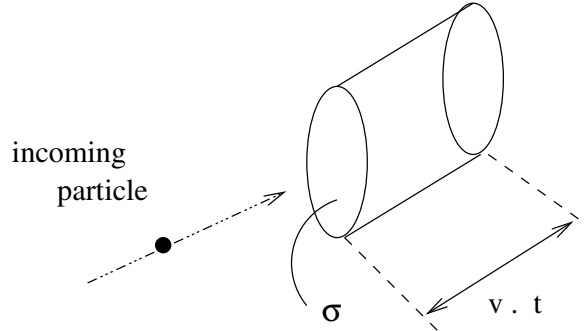
Figure 1.8: *Volume in which the particle moving with velocity v during time t is contained.*

The probability per time unit W_x that $A \to x + B$ is given through the following relation (see [6]):

$$W_x . d\varepsilon_x = \omega_x . N_x . \left(\frac{\rho_B}{\rho_A} \right) \tag{1.26}$$

with :

$$N_x = V . g . \left(\frac{4\pi p_x^2 . dp_x}{h^3} \right) \tag{1.27}$$

N_x is the number of available states.

In equation 1.27, g is the spin degenerescence of x, $g = 2s + 1$, $\frac{4\pi p_x^2.dp_x}{h^3}$ is the number of states with a momentum between p_x and $p_x + dp_x$ (its is equal to the volume contained between the sphere of radius $p_x + dp_x$ and sphere of radius p_x, divided by the elementary volume in the space of the momenta i.e. h^3).

Furthermore :

$$p_x^2 = 2m_x\varepsilon_x \tag{1.28}$$

$$p_x dp_x = m_x d\varepsilon_x \tag{1.29}$$

Using equations 1.25 and 1.27 in 1.26 one gets :

$$W_x.d\varepsilon_x = \sigma(E_A,\varepsilon_x)\frac{p_x}{m}g\frac{4\pi p_x^2 dp_x}{h^3}\left(\frac{\rho_B}{\rho_A}\right) \tag{1.30}$$

And finally, using equation 1.28, equation 1.29 and $h = 2\pi\hbar$ in 1.30, one gets :

$$W_x.d\varepsilon_x = \sigma(E_A,\varepsilon_x).\frac{g.m_x}{\pi^2.\hbar^3}.\frac{\rho_B}{\rho_A}.\varepsilon_x.d\varepsilon_x \tag{1.31}$$

The total transition probability Γ_x is obtained by integrating equation 1.31 over all possible energies. Γ_x is the width of transition $A \rightarrow x + B$. One has :

$$\Gamma_x = \int_0^\infty W_x(\varepsilon_x).d\varepsilon_x \tag{1.32}$$

One of the problems of this model is that it uses capture cross-sections for the reverse capture in excited states. These cross sections can not be determined with experiments. Nevertheless, for a particle hitting a nucleus and beeing absorbed, Weisskopf shows [29] that the reverse capture cross-section is :

$$\sigma(E_A,\varepsilon_x) = \begin{cases} 0 & \text{if } \varepsilon_x < V_{Coulomb} \\ \\ \sigma_0.\left(1 - \frac{V}{\varepsilon_x}\right) & \text{if } \varepsilon_x \geq V_{Coulomb} \end{cases}$$

where $\sigma_0 = \pi R^2$ and $V = \frac{ZZ'e^2}{r}$, with Ze the charge of the nucleus, r its radius, Z'e the charge of the particle.

As already mentioned, Schmidt has developed an evaporation model based for some part on the Weisskopf-Ewing model. The version called KHSv3p has been recently coupled to the last version of the Cugnon INC model called INCL4 [26]. Production of spallation products can thus be estimated by the *INCL4 + KHSv3p* ensemble, INCL4 predicting the nuclei with mass number around the one of the target, KHSv3p doing the simulation in the fission-evaporation area.

In the Schmidt model, the emission of p, n and α particles is described by the Weisskopf-Ewing model. A special fragment mass distribution function has been integrated in the model for

describing the fission. Friction is also taken into account. More informations about the Schmidt model as well as a description of the Schmidt code can be found in [27].

1.3.2 Fission

The case of fission is more complicated and there is no real way to describe it properly. The description of the evolution of the fission probability as evaporation goes on, and also the prediction of the fission products are both not very well managed. Bohr and Wheeler [30] have proposed a formalism which let them find the fission width associated to a special state of the compound nucleus, the state is defined by Z, A, E^*. They obtained that :

$$\Gamma_f = \frac{N^*}{2\pi\rho(E)} = \frac{1}{2\pi\rho(E)} \cdot \int \rho^*(E - E_f - E_{kin})dE_{kin} \tag{1.33}$$

where N^* is the number of levels in the transition state available with the given excitation. ρ^* is the density of levels of the compound nucleus in the transition state (at the saddle point) which are above the fission barrier. E^* is the energy of the compound nucleus at saddle point.

In the cases we are considering in this work, fission may be induced by high-energy interactions. Two models are available in MCNPX for describing high-energy fission, the ORNL model and the RAL model (Rutherfords Appleton Laboratory) [34]. The RAL model allows fission for nuclei with Z above 71. It is the default option in MCNPX and it is the option we used for all our calculations. The ORNL model simulates only fission for actinides.

1.3.3 The emission of photons and the nuclear decay

The $\gamma-emission$ is not very important when other de-excitation channels are open. The probability of $\gamma-emission$ is given by :

$$P_\gamma = \frac{\Gamma_\gamma}{\Gamma_\gamma + \sum_i \Gamma_i} \tag{1.34}$$

where the Γ_i are the transition widths for the different open channels and Γ_γ the width for $\gamma-emission$.

As already said, nuclear decay is also a possible channel of de-excitation. Suppose that we have a given nucleus which can decay through different nuclear decay channels as shown in fig. 1.9.
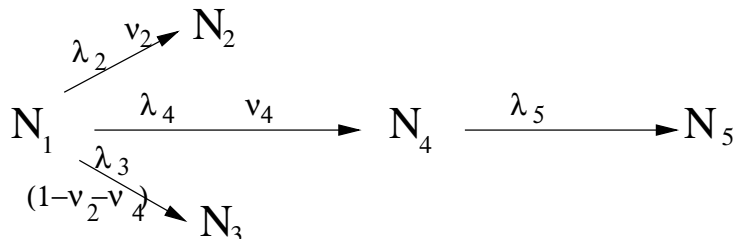
Figure 1.9: *Nuclear decay.*

For example, the decay of nuclides N_1 and N_4 is described with :

$$\begin{cases} \frac{dN_1(t)}{dt} = -\nu_2\lambda_2 N_1(t) - \nu_4\lambda_4 N_1(t) - (1-\nu_2-\nu_4)\lambda_3 N_1(t) \\ \\ \frac{dN_4(t)}{dt} = \nu_4\lambda_4 N_1(t) - \lambda_5 N_4(t) \end{cases}$$

where $N_i(t)$ is the number of nuclides of type "i" at time "t", λ_i is the decay constant and ν_i is the branching ratio for decaying to nucleus j (see also Appendix A).

Supposing that $N_1(0) = N_{1,0}$ and $N_4(0) = N_{4,0}$, the solution is :

$$\begin{cases} N_1(t) = N_{1,0}e^{-[\nu_2\lambda_2+\nu_4\lambda_4+(1-\nu_2-\nu_4)\lambda_3]t} = N_{1,0}e^{-\alpha_1 t} \\ \\ N_4(t) = (N_{4,0} + \frac{\nu_4\lambda_4 N_{1,0}}{\alpha_1-\lambda_5})e^{-\lambda_5 t} - \frac{\nu_4\lambda_4 N_{1,0}}{\alpha_1-\lambda_5}e^{-\alpha_1 t} \end{cases}$$

1.3.4   Competition between the de-excitation channels

Evaporation and fission are the two major de-excitation channels. The probability that fission occurs is given just as for $\gamma - emission$ by :

$$P_f = \frac{\Gamma_f}{\Gamma_f + \Sigma_{i \neq f}\Gamma_i}$$

It is exactly the same for evaporation.
Usually evaporation and fission have the largest widths, thus one can write :

$$P_f \simeq \frac{\Gamma_f}{\Gamma_f + \Gamma_{evap}} = \frac{1}{1 + \frac{\Gamma_{evap}}{\Gamma_f}}$$

and

$$P_{evap} \simeq \frac{\Gamma_{evap}}{\Gamma_f + \Gamma_{evap}} = \frac{1}{1 + \frac{\Gamma_f}{\Gamma_{evap}}}$$

Important is then the ratio $\frac{\Gamma_{evap}}{\Gamma_f}$.

Chapter 2

Simulation codes

For the simulation of the interaction of high energy light particles with matter, two development lines may be recognised. In the western community, the HETC Code [14] from Oak Ridge National Laboratory is the basis for the developments. In the eastern community, the CEM code [31] from JINR Dubna plays a similar role. In the following, we will discuss the HETC line in some details presenting the succesive developments of HETC : HETC, LCS, MCNPX. It should also be mentioned that the CEM model has been integrated in the actual code MCNPX. Here we concentrate on the HETC development line.

2.1   HETC

HETC, High Energy Transport Code, is a Monte Carlo code for treating the transport problems of nucleons, pions and muons. It was developed at Oak Ridge National Laboratory (ORNL). HETC has been used afterwards at Los Alamos National Laboratory (LANL) which has developed its own version of the code.
HETC uses the Bertini intra nuclear cascade model [18], to describe the physics of the nuclear interactions (see 1.2.3). It treats all interactions involving protons, pions and muons. For interactions involving neutrons, it only treats those which are above a given cut off energy, for example 20 MeV at LANL. In the case of neutrons created from a nuclear reaction with an energy below the cut off energy, their kinetic parameters are stored in a special file NEUTP (neutron file). NEUTP can be used afterwards by another Monte Carlo code such as MCNP which is able to solve the transport problem by using the NEUTP file combined with neutron cross-section libraries.
For the description of the intra nuclear cascade, HETC is based on the Bertini model [14]. We will shortly describe its main caracteristics hereafter.

- *Nucleon density in the nucleus :*
  For heavy or intermediate mass nuclei, the nucleon density in the nucleus can be written as :

$$\rho(r) = \rho_1 \left[1 + exp\frac{(r-c)}{a}\right]^{-1}$$

  ρ_1 is a parameter chosen for the normalisation, c is defined through $cA^{1/3} = 1.07$ fm where A is the mass number of the nucleus, r is the distance from the centre of the nucleus and $a = 0.545$ fm.

In HETC, the nucleus is described as three concentrical spheres. The radius of each sphere corresponds respectively to 0.9, 0.2 and 0.01 of the maximal density. The normalisation is the same as explained in section 1.2.3.

- *Momentum distribution in the nucleus :*
  The interactions between the nucleons are neglected. The momentum distribution is then a Fermi distribution at zero temperature and one has in each density area :

$$f(p) = cp^2 \quad \text{with} \quad \int_0^{P_f} f(p)dp = n_i$$

where n_i means n_n or n_p, number of neutrons, respectively protons in the area.

P_f is the momentum corresponding to the Fermi energy E_f which depends of the density $\frac{n}{V}$ of particles. E_f is therefore different for each zone of density and each type of particle. One has :

$$E_f = \frac{P_f^2}{2m} = \frac{\hbar^2}{2m}\left(\frac{3\pi^2 n}{V}\right)^{2/3}$$

The global momentum distribution is not a Fermi distribution anymore because it is discontinuous at each zone boundary.

- *Potential energy distribution in the nucleus :*
  The separation energy of the least bound nucleon is considered to be 7 MeV for all the nucleons and all the density zones. The distribution of the potential energy is obtained by adding this binding energy to the Fermi energy of the nucleons in each zones. This distribution is then also depending of the nucleons and the density zones.

- *Nucleon-nucleon cross-sections :*
  HETC uses free nucleon-nucleon interaction cross-sections to compute the probability of interaction during the intra nuclear cascade. These cross-sections have been derived from experimental results and implemented in the code in a parametrised form. They are elastic cross-sections and pion production cross-sections. The pion-nuclei interactions (such as elastic diffusion, charge exchange, absorption) are also computed.

- *The Pauli principle :*
  According to the Pauli principle, an interaction which would lead to an already occupied state is forbidden. As already said, in HETC the nucleons are considered as a Fermi gas (see momentum distribution). In such a gas, all the states with an energy smaller or equal to the Fermi energy are occupied. Therefore, the Pauli principle is applied in the HETC calculations by neglecting afterwards all interactions wich have led to a state with an energy smaller than the Fermi energy for the considered zone and particles.

As far as the evaporation stage is concerned, the method used in HETC is based on the Weisskopf theory (see section 1.3.1). The main parameters are set as follows :

- **Probability $P_i(\varepsilon)$:**
  $P_i(\varepsilon)$ is the probability that a nucleus excited at energy E^* emits a particle of type i with energy ε.

$$P_i(\varepsilon) \sim g_i m_i \varepsilon \sigma_{ci}(\varepsilon) \rho(E)$$

  where E is the excitation energy of the remnant nucleus, $E = E^* - B_i - \varepsilon$. g_i is the number of spin states, B_i is the binding energy of the particle i, and $\rho(E)$ the state density in the remnant nucleus. σ_{ci} is the inverse cross-section for the reaction.

- **State density in the remnant nucleus, $\rho(E)$:**
  $\rho(E) \sim e^{(a[E-\delta])^{1/2}}$
  where δ is the pairing energy and $a = \frac{A}{8}[1 + \frac{3}{2}(1 - \frac{27}{A})^2]$

- **Cross-sections :**
  They are inverse cross-sections i.e cross-sections for formation of the compound nucleus by bombarding the remnant nucleus with particle i.
  - *For neutrons :*

$$\sigma_{cn}(E) = \pi R^2 \alpha (1 + \tfrac{\beta}{E})$$

  with $\alpha = 0.76 + 1.93 A^{-1/3}$, $\quad \alpha\beta = 1.66 A^{-1/3} - 0.05$ and $\quad R = 1.74 A^{1/3}$

  - *For charged particles :*

$$\sigma_{ci}(E) = \begin{cases} \pi R^2 (1 + c_i)(1 - \frac{K_i V_i}{E}) & \text{if } E > K_i V_i \\ \\ 0 & \text{if } E < K_i V_i \end{cases}$$

  Only five charged particles are considered in HETC : p, d, t, He^3, α. For these five particles K_i, V_i and c_i are defined as follows, depending on the charge number Z of the target nucleus (see table 2.1).

$V_i = \frac{Z_i Z e^2}{R + R_i}$ with $R_i = 0$ fm for the protons, 1.2 fm for the four other particles.
$$K_d = K_p + 0.06 \qquad c_d = \tfrac{c_p}{2}.$$
$$K_t = K_p + 0.12 \qquad c_t = \tfrac{c_p}{3}.$$
$$K_{He^3} = K_\alpha - 0.06 \qquad c_{He^3} = c_\alpha = 0.$$

Charge number Z	K_p	c_p	K_α
0 to 10	0.60	0.08	0.77
11 to 20	0.51	0.00	0.81
21 to 30	0.60	-0.06	0.85
31 to 40	0.66	-0.10	0.89
41 to 50	0.68	-0.10	0.93
51 to 60	0.69	-0.10	0.97
> 61	0.69	-0.10	1.00

Table 2.1: *Values of K_p, c_p and K_α for p, d, t, He^3 and α as defined in HETC [14].*

2.2   LCS

The LAHET Code System (LCS) was developed at Los Alamos National Laboratory [32]. LAHET (Los Alamos High Energy Transport Code) is an improved version of HETC. LAHET includes as user option an alternative intra nuclear cascade model called ISABEL. To complete the particle transport below a cut-off energy (default 20 MeV) a direct coupling to the Monte Carlo Code MCNP was realised with the help of the interface file NEUTP. In a first version, a modified version of MCNP4B, called HMCNP, was issued for this coupling (see fig. 2.1). In a next step, starting from the version MCNP4C, the coupling was realised on the basis of new interface files and no special version of MCNP4C was needed.

In the last stage, LAHET was fully integrated in the MCNP code environment, leading to the MCNPX code discussed in the next section.
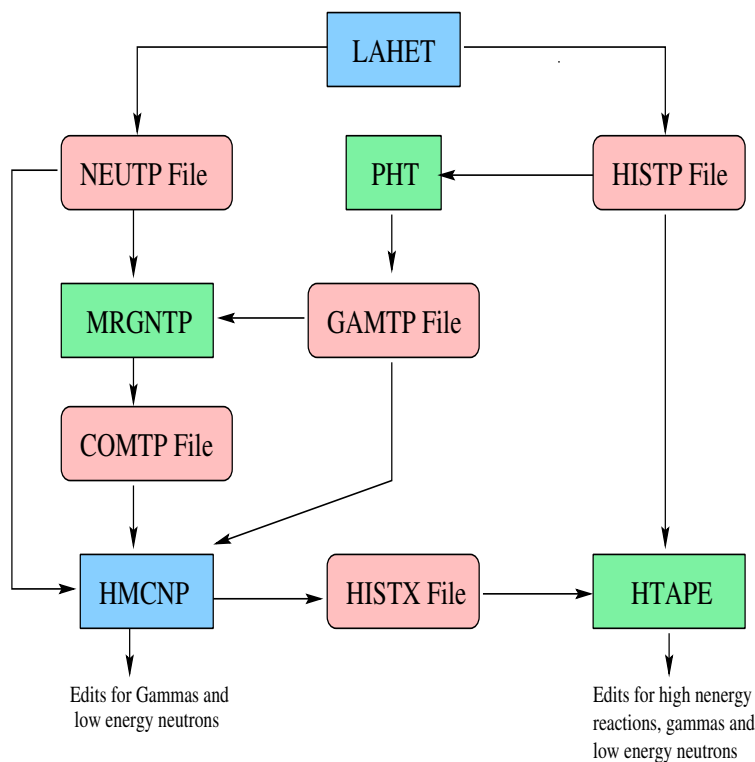
Figure 2.1: *The LAHET Code System [32].*

2.3 MCNPX

The MCNPX code [34] was designed to replace the already existing LCS [35]. It is a coupling of two previous calculations codes : LAHET and MCNP [33]. MCNPX only needs one input file for both codes and avoids the transfer of large data files. It allows the treatment of transport problems in a large range of energies, from thermal energy (25 meV) to a few GeV. For energies lower than 20 MeV, quite complete sets of cross sections are available for the major part of the stable nuclei. International cross-sections libraries such as ENDF, JEF, JENDL, are available and are regularly updated. To treat the transport, MCNP uses data deduced of these libraries after processing them with *NJOY/ACER* for instance. For energies larger than 20 MeV, there are less cross-section data. The cross-sections which are needed for the treatment of the transport problems have to be calculated by using nuclear physics models available in the code. LAHET is a very complete code in this field. Presently the preparation of complete data files up to 150 MeV is in progress in several projects. After running an MCNPX-job, several evaluations can be performed with an auxilliary code, HTAPE3X, to obtain specific informations (neutron spectrum, energy deposition, residual nuclei...)

Most LCS options are used in MCNPX. They include for example the following models :
- the Bertini and the ISABEL INC models as in LCS,
- a third INC model : the CEM model [31],
- a multistage pre-equilibrium model,
- an evaporation model,
- a nucleon elastic scattering model,
- a gamma production model...

For high energy fission, two models are available in MCNPX, the ORNL model and the RAL model (Rutherfords Appleton Laboratory) [34]. The RAL model allows fission for nuclei with Z above 71. It is the default option in MCNPX and it is the option we used for all our calculations. The ORNL model simulates only fission for actinides.
A summary of the MCNPX variables and physics models is given in tables 2.2 and 2.3.

Variable	Bertini	ISABEL	CEM
Nuclei	all	all	Carbon and heavier
Incident particles	p, n, pions	$A <= 4+$ antiprotons	p, n, pions
Upper energy	3.5 GeV for nucl-nucl 2.5 GeV for pion-nucl	1 GeV	5 GeV
Lower energy	20 MeV - 150 MeV	20 MeV - 150 MeV	$\simeq$ 100 MeV

Table 2.2: *MCNPX variable range [34].*

We will now explain how an MCNPX input file is created. An MCNPX input file is constituted of six major parts generally labelled "Cells", "Surfaces", "Materials", "Source", "Options", "Tallies".
In the "Cells" definition, one gives the list of the cells (i.e volumes) constituing the geometry describing the problem. The cells are defined by their surrounding surfaces.
In the "Surfaces" definition, one gives the list of the surfaces which are needed to define the cells of the problem. Note that in some cases, special surfaces are used for the source definition.
In the "Materials" definition, one gives a list of the materials involved in the problem. The composition of each material is fully written by listing all its constitutive elements or isotopes whith their relative amount (in atomic fraction or weight fraction). All the data libraries used

Physics Process	Bertini	ISABEL	CEM
Method	$INC + EQ$ or $INC + EQ + PE$	$INC + EQ$ or $INC + EQ + PE$	$INC + EQ + PE$
Intranuclear Cascade Model	Bertini INC	ISABEL INC	improved Dubna INC
Nuclear density distribution	$\rho(r) = \rho_0[1 + exp\frac{(r-c)}{a}]^{-1}$ $c = 1.07A^{1/3} fm$ $a = 0.545 fm$ $\rho(r) = \alpha_i \rho_0; i = 1,2,3$ $\alpha_1 = 0.9, \alpha_2 = 0.2, \alpha_3 = 0.01$	$\rho(r) = \rho_0[1 + exp\frac{(r-c)}{a}]^{-1}$ $c = 1.07A^{1/3} fm$ $a = 0.545 fm$ $\rho(r) = \alpha_i \rho_0; i = 1,...,16$	$\rho(r) = \rho_0[1 + exp\frac{(r-c)}{a}]^{-1}$ $c = 1.07A^{1/3} fm$ $a = 0.545 fm$ $\rho(r) = \alpha_i \rho_0; i = 1,...,7$ $\alpha_1 = 0.95, \alpha_2 = 0.8, \alpha_3 = 0.5$ $\alpha_4 = 0.2, \alpha_5 = 0.1, \alpha_6 = 0.05$ $\alpha_7 = 0.01$ $\frac{\rho_n(r)}{\rho_p(r)} = \frac{N}{Z}$
Nucleon potential	$V_N = T_F + B_N$	Nucleon kinetic energy T(N) dependant potential $V_N = V_i(1 - \frac{T_n}{T_{max}})$	$V_N = T_F + B_N$
Pion potential	$V_\pi = V_N$	$V_\pi = 0$	$V_\pi = 25 MeV$
Mean nucleon binding energy	$B_N \simeq 7 MeV$	initial B_N from mass table the same value is used throughout the calculation	$B_N \simeq 7 MeV$
Elemantary cross sections	standard Bertini INC (old)	standard ISABEL INC (old)	new CEM97 last update March 1999

Table 2.3: *MCNPX physics models [34].*

for the different elements are also specified in this part.

In the "Source" part, one gives all the informations which are needed to define the source especially the type of the source particles, their energy, the shape of the beam, its direction, the place where the beam encounters the target material, etc.

In the "Options" definition, one gives the specific computing options which will be used in the calculation. For example, one may choose for which type of particles the summaries will be written in the ouptput file, which INC model will be used, and one can set several cut off energies.

In the "Tallies" part, one tells what is to be calculated for the particles. For example a flux through a given surface or a neutron current. The way how the tally-results will be written in the output file is also specified. For example, one can specify the print out of a neutron flux through several given surfaces in a table where for each surface the flux is given as a function of the energy.

At the end of the input file, one gives also the stop criterium which is to be used for the calculation (time to run or number of simulated particles).

A simple example of an MCNPX input file is given hereafter in table 2.4. Note that there is an empty line at the end of the "Cells" part and also at the end of the "Surfaces" part. These blank lines are needed and may not be forgotten otherwise MCNPX does not run and one may loose quite a lot of time in finding where the error is. The meaning of some terms of the MCNPX example file is explained in table 2.5.

As already said, MCNPX is based on MCNP and LAHET. Here we want to explain a bit more the physics used in MCNP. The very essence of MCNP is the calculation of neutron transport by applying the Monte Carlo method (note that MCNP stands for Monte Carlo N-Particle transport code). In fig. 2.2 we give a schematic representation of the history of a neutron simulated by a Monte Carlo method (fission is represented as part of absorption without further detail).

```
c MCNPX test problem
c ——————————————————————————————————————————
c 600 MeV protons on a cylindrical Pb target of 20 cm radius and
c 50 cm thickness. Source uniformly distributed over circle of
c 2 cm radius. Tally of neutron current.
c ——————————————————————————————————————————
c Cells
c ——————————————————————————————————————————
1   1    -11.30   -1 2 -3
2   0    -4    (1:-2:3)
3   0    4


c ——————————————————————————————————————————
c Surfaces
c ——————————————————————————————————————————
1   cz   20.0
2   pz   0.0
3   pz   50.0
4   sz   25.0   50.0


c ——————————————————————————————————————————
c Materials
c ——————————————————————————————————————————
m1   82000.42c   1
c ——————————————————————————————————————————
c Source
c ——————————————————————————————————————————
sdef   par = 9   erg = 600   sur = 2   dir = 1   pos = 0 0 0   rad = d1
si1   2.0
ssw   1   2   3   4   CEL 1
c ——————————————————————————————————————————
c Options
c ——————————————————————————————————————————
imp:n    1 1 0
imp:h    1 1 0
phys:n   660
phys:h   660
mode    n h p
histp   1
lca   2 1 2
c ——————————————————————————————————————————
c Tallies
c ——————————————————————————————————————————
E0   100   200   300   400   500   600
FC1    Neutron current integrated over surface 4 (unit:particles)
F1:n   4
FQ1   f e
c ——————————————————————————————————————————
print
nps   2000
```

Table 2.4: *Example of an MCNPX input file for calculating the neutron current produced over a cylindrical lead target irradiated by a 600 MeV proton beam.*

	Input command	Meaning
	c MCNPX test problem c —————— c 600 MeV protons...	the letter "c" at the beginning of a line is used to write a comment in the input file. The line will not be read by MCNPX as input key-words.
Cells	1 1 -11.30 -1 2 -3	Cell Nr 1 is made of material Nr 1, the density of which is 11.30 g/cm^3. The volume of cell 1 is made of the intersection of three volumes : the inner volume of cylinder 1, the volume above plane 2 and the one below plane 3.
Surfaces	1 cz 4.0	Cylinder of 4.0 cm radius, axis of which is Z-axis.
	2 pz 0.0	Plane $Z = 0.0$
	4 sz 25.0 50.0	Sphere of radius 50.0 cm and center on Z-axis at $Z = 25.0$.
Materials	m1 82000.42c	Material Nr 1 is natural lead (82000) and the ENDL92 library (.42c) is used.
Source	sdef par=9 erg=600 sur=2 dir=1 pos=000 rad=d1 si1 2.0	The source is a 600 MeV (erg=600) proton (par=9) beam, encountering the target on surface Nr 2 (sur=2) at the point (0,0,0) (pos=000). The beam is going in the target along the Z-axis (dir=1). The source is uniformly distributed over a circle of radius d1=2cm (rad=d1, si1 2.0).
	ssw 1234 CEL1	An HISTX file called wssa will be written. It will be an input file for the HTAPE3X Code.
Options	mode n h p	The summary for neutrons, protons and photons will be printed in the output file.
	histp 1	An history file HISTP will be written. It will be an input file for the HTAPE3X Code. This code was used in this work for the calculation of the spallation residual nuclei production.
	lca 2 1 2	One considers elastic scattering for neutrons and protons (2), one uses a pre- equilibrium model after the cascade (1), the ISABEL model is used (2), all the 6 other entries of the card are left to their default value.
Tallies	E0 100 200 300 400 500 600 FC1 F1:n 4 FQ1 f e	Neutron current integrated over surface Nr 4 (F1:n 4). The results will be written in a table with the current (f) as a function of the energy (e). The energy bins are 0 to 100MeV, 100 to 200, etc...
	print	A list of specific tables will be printed in the output file.
	nps 2000	The run will be terminated after 2000 simulated source particles.

Table 2.5: *Meaning of some terms of the input file.*

```
                          ┌─────────────────┐
                          │    EMISSION     │
                          └─────────────────┘
                                   │
                          ┌─────────────────┐
                          │ random choice   │
                          │  of the point   │
                          └─────────────────┘
                                   │
                          ┌─────────────────┐
                          │ random choice   │
                          │  of the energy  │
                          └─────────────────┘
                                   │
                          ┌─────────────────┐
                          │ random choice   │
                          │ of the direction│
                          └─────────────────┘
                                   │
                          ┌─────────────────┐
                          │ random choice   │
                          │of the optical path│
                          └─────────────────┘
                                   │
                          ┌─────────────────┐
                          │ Calculation of  │
                          │ the impact point│
                          └─────────────────┘
```

Goes through the limit   *Impact in medium*   *Goes through an interface*

┌─────────────────┐   ┌─────────────────┐   ┌─────────────────┐
│ random choice of the │   │ Position at the interface │
│ encountered element │
└─────────────────┘

Reflexion   *Leakage*

┌─────────────────┐
│ random choice   │
│ of the interaction │
└─────────────────┘

non isotropic   *isotropic*

| Calculation of the direction | random choice of the direction |

Absorption   *Scattering*

Inelastic   *Elastic*

┌─────────────────┐
│ **END OF THE HISTORY** │
└─────────────────┘

| random choice of the excitaion energy | random choice of the direction |

┌─────────────────┐
│ Calculation of the energy │
└─────────────────┘

Figure 2.2: *History of a neutron simulated by a Monte Carlo method.*

Chapter 3

Validation of the applied procedures

As already said, the present work is based on the use of MCNPX, a code which is still under development in the moment. Therefore, before making any simulation of specific problems with this code, it is necessary to validate its use. As MCNPX becomes the international standard code for this area of applications, several validation tests were done by other groups and some other are still in progress in many research teams. Nevertheless we have performed our own validation investigations. Special emphasis was devoted to the generation of reaction products which is the main issue of this study. Our validation tests as well as most of the international tests presented previously are made in the scope of the BETA-testing of MCNPX. Some of our validation investigations will be presented in the following sections.

3.1   Estimation of the neutron production

One of the important parameters of a spallation target is the neutron production per proton. Therefore we wanted to test MCNPX abilities for the prediction of the neutron production in an irradiated target. For this purpose, we based our study on recent experimental data of spallation neutron production measurements [37]. We considered a cylindrical target of 10.2 cm radius and 61 cm thickness made of natural lead. This target was irradiated by a beam of protons on its axis. The energy of the beam varied between 0.3167 GeV and 1.47 GeV. A schematic representation of the experiment, taken from [37] is given in fig. 3.1. The results of the experiments and code predictions are given in table 3.1 and can be seen in fig. 3.2.
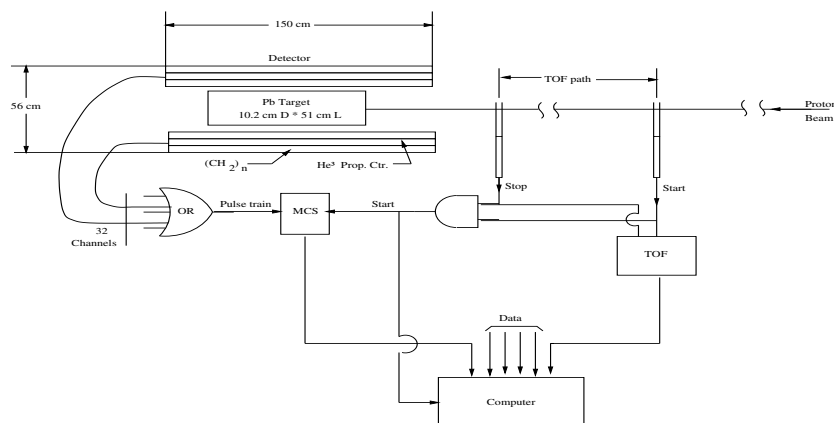
Figure 3.1: *Schematic representation of the experiment for spallation neutron measurements [37].*

Beam energy (GeV)	Experiment	MCNPX
0.3167	3.130	2.731 ± 0.008
0.5024	7.091	6.966 ± 0.021
0.54	7.960	7.959 ± 0.022
0.66	10.614	11.082 ± 0.027
0.72	11.760	12.707 ± 0.028
0.80	13.600	14.731 ± 0.029
0.8287	14.252	15.542 ± 0.030
0.96	16.640	18.819 ± 0.032
0.9899	17.288	19.546 ± 0.033
1.00	17.380	19.801 ± 0.034
1.20	22.310	24.314 ± 0.039
1.40	26.210	28.347 ± 0.043
1.47	26.400	29.665 ± 0.044

Table 3.1: (n/p) *ratio : MCNPX predictions compared with experimental data. Experimental data taken from [37].*
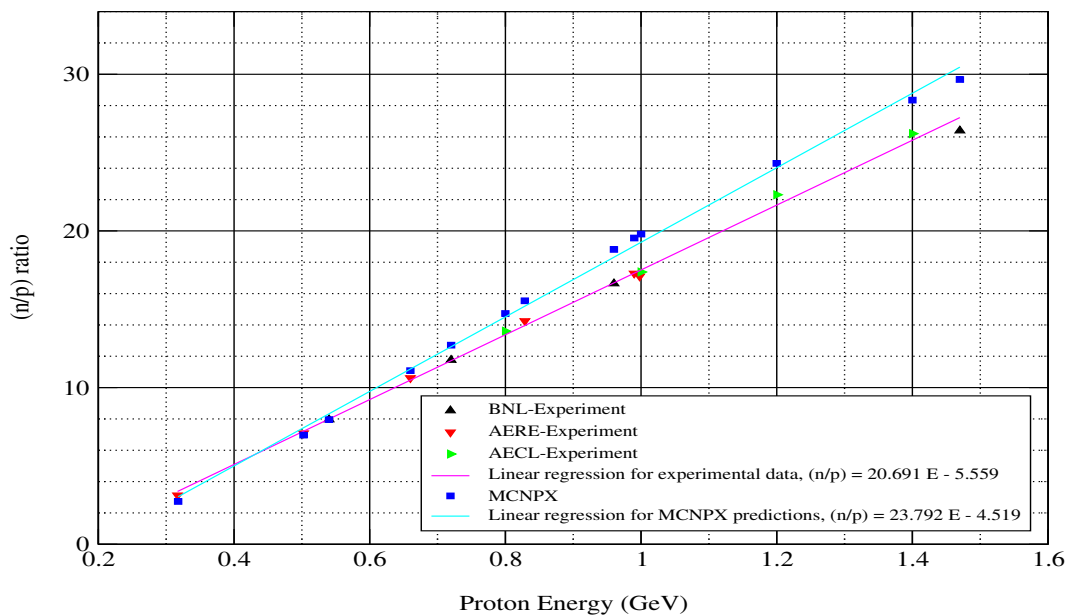
Figure 3.2: *Neutrons produced in the lead target and leaving it.*

The experimental data are coming from three experiments which were carried out for different energy ranges by different groups using different accelerators and measurement techniques. One can see that the three experimental data sets are in good agreement one with the other, one can fit these sets with the same straight line represented by $y = 20.691x - 3.181$. The correlation coefficient for this linear regression is $R^2 = 0.9986$. Therefore, one can be sure that the systematics errors made in the measurements are not significant. Uncertainties in the experimental data are about 1.3% at the 2σ level.

Spectrum of the neutrons coming out of the target

Cumulative neutron fraction as a function of the neutron energy in MeV.
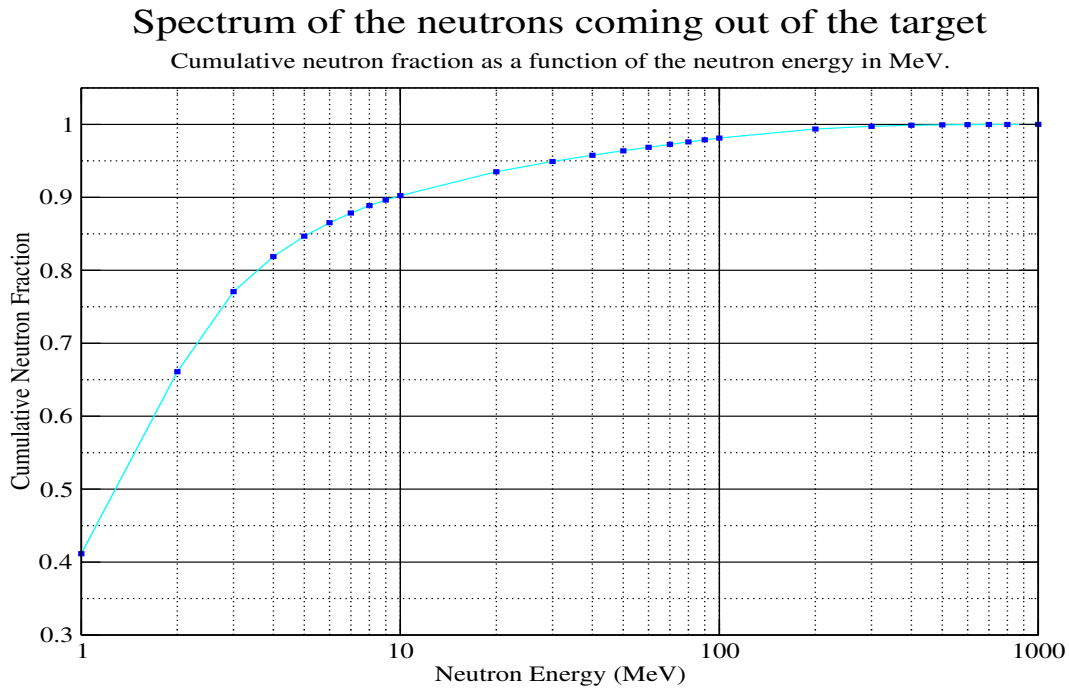
Figure 3.3: *Cumulative spectrum of the neutrons leaving the target.*

These experimental results were compared with predictions of MCNPX. For this numerical simulation, the target was supposed to be irradiated by a pencil beam of protons, the energy was varying in the range mentioned before. MCNPX was used to estimate the neutrons coming out of the target i.e going outwards through the lateral and the bottom surfaces of the target. As shown on fig. 3.2, the MCNPX data can be fit with a straight line too. In this case the equation is $y = 23.792x - 4.519$ and the correlation coefficient is $R^2 = 0.9985$. For energies larger than 0.5 GeV, the calculated (n/p) ratio is higher than the measured ratio. This discrepancy is becoming more significant with increasing energy of the proton beam. For instance at 1 GeV, MCNPX overestimates the neutron production by about 14%. Such a situation had already been observed by simulations with codes such as HETC or LAHET. The calculation of the neutron production in this target had been performed whith LAHET at the time when the experiments were carried out and LAHET was also overestimating the neutron production. To make a comparison, at 1.0 GeV LAHET predictions were also about 14% higher than the measurements.

One can suppose that the explanation for this discrepancy is that MCNPX takes into account all the neutrons encountered during the calculation. That means that there is no energy threshold below which the neutrons are not taken into account any more. On the contrary, for the experiment, one can suppose that the detectors do not detect all neutrons. Therefore, one can expect that MCNPX predicts more neutrons than the experiments.

The neutron energy spectrum was also determined and it is shown for 1 GeV protons in fig.3.3. In principle, spallation can produce neutrons with an energy up to that of the source particle, i.e 1 GeV, but one can notice in the neutron spectrum that about 94% of the neutrons have an energy smaller or equal to 20 MeV. Note that these neutrons are therefore well in the scope of MCNP. It is also to be mentioned that about 98% of the neutrons are below 100 MeV, which is only a few scatterings away from the 20 MeV range.

3.2   NEA benchmark

The evaluation of spallation products predicted with MCNPX was the most important parameter to be tested in this study. For this purpose, we made a comparison between the results given by MCNPX and by the so called Thick Target NEA benchmark. The NEA benchmark we used [36] was analysing the results of a code comparison exercise in which twelve institutions or laboratories took part. The specifications for this work were the following:

For the incident beam : a pencil beam of 800 MeV protons on the target axis.

For the target : a cylindrical target of diameter 20 cm and 60 cm length, made of lead (density $11.34g/cm^3$).

We estimated the residual nuclei production over the whole target. The running time of the calculations was set to 500 000 histories. We obtained the following results as shown in fig. 3.4.

These results are quite interesting because we see that our MCNPX results, using the Bertini model, are in good agreement with the residual nuclei production estimated by the other simulation codes. Important is also that the prediction of MCNPX agrees perfectly with the prediction made by the LANL simulation. As the LANL simulation was made by using LAHET and as MCNPX is a merged version of LAHET and MCNP, such a result was expected and it was encouraging that it could be verified by this investigation.
We also compared the prediction made by MCNPX using the three available INC models : Bertini, ISABEL and CEM. The calculation using the Bertini model was the fastest, the one with CEM lasted the longest time.

We can see in fig. 3.5 that the residual nuclei production estimated by using these models are a bit different. The predictions of the Bertini and ISABEL models are quite the same over the mass number range $A = 1$ to $A = 150$. For $A > 150$, i.e. for mass numbers close to the mass number of the target nucleus, i.e. also in the spallation area, the residual nuclei production estimated by using ISABEL is lower than the one estimated by using Bertini. We can infer that this comes from the fact that the nuclear models used to describe the spallation process are slightly different. For example the nucleus charge density is represented with eight steps in the ISABEL model but with three steps in the Bertini model. Although the predictions of CEM are in good agreement with Bertini and ISABEL in the area of the fission fragments (especially around the maximum in this zone), they are lying well below the predictions of those two models in the major part of the considered mass range. The shape of the CEM data set is close to the ones of Bertini and ISABEL, but the discrepancies between the predictions can be up to a factor of 100 for $A = 160$, CEM predictions being lower than the other ones.
At this state of the present work, it was not possible to assess which one of the three models would be best suited for evaluating the residual nuclei production in a target irradiated with a proton beam. This should be explored in more detail by making comparisons to experimental data, that will be done in the next chapter. Nevertheless, with these first model comparisons, one can point out the fact that the code predictions are very sensitive to the model chosen for describing the spallation processes. It is therefore advisable to make an experimental validation of the codes.

Spallation product yield distributions over A (whole target) after beam shutoff
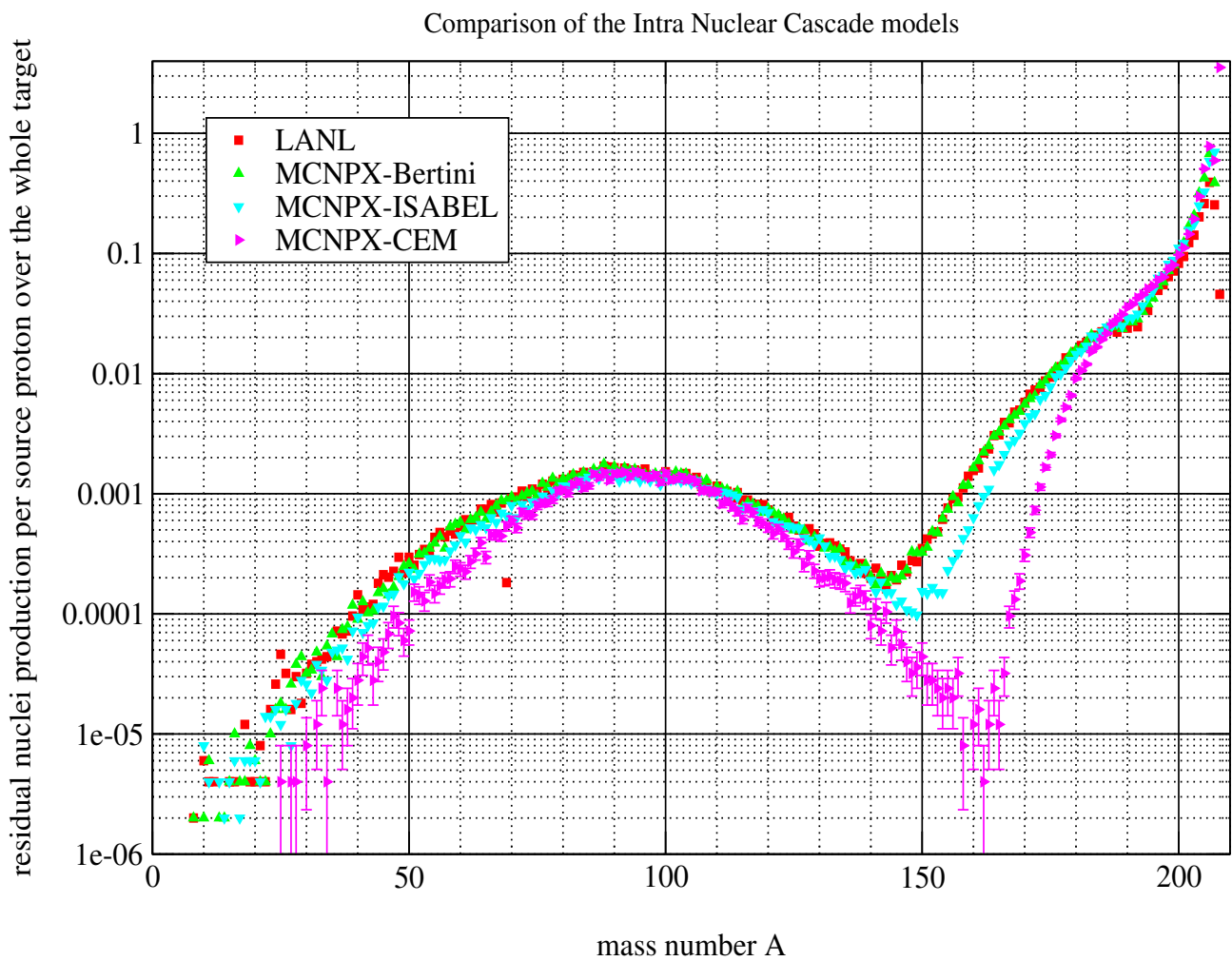
Comparison of MCNPX results with OECD thick target benchmarks (1995) for lead

Figure 3.4: *Residual nuclei production in a lead target irradiated by 800 MeV protons.*

3.3 Thick target experiments

The use of MCNPX for estimating the production of spallation products has been validated first by making code comparisons as already explained in section 3.2. The results we obtained in this validation job were good as the agreement between the codes was reasonable and gave confidence that we apply MCNPX properly. But these results did not give any proof that MCNPX is representative of what is really happening in a spallation target. Therefore it was still necessary to compare MCNPX predictions to experimental data for thick target proton irradiations.

A recent experiment on a thick lead target is related to the SAD project which is in progress in Dubna, Russia [40]. In the scope of the preparation of this project, several quantities relative to the spallation products were measured, among them the activity due to these products. In this experiment, a cylindrical Pb^{208} target, 8 cm diameter and 30.6 cm length, was irradiated by a 600 MeV proton beam. For a given spallation product, the activity due to this element was measured in the target at several distances from the target front. The preliminary experimental data have been provided to us by the research community of Cracow, Poland, one participant to the SAD project [41]. In our simulation with MCNPX, we focussed on estimating the activity due to spallation products. The results we obtained for Bi^{205} and Bi^{206} are shown respectively in fig. 3.6 and fig. 3.7.
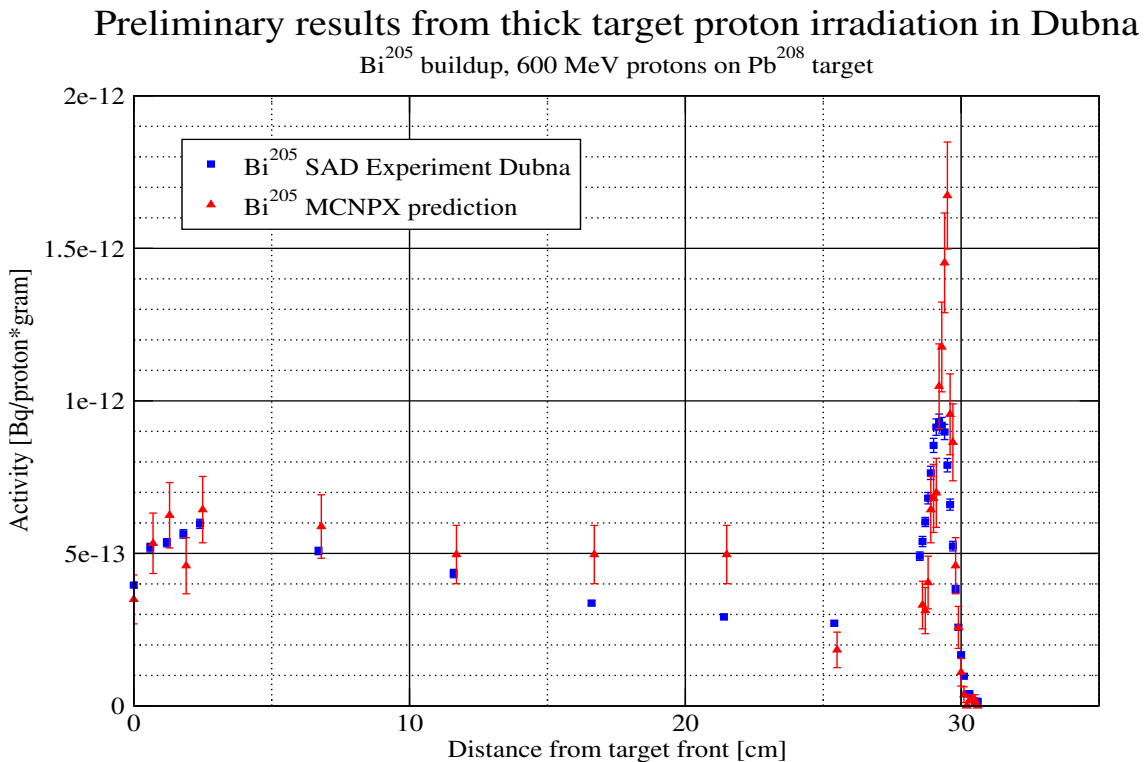
Figure 3.6: *SAD Experiment in Dubna : Activity due to Bi^{205} buildup in a Pb^{208} target irradiated by 600 MeV protons. Experimental data from the university of Cracow, Poland [41].*

Preliminary results from thick target proton irradiation in Dubna
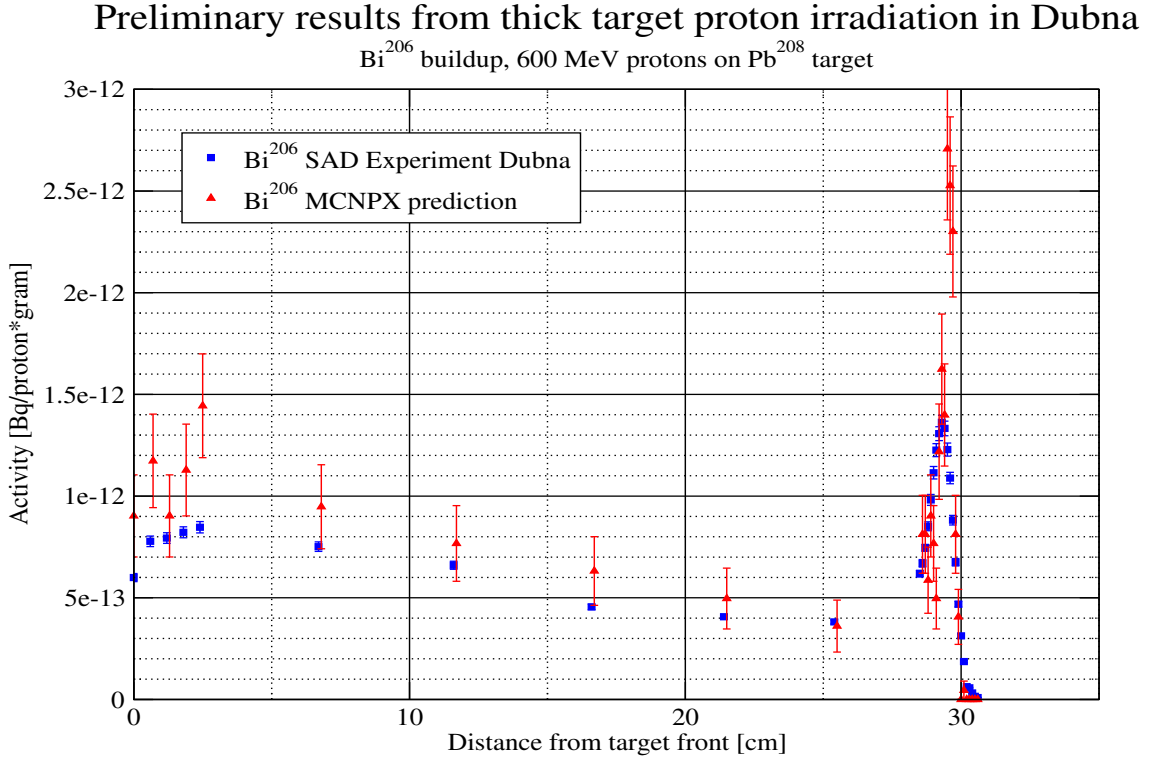
Figure 3.7: *SAD Experiment in Dubna : Activity due to Bi^{206} buildup in a Pb^{208} target irradiated by 600 MeV protons. Experimental data from the university of Cracow, Poland [41].*

To obtain our absolute results, we first calculated the number of Bi^{205} nuclei and of Bi^{206} nuclei which are produced per source proton. Then we simplified a little bit the problem in considering only the major mode of decay which is the electron capture for both isotopes. Knowing the half-life of each isotope, we could then estimate the activity due to each isotope. Per definition, the activity in Bq is the number of decays per second. As the time dependent evolution of the number of Bismuth nuclei can be written as :

$$N(t) = N_0 e^{-\lambda t}$$
$$\text{with } \lambda = \frac{ln(2)}{T_{1/2}}$$

we can determine the number of decays per second A, and we get :

$$A = N_0 - N(1sec) = N_0(1 - e^{-\frac{ln(2)}{T_{1/2(sec)}}})$$

For Bi^{205}, $T_{1/2} = 15.31$ days and for Bi^{206}, $T_{1/2} = 6.24$ days so that we get :

$$A_{Bi^{205}} = 5.240 10^{-7} N_0 \ Bq/proton$$
$$A_{Bi^{206}} = 1.286 10^{-6} N_0 \ Bq/proton$$

To obtain the activity in $Bq/proton.gram$ one has only to devide by the mass of lead.

In fig. 3.6 and fig. 3.7, one can notice the sharp peak in the activity at about 29 cm from the target front. Such a behaviour was to be expected : because of their high energy, the protons are going through the target for a while. They are stopped at a given distance from the target front (depending on their energy). This distance is their depth of penetration in lead at 600 MeV. Therefore there is a larger rate of reactions at this point, the amount of produced nuclei is larger and that is why the peak of Bi-activity stands there. One can also notice the good agreement between MCNPX prediction and the experimental data, both for the axial dependency and for the presence of the maximum at about 29 cm. At the maximum, we can notice on both figures that the experimental data are well below MCNPX predictions (about a factor 2). This is in contrast to the results of LAHET reported in [41]. The reason for this discrepancy between MCNPX and LAHET has to be analysed in more detail.

3.4   Thin target experiments

As we have seen in sections 3.2 and 3.3, MCNPX simulates the chains of spallation processes occuring in thick targets quite good. It allows to predict spallation yields in reasonable agreement with other codes and also with experimental results. Another experimental property of spallation processes is the isotopic spallation cross section. From an experimental point of view, the measurement of spallation cross sections is realised by carrying out irradiation experiments on thin targets. Using a thin target allows indeed to consider only the first spallation reaction i.e only the reaction initiated by the source particle.

Such an experiment has been recently carried out at GSI Darmstadt, Germany, for $Pb^{208} + 1 GeV p$ reactions [38]. The isotopic production cross-sections were measured for all elements from $Z = 22$ (Titanium) to $Z = 82$ (Lead) using the inverse-kinematics reaction : 1 GeV Pb^{208} were hitting a liquid-hydrogen target. The primary beam of Pb^{208} was delivered by the heavy-ion synchrotron SIS. The reaction products were separated and identified by the fragment separator FRS. A simplified drawing of the experiment is shown in fig. 3.8. In this experiment, the beam monitor was used to measure the proton beam intensity, the two scintillators to measure horizontal positions and time of flight. The MUSIC detector was used to measure the nuclear charge of elements from titanium to gadolinium, for elements heavier than gadolinium the degrader was used [38].
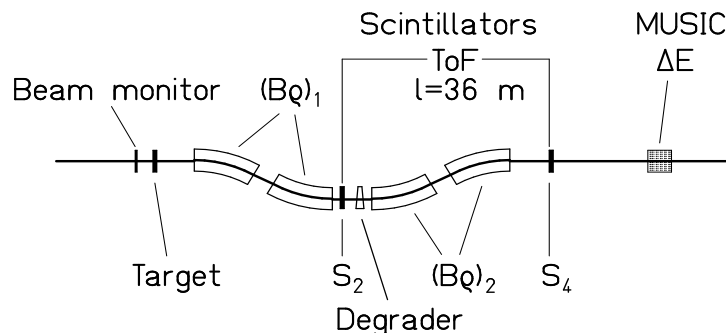
Figure 3.8: *Schematic drawing of the fragment separator FRS with the detector equipment taken from [38].*

The experiment carried out at GSI was simulated with MNCPX using the three available models, Bertini, ISABEL and CEM. It was also simulated with LAHET using Bertini and ISABEL models. In addition, this experiment was simulated with the Cugnon code (INCL4) kindly provided by the team of J. Cugnon, University of Liège, Belgium [39]. The results of the different simulations can be seen in fig. 3.9 to fig. 3.13 for mass yields in mb according to mass number and in fig. 3.14 to fig. 3.16 for mass yields in mb according to charge number. In these pictures, we have also given the experimental results obtained in a framework of ISTC, Russia, (project ISTC839) for the same experiment done for the direct-kinematics reaction. The direct-kinematics reaction is much more difficult to carry out, therefore isotopic cross-sections could only be measured for fewer elements in this work.
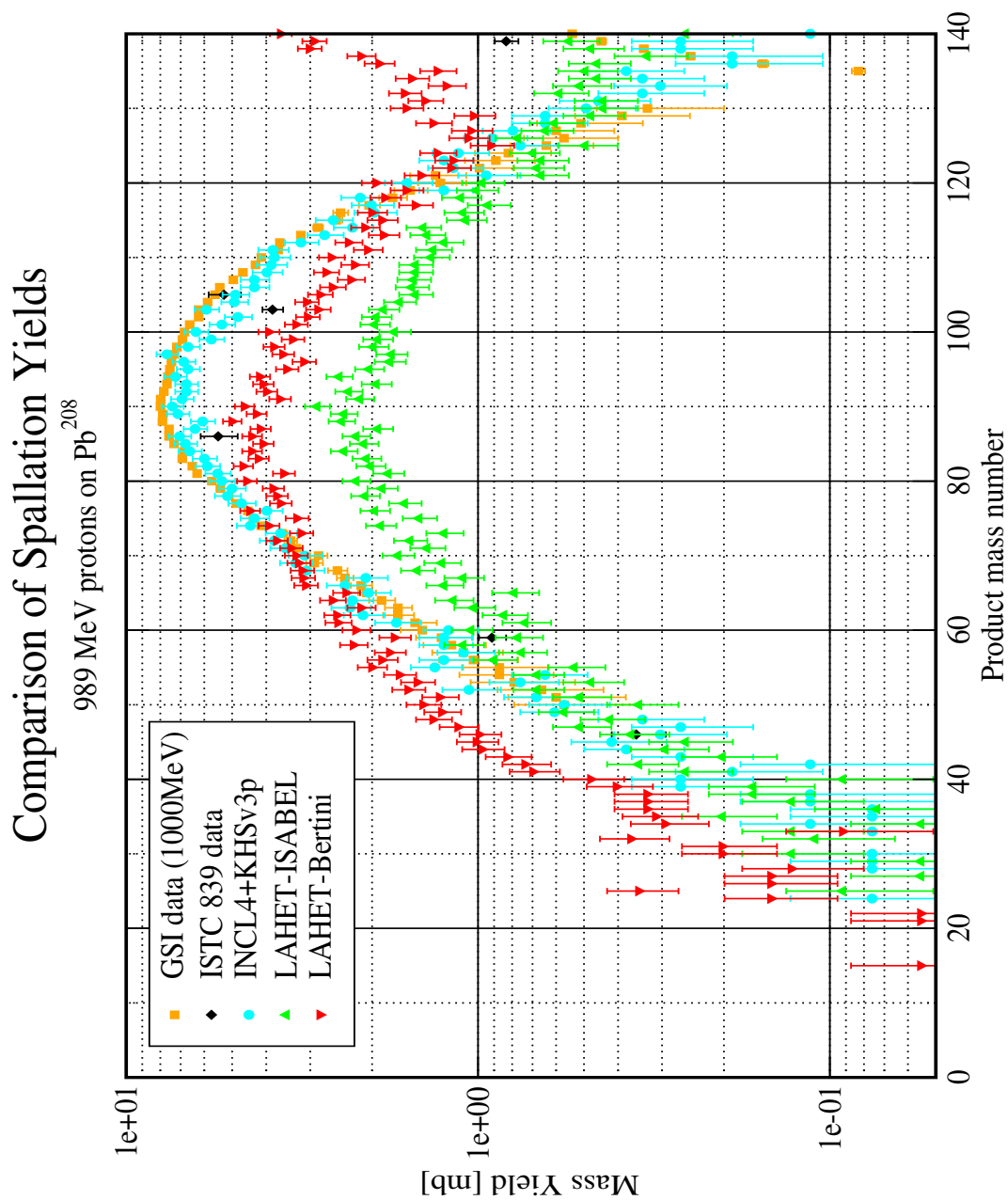
Figure 3.9: *Comparison of experimental spallation yields (ISTC, GSI) and Code computed spallation yields (INCL4, LAHET-Bertini, LAHET-ISABEL). Mass yields in millibarns (mb) according to mass number A for A < 140. GSI experimental data taken from [38].*
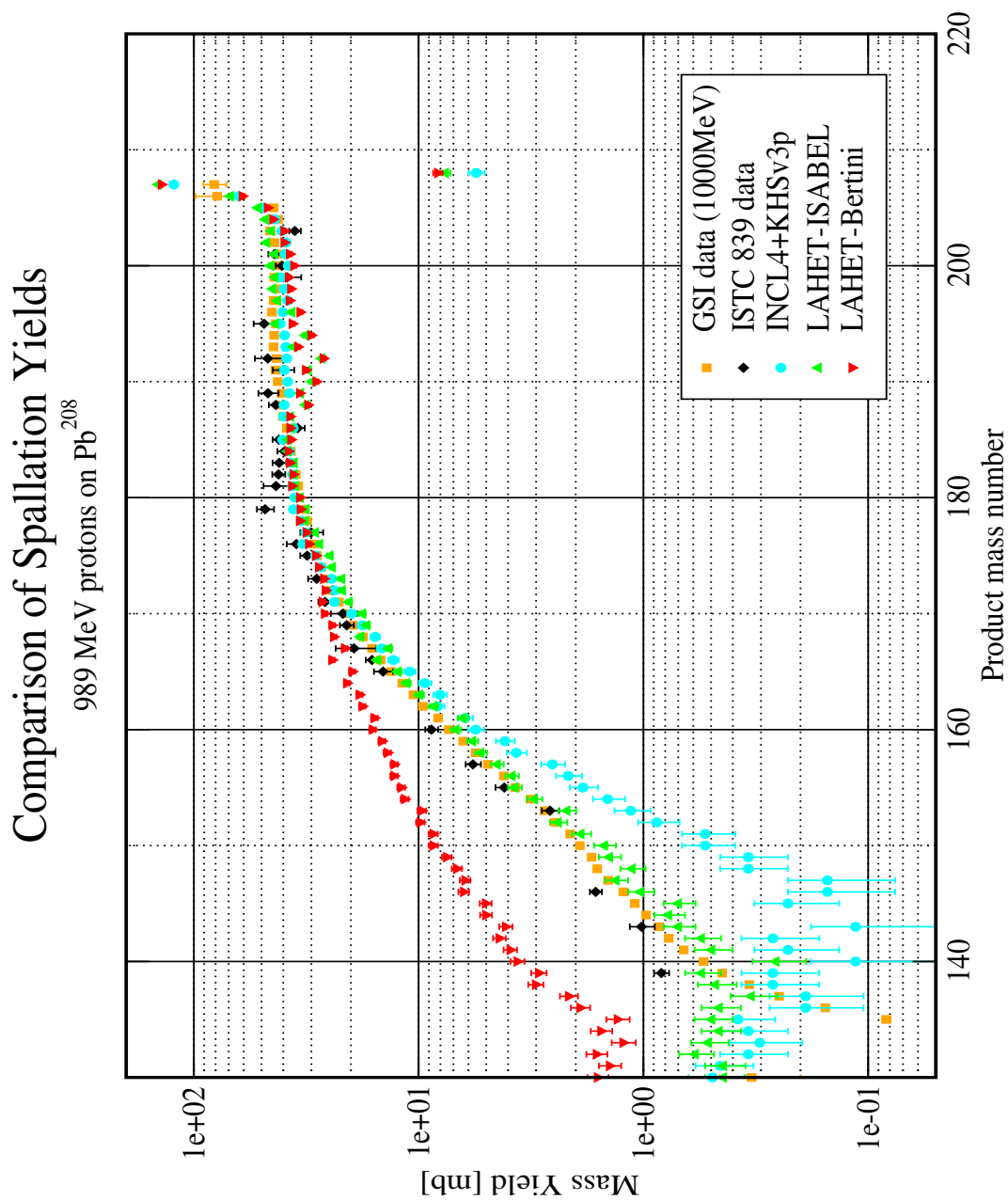
Figure 3.10: *Comparison of experimental spallation yields (ISTC, GSI) and Code computed spallation yields (INCL4, LAHET-Bertini, LAHET-ISABEL). Mass yields in millibarns (mb) according to mass number A for A > 140. GSI experimental data taken from [38].*
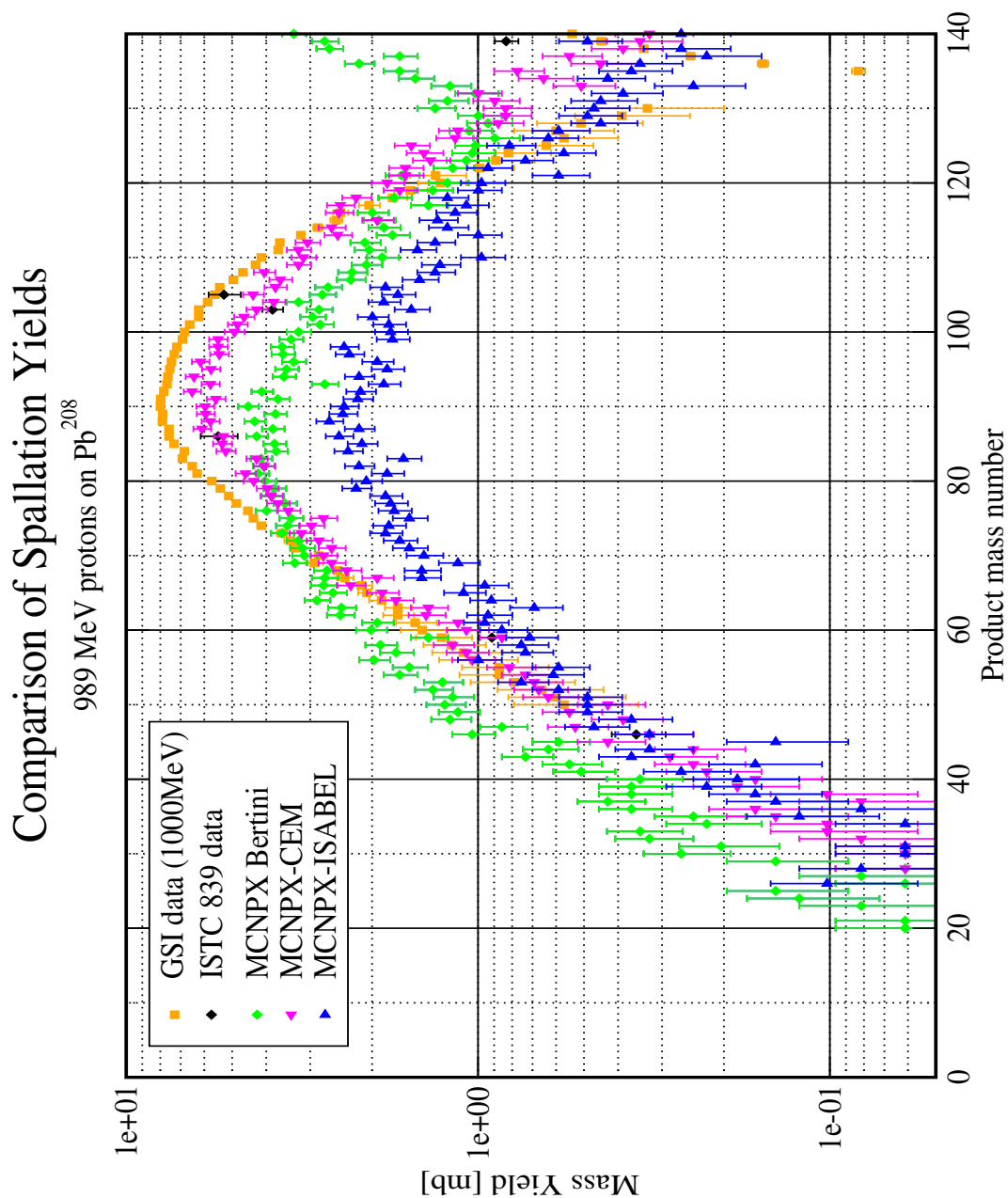
Figure 3.11: *Comparison of experimental spallation yields (ISTC, GSI) and Code computed spallation yields (MCNPX-Bertini, MCNPX-ISABEL, MCNPX-CEM). Mass yields in millibarns (mb) according to mass number A for A < 140. GSI experimental data taken from [38].*
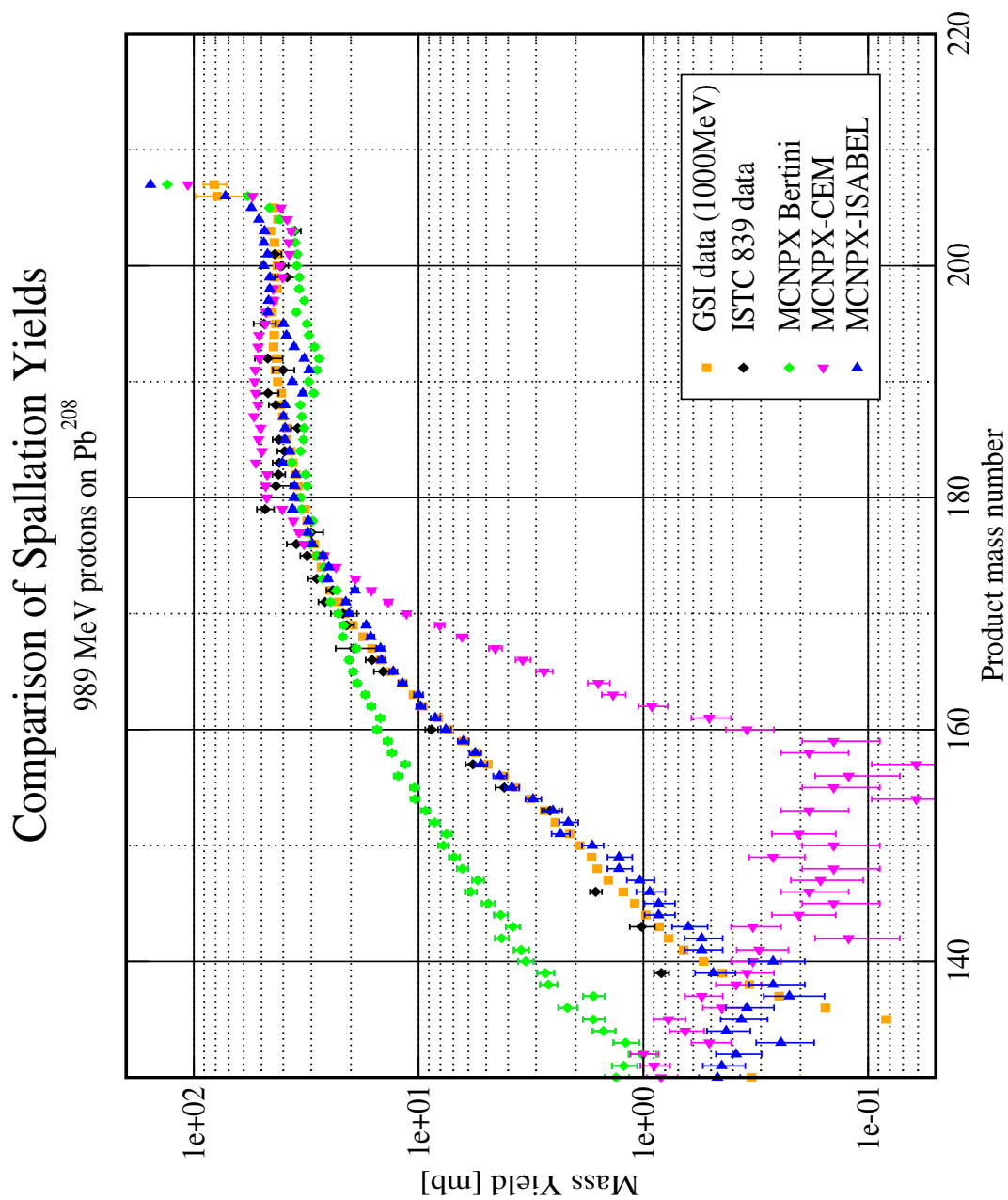
Figure 3.12: *Comparison of experimental spallation yields (ISTC, GSI) and Code computed spallation yields (MCNPX-Bertini, MCNPX-ISABEL, MCNPX-CEM). Mass yields in millibarns (mb) according to mass number A for A > 140. GSI experimental data taken from [38].*
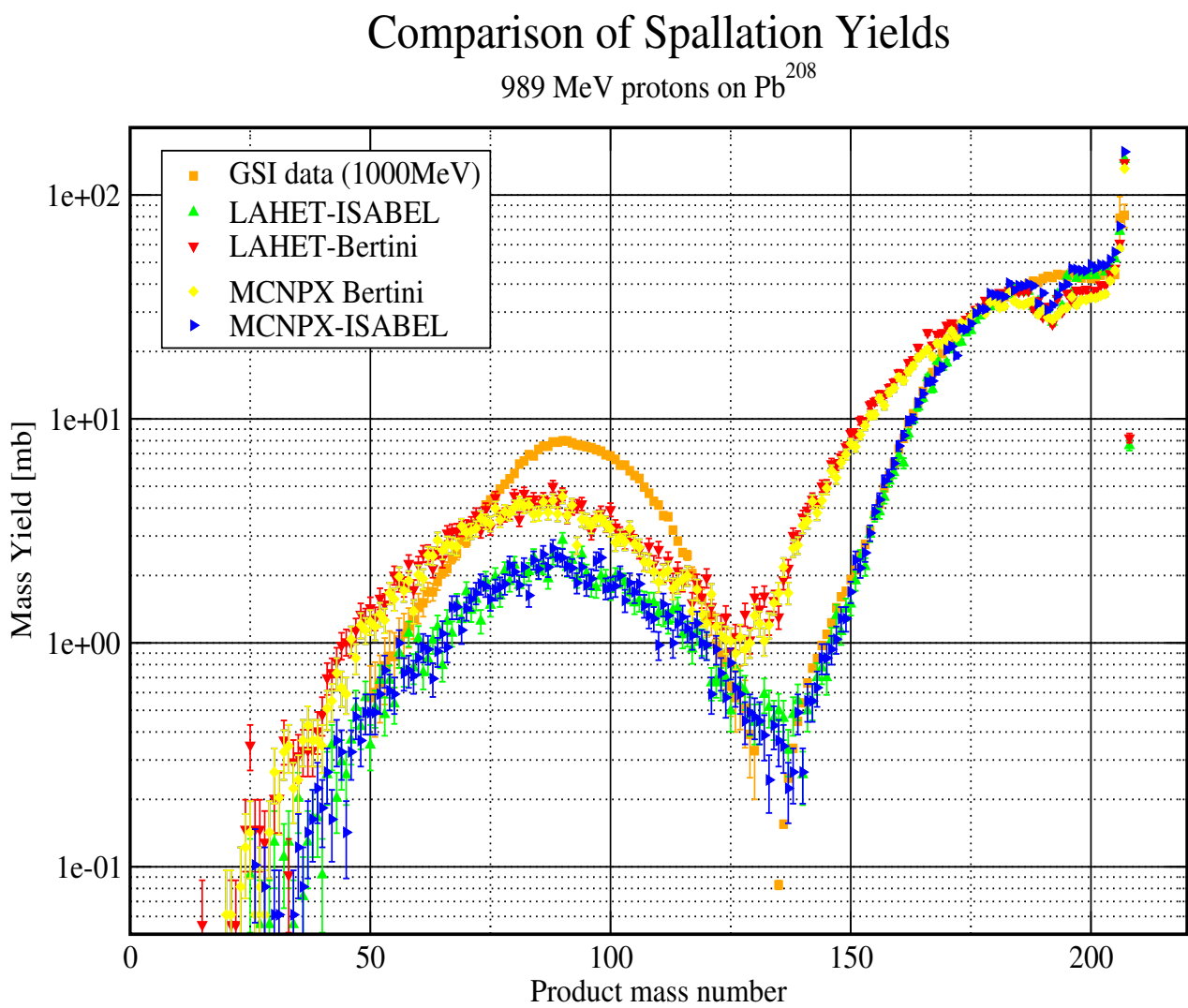
Figure 3.13: *Comparison of LAHET and MCNPX computed spallation yields. Mass yields in millibarns (mb) according to mass number A. GSI experimental data taken from [38].*
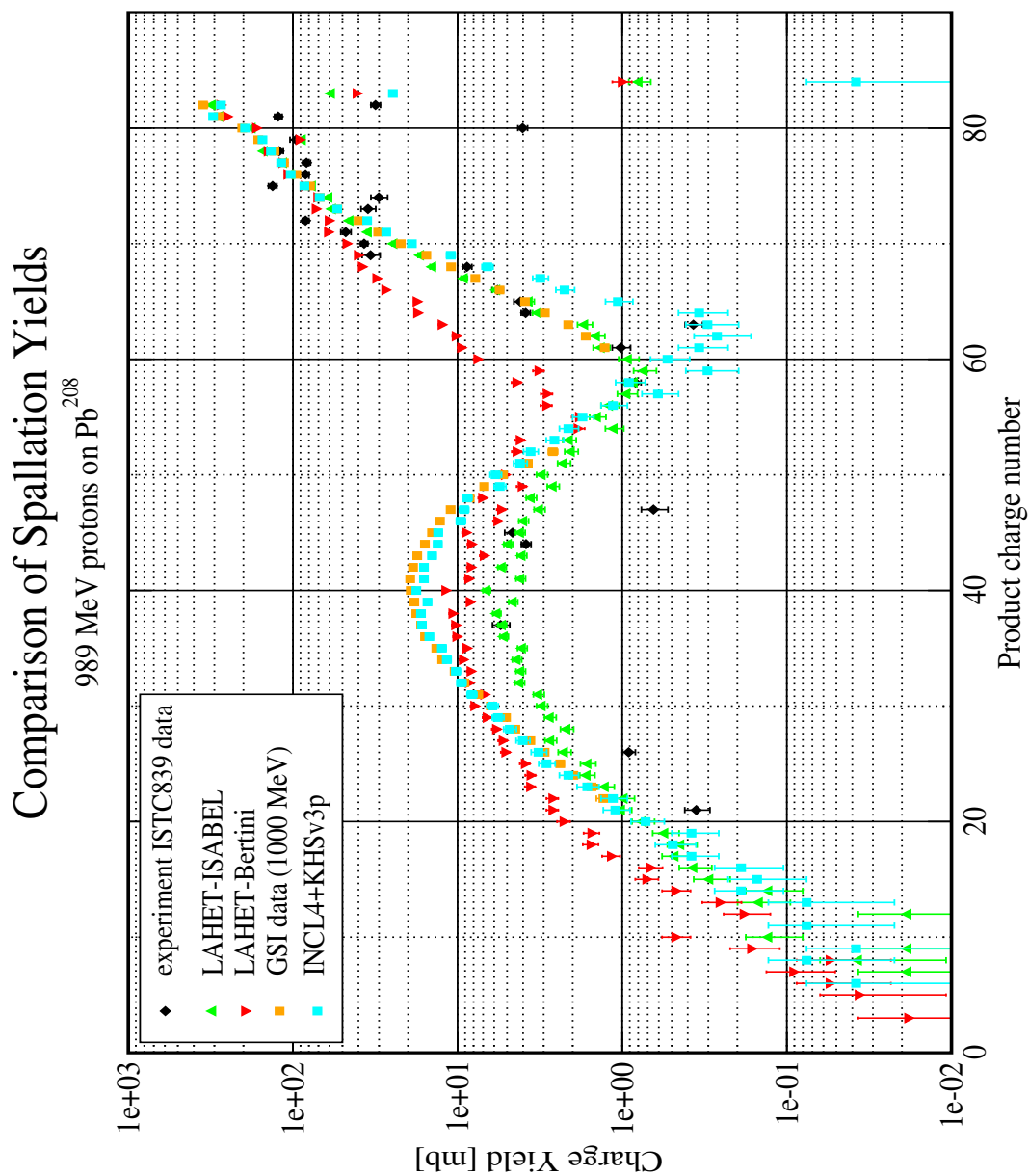
Figure 3.14: *Comparison of experimental spallation yields (ISTC, GSI) and Code computed spallation yields (INCL4, LAHET-Bertini, LAHET-ISABEL). Mass yields in millibarns (mb) according to charge number Z. GSI experimental data taken from [38].*
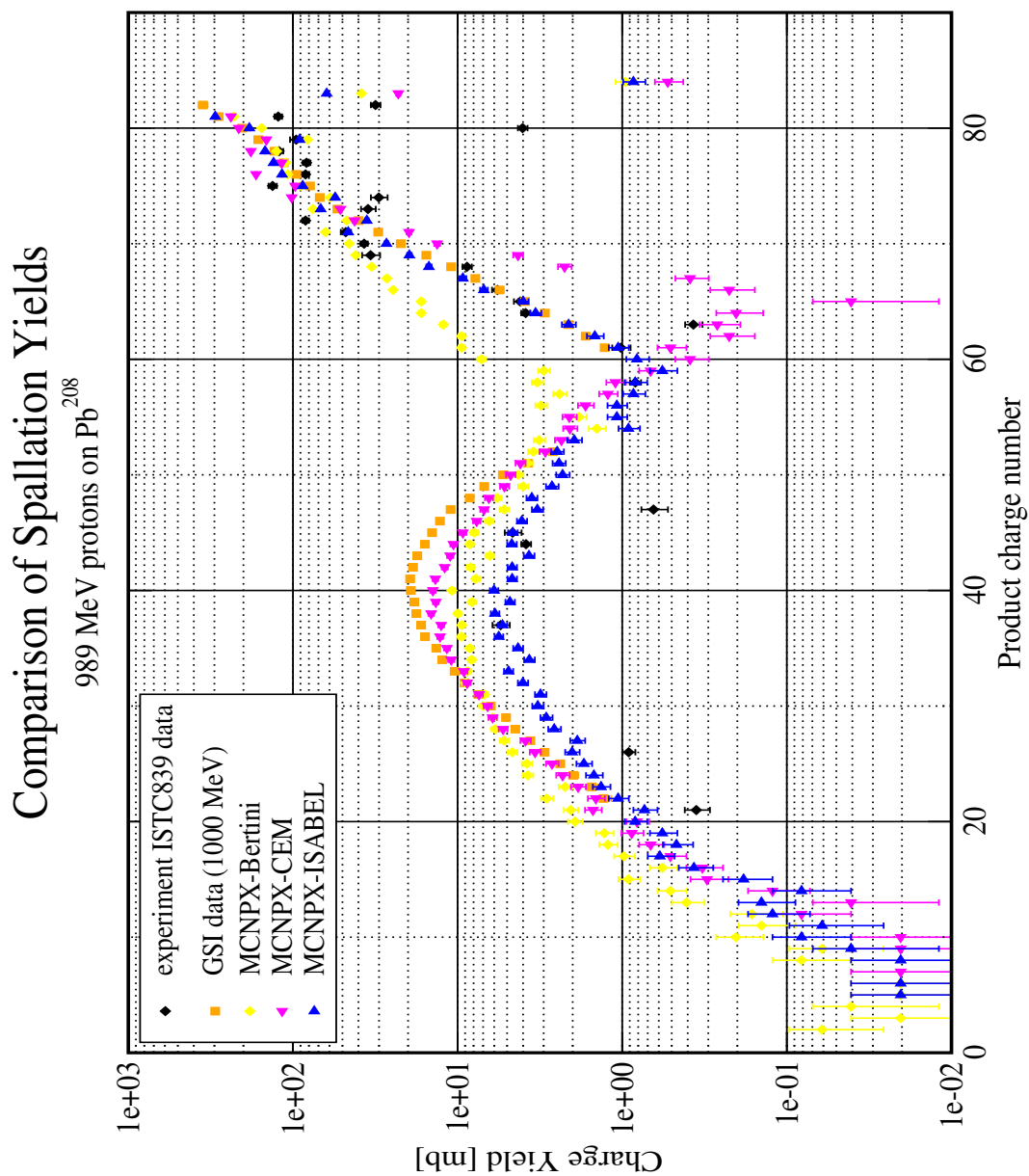
Figure 3.15: *Comparison of experimental spallation yields (ISTC, GSI) and Code computed spallation yields (MCNPX-Bertini, MCNPX-ISABEL, MCNPX-CEM). Mass yields in millibarns (mb) according to charge number Z. GSI experimental data taken from [38].*
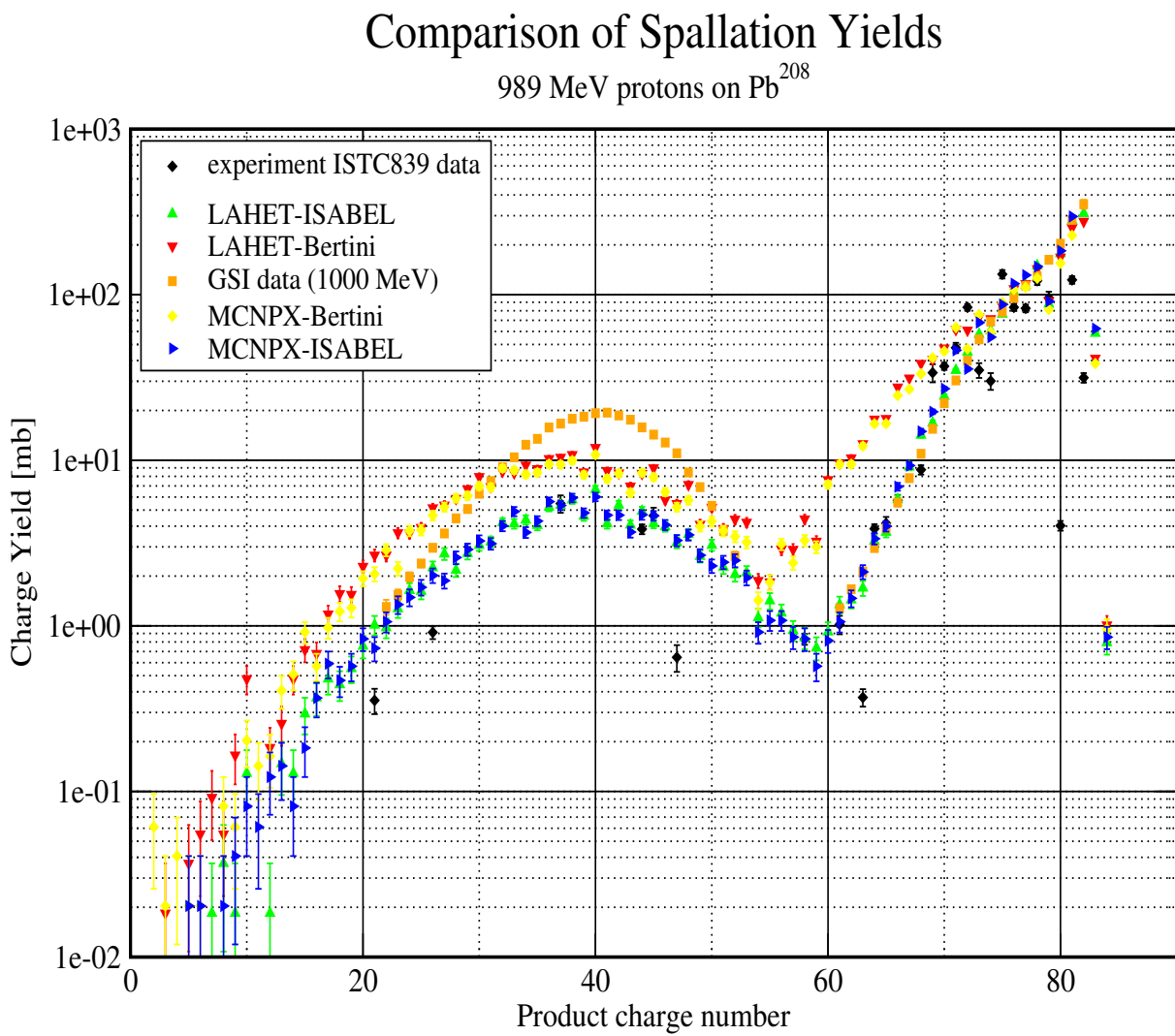
Figure 3.16: *Comparison of LAHET and MCNPX computed spallation yields. Mass yields in millibarns (mb) according to charge number Z. GSI experimental data taken from [38].*

In these figures, one can notice that the predictions of the different codes agree more or less with the experimental data depending on the model used and on the range of the mass number of the products (fission range until $A \simeq 130$, spallation range above $A \simeq 130$).

First of all, a good thing is that, for a given model i.e. Bertini or ISABEL, MCNPX predictions agree perfectly with LAHET predictions. We had already observed such a behaviour in the code comparison in section 3.2.

Second good thing is that the shape of the predicted results is quite the same as the shape of the experimental data : one can allways distinguish two regions in the plots at each side of a local minimum which is at about $A = 130$. On the left side of the minimum is the fission area, on the right is the spallation area.

Let us consider now more precisely the predictions of MCNPX. One notices immediately that the Bertini model does not suit very well for estimating spallation cross-sections. There is a discrepancy between MCNPX-Bertini and the experimental data almost over the whole range of the considered mass numbers. This discrepancy can be up to a factor two or three. In the fission area, MCNPX-Bertini underestimates the cross-section whereas it overestimates them in the spallation area.

MCNPX-ISABEL seems to be more efficient for predicting production cross-sections. The results obtained with the ISABEL model are in very good agreement with experimental data for mass number $A > 130$. Nevertheless, for $A < 130$, MCNPX-ISABEL underestimates much more the cross-sections than MCNPX-Bertini did, the discrepancy with the experimental data can be up to a factor six or seven.

Just as MCNPX-ISABEL, MCNPX-CEM seems to be more adapted than MCNPX-Bertini. The results obtained with the CEM model are in good agreement with the experiments for $A < 130$. Nevertheless, for $A > 130$, MCNPX-CEM underestimates significantly the production cross-sections, for $A > 180$ there is reasonable agreement between the experiments and the CEM model.

A good solution for estimating isotopic production cross-sections with the present models available in MNCPX would then be to run two MCNPX jobs, one with ISABEL, one with CEM. The corresponding results are crossing at about $A = 130$. One would then have to take the CEM predictions below this point and the ISABEL predictions above it.

The "best" code among the ones we have tested to compute the production cross-sections is certainly the Cugnon-Code in its fourth version INCL4, combined with the K.-H. Schmidt evaporation model. Its agreement with the experimental data is very good over the whole mass number range unless for $130 \leq A \leq 155$ where it slightly underestimates the cross-sections. More informations about INCL4 can be found in [26].

We also estimated the production cross-section of several isotopes of given elements such as Zn, Sn, Hg. Why we have focussed on these three elements is explained in chapter 4. The computed cross-sections for mercury isotopes, with mass number between 180 and 205, are compared to the experimental data from GSI in fig. 3.17. We can notice that the computed data are quite in good agreement with the experimental data. The shape of the experimental curve is very well reproduced by MCNPX, although MCNPX slightly underestimates the production cross-sections for mass numbers lower than 190. For mass numbers above 190, the agreement is very good : the discrepancy between calculated and experimental data is less than 5 %.
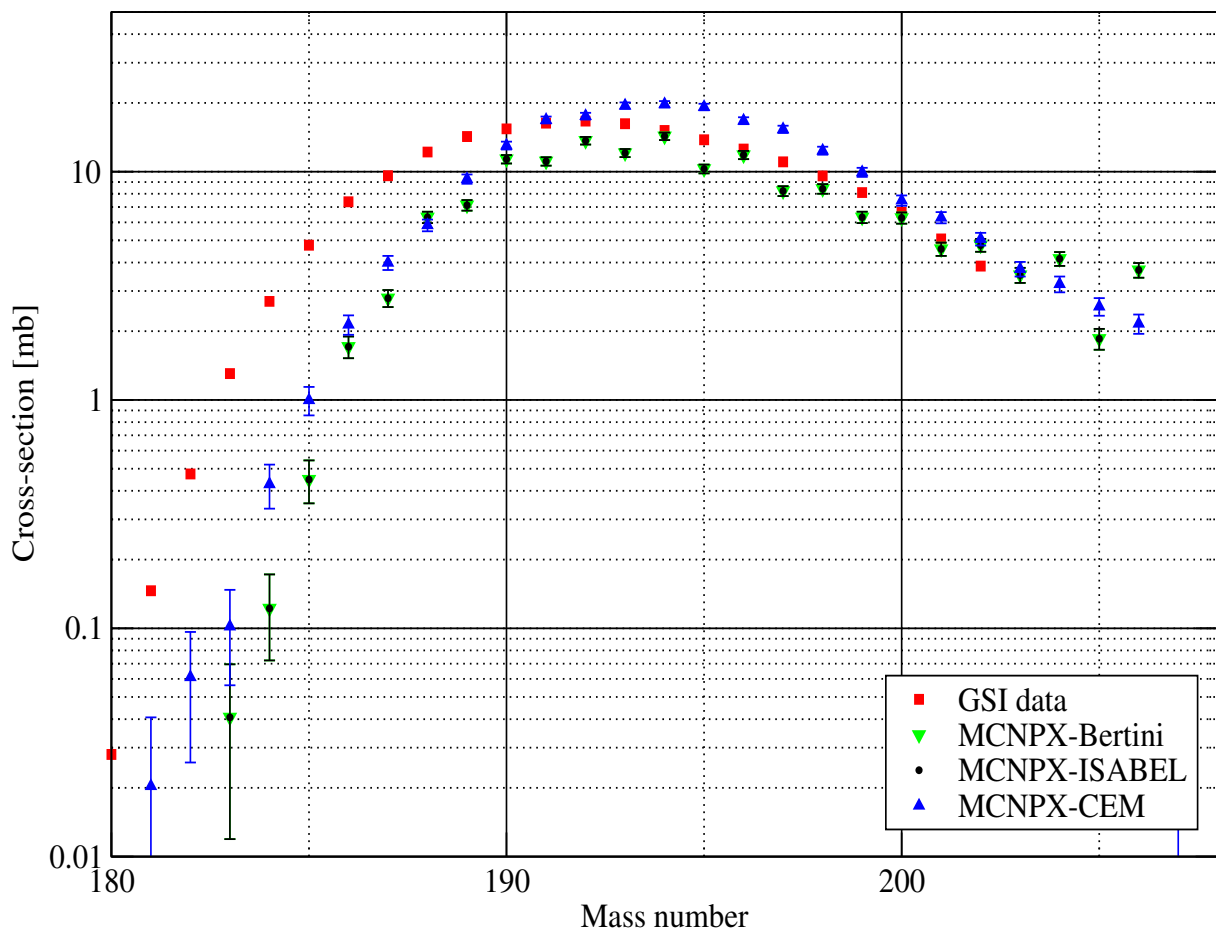
Figure 3.17: *MCNPX computed production cross sections for Hg compared to experimental data from GSI [38].*

Chapter 4

MEGAPIE

MEGAPIE is a joint initiative from European research institutions (among them PSI, FZK, CEA, CNRS, ENEA) and the Japanese institution JAERI. The aim of the MEGAPIE project is to design and to operate a liquid PbBi spallation target for the 1MW proton beam available in the SINQ facility at PSI. A simplified representation of the SINQ facility is given in fig. 4.1.
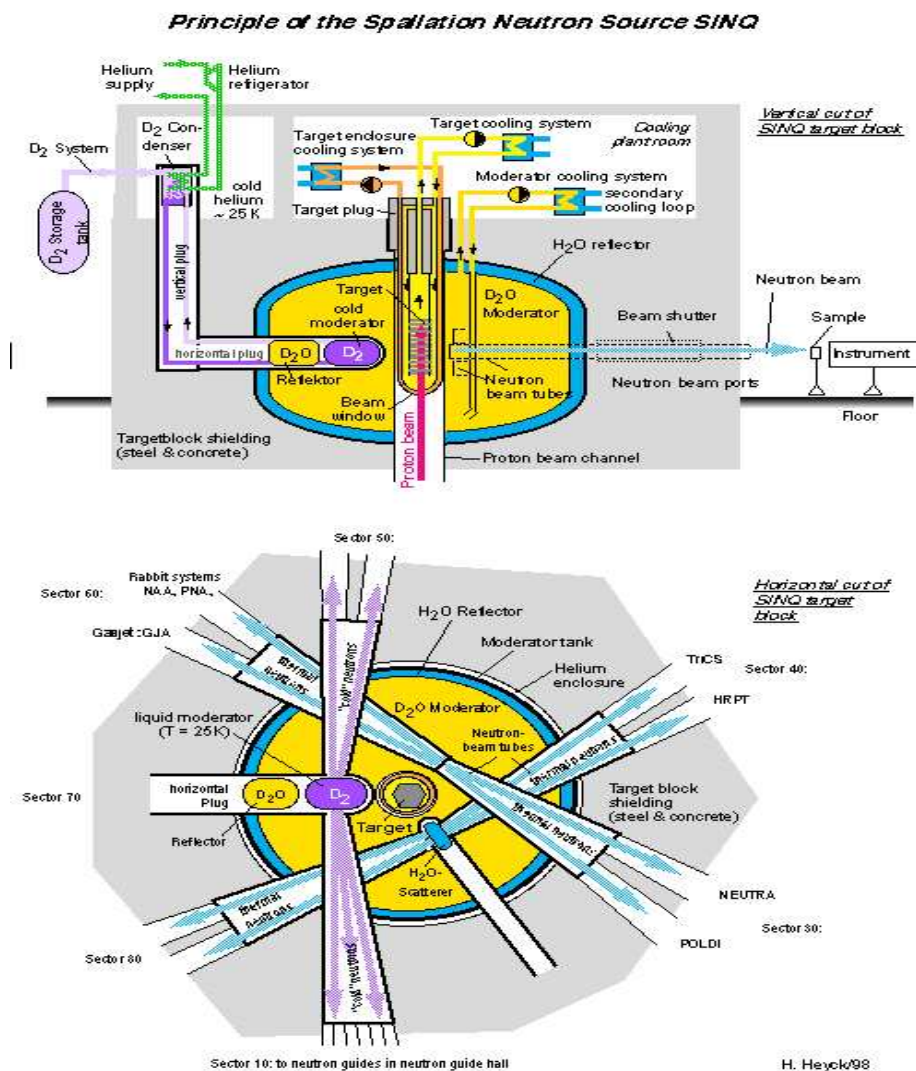
Figure 4.1: *SINQ spallation source. Picture taken from [45].*

The MEGAPIE project started in the year 2000 with the aim of installing a LBE (Lead-Bismuth Eutectic) target in the SINQ facility in the year 2004. At present the project is progressing well with small time delay. A final design of the target has already been proposed, see fig. 4.2.
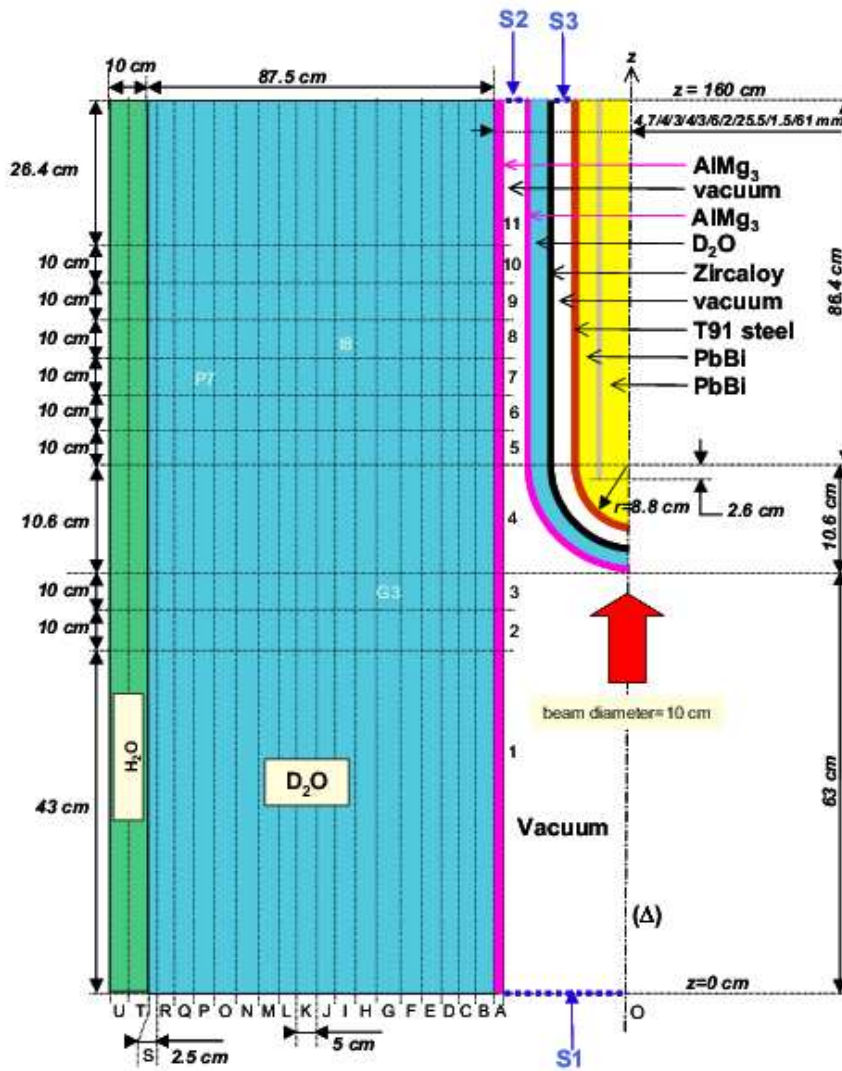
Figure 4.2: *Schematic representation of the MEGAPIE target surrounded by a water tank. Picture taken from [46].*

The MEGAPIE target will be designed and conceived so that contamination of the accessible areas in SINQ is not likely to happen under any imaginable condition. The target will stay for one complete year of experiments in the SINQ facility. There it will be irradiated by a 1 MW proton beam at a proton energy of 575 MeV and a total proton current of 1.74 mA [1, 46]. The neutrons which will be produced in the target will be slowed down in the heavy water tank and then used for experiments as shown on fig. 4.1.

4.1 Estimation of the prompt spallation source

To estimate the prompt spallation source, we performed simulations based on MEGAPIE neutronic benchmarks [46]. The configuration we had to simulate is shown on fig. 4.2. The estimated characteristics of the incoming proton beam are the following [46]:

- **Incident proton energy :** 575 MeV

- **Total beam power :** 1 MW

- **Total beam current :** 1.74 mA

- **Radial distribution of proton current density :** $i(r) = I_0.exp\left(-\dfrac{\frac{1}{2}\cdot\frac{r^2}{\sigma^2}}{2\pi\sigma^2(1-e^{-\frac{c^2}{2}})}\right)$

  $i(r) =$ radial current density
  $I_0 = 1.74\ mA$
  $r =$ radius from the centre of symmetry axis in cm
  $\sigma = 2.5\ cm$
  $c = 2$
  gaussian profile truncated at $c.\sigma = 5.0\ cm$

We performed the calculation whith MCNPX and HTAPE3X and we obtained the following results for the prompt spallation source as shown on fig. 4.3 and fig. 4.4.

In these two figures, one recognizes the typical shape of the curves with some discrepancies between the predictions of the three models, as we could already notice it during our investigations related to the validation of the code. From these results concerning the spallation source in the target, we could study more precisely the behaviour of specific nuclides as explained in the next section. In particular, the predicted nuclei production in the target was the basis for the work we carried out on elements responsible for the target contamination.
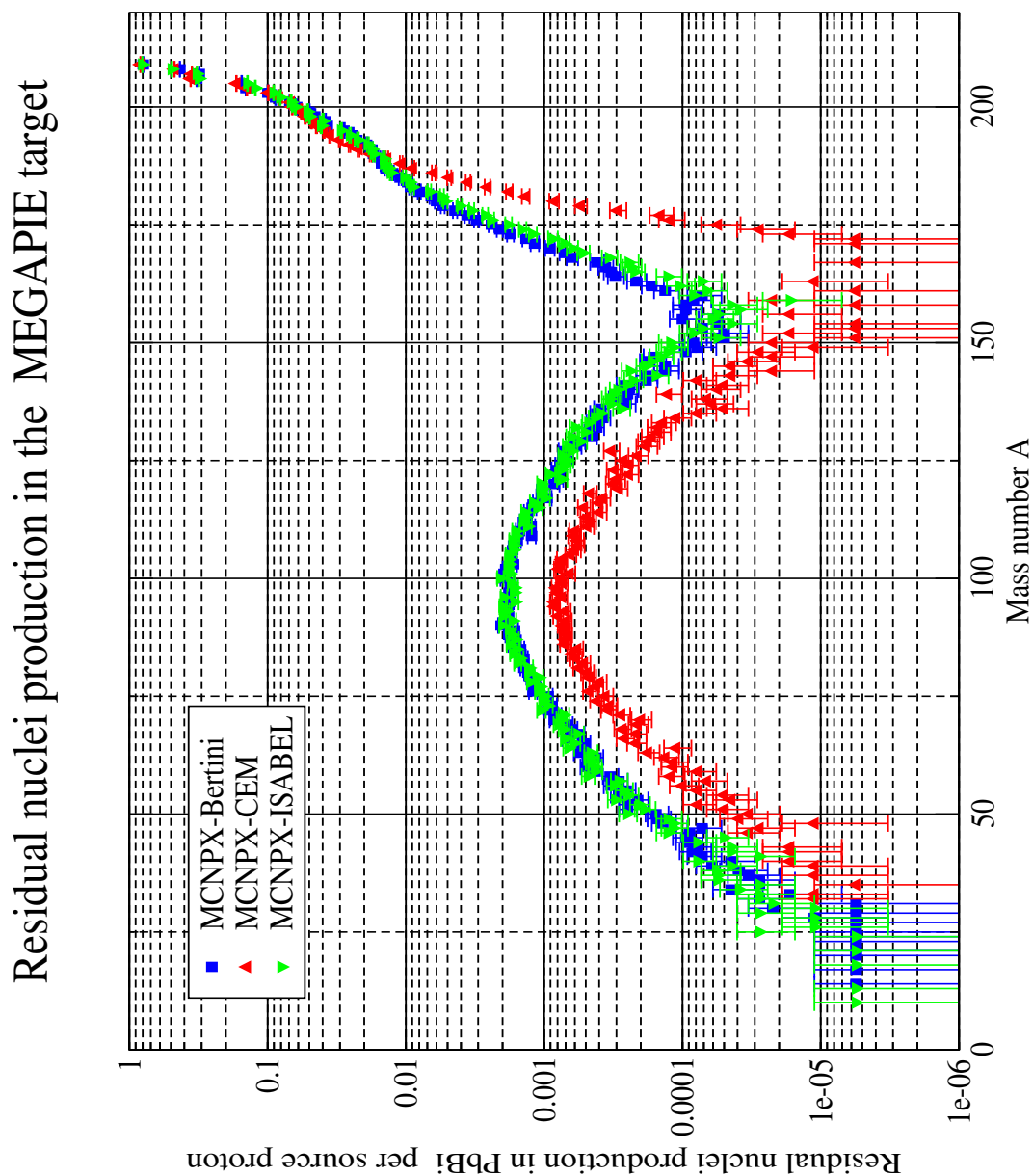
Figure 4.3: *Estimation of the prompt spallation source in the MEGAPIE target irradiated by the 575 MEV proton beam of the SINQ facility. Residual nuclei production according to mass number A. Target specifications taken from [46].*
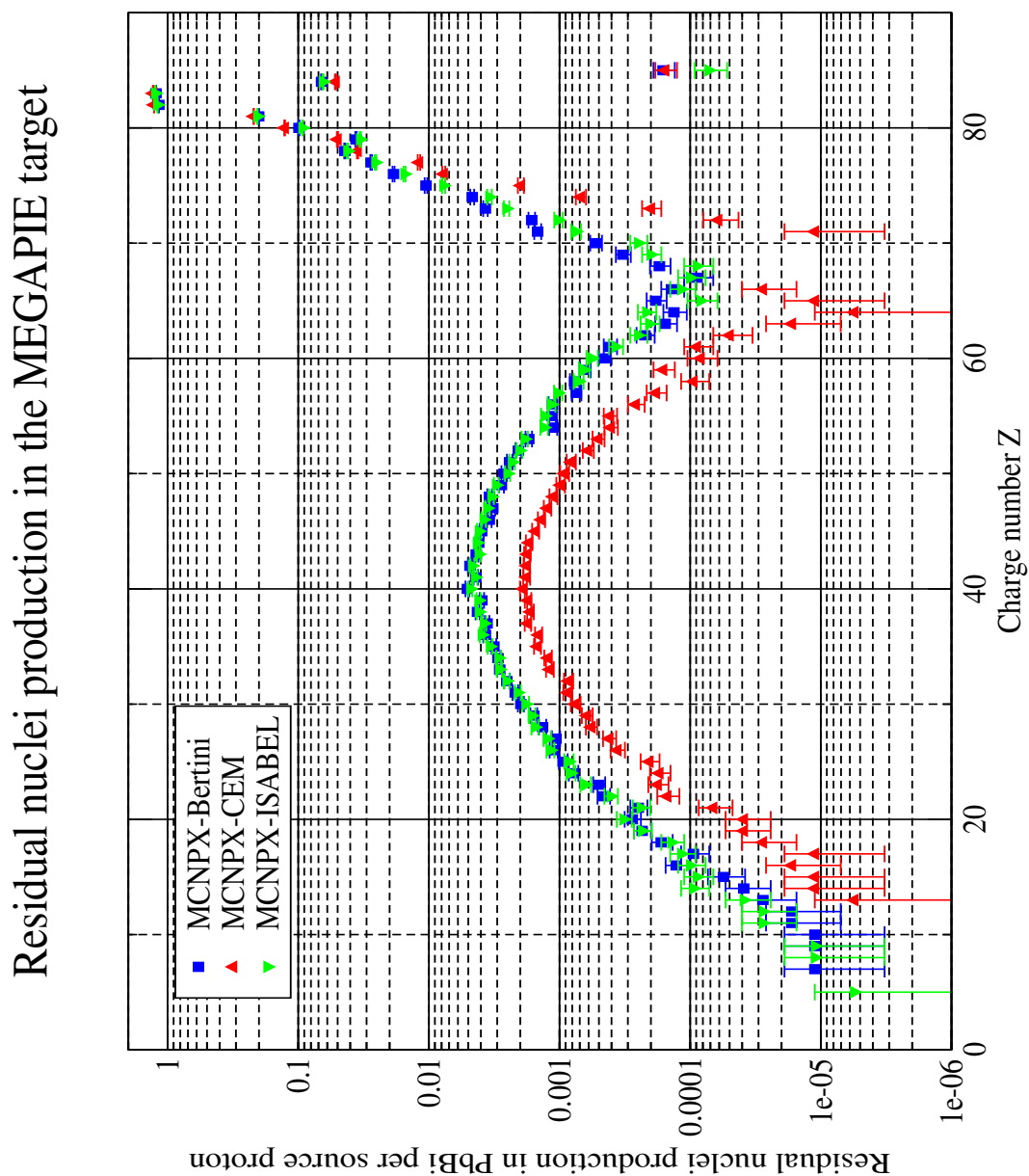
Figure 4.4: *Estimation of the prompt spallation source in the MEGAPIE target irradiated by the 575 MEV proton beam of the SINQ facility. Residual nuclei production according to charge number Z. Target specifications taken from [46].*

4.2   Time dependent behaviour

4.2.1   Depletion calculations : use of ORIHET3

The MEGAPIE target which will be used in the SINQ facility must be taken out after the spallation experiments, so that other experiments can be started very rapidly afterwards. Thus it is quite important to know the state of the MEGAPIE target after given times of irradiation and cooling. In other words, one should have a precise idea of the time dependent behaviour of the target radioactivity. For safety reasons, for target maintenance or handling, one should be able to predict the amount of "dangerous" isotopes which will have been created after a given time. Interesting isotopes are for instance Polonium 210 which is an alpha-emitter or Zn, Sn, and Hg which can probably damage the target material by causing chemical reactions.

To estimate this time dependent behaviour, we could use the ORIHET3 code which was kindly provided to us by Dr. F. Atchinson of PSI Villingen [42]. ORIHET3 is an adaptation of ORIGEN (Oak Ridge Isotope GENeration code). Knowing the nuclide production rates and the nuclide concentrations in the target, we may study the build-up and the decay of the activity in the target. In order to calculate the build-up and the decay of activity, ORIHET3 solves the Bateman equations (Eq. 4.1) for the concentrations of the nuclides.

$$\frac{dN_i}{dt} = -\tau_i N_i + \sum_k f_{ik}\tau_k N_k + B_i, \quad i = 1...N \tag{4.1}$$

where N_i is the concentration, τ_i the decay constant, f_{ik} the branching ratio for the nuclides k that have nuclides of species i as a direct decay product. B_i are the production rates for nuclides of species i.

For solving these equations, the so called *matrix exponential method* realised in three routines (called EQUIL, DECAY and TERM) taken from ORIGEN are used. One can write the N coupled differential equations of eq. 4.1 as :

$$\left[\frac{dN}{dt}\right] = [A][N] + [B] \tag{4.2}$$

A particular solution of equation 4.2 is [42] :

$$[N(t)] = (e^{[A]t} - [I])[A]^{-1}[B] = \left(\sum_m \frac{[A]^m t^m}{(m+1)!}\right)[B]t \tag{4.3}$$

The nuclides treated as both matrices $[A]$ and $[B]$ are defined from the input file of initial production rates of the problem and from nuclide decay data libraries. With these values the code calculates the nuclide concentrations for given conditions and after several given time intervals chosen by the user. The required derived quantities, which are also specified by the user, are computed and written in the output file. The output file contains thus parameters such as activity, power dissipation, gamma spectra, etc.[42]

The input production rates are derived from the MCNPX calculations and they should be given in *g.atom/sec*. Lets first define what the unit *g.atom/sec* means. As Dr. F. Atchinson kindly explained [43] : "The definition is that 1 gram.atom is the mass in grams numerically equal to the atomic weight. That is why the factor $1/(6.022.10^{23})$ is the conversion to the number of lots of "A" grams (where A is the atomic/nuclear mass in AMU). For example,

the weight of the proton in nuclear units is 938.27231 MeV/c^2, 1 unified atomic mass unit is 931.49432 MeV/c^2 which means that $A = 1.00727647$. Dividing by the Avagadro constant 6.0221367 10^{23} we get 1.6726231 10^{-24} g."

Thus we first made an MCNPX calculation followed by a post-processing with HTAPE3X to get the spallation yields in the target that is to say for each type of nuclide produced we had the number N_i of this nuclide created in the whole target per source proton. This was obtained for the beam and target specifications as explained above. For the calculation of the decay and continuous feed, we then needed to have this production rates $[N_i]$ in g.atom per second for 1 mA beam current. Thus we made the conversion as follows :

$$\left. \begin{array}{rcl} 1A & = & 1C/s \\ 1proton & = & 1.60219 \times 10^{-19}C \end{array} \right\} \quad thus \quad 1mA = \frac{10^{-3}}{1.60219 \times 10^{-19}} \; proton/sec$$

and then we get

$$\boxed{[N_i] = N \times \frac{10^{-3}}{N_{avogadro} \times 1.60219 \times 10^{-19}} \; g.atom/sec}$$

where $N_{avogadro} = 6.022 \times 10^{23}[1/Mol]$

The nuclide decay data libraries contain the decay modes and the half-lives of the nuclides. Two libraries can be used with ORIHET3 : the original ORIHET library and the NUBASEX library [42]. The ORIHET library has been issued in its first form already more than twenty years ago as it was supplied with the ORIGEN code. Since this time, several updates have been made, once in 1979 to add new isotopes with mass above 40, then later to include neutron emitters and to update the gamma data (1981). The last modification was done in 1983 to add decay data for nuclides in the mass range below 40. The present version of the ORIHET library contains decay data for 2456 nuclides. The NUBASEX library is an upgrade of a previous library called NUBASE. In the present form of NUBASEX, data for the decay of the isomeric states of some daughter nuclides have been added. The library contains now the decay data for 3738 nuclides and it uses more than 40 decay modes. Note that the work to complete the data for the isomeric state is still in progress, the present NUBASEX library is therefore a preliminary version of what should be a quite complete library soon.

Let us explain now what is needed to launch an ORIHET3 calculation. One needs a deck file in which all the parameters for the calculations are set and were the input data file and library files are specified. One needs then the input data file whith the element concentrations in gram.atom/sec. The results of the MCNPX-HTAPE3X calculations are to be converted as explained before to create this file. One needs also the library file. An example of the input deck file is given and commented in tables 4.1 and 4.2 respectively :

```
%time_step 10 100.0 1e3 1e4 1e5 1e6 1.73e7 3e7 1e8 3e8;
%title SINQ Target activity build up [with fission];
%basis In total target mass for 1 mA;
%nuclide_library nubasex ;
%output none grammes/thresh=1.0e-7 activity/nucl /thresh=1.0e-3 gamma check=5;
%output unit = ci neutr/nucl alpha/nucl;
%conc zero;
%prod file="nucdat.dat";
%calculate logfile = 200EFPD.bup ;
%time_step 0.5 1.0 12.0 24.0 744.0 2192.0 4383. 8766. 17532. 8.77E+04 unit=h;
%output check=1 ;
%title SINQ Target activity decay following 1 year irradiation;
%prod zero;
%concen time_step=7 ;
%calculate logfile = 200EFPD.dec ;
%end ;
```

Table 4.1: *Example of an ORIHET3 input file.*

Term	Meaning
time_step 10 100...	irradiation time in seconds. The results will be printed for 10 sec, 100 sec ...
title SINQ...	Title to be printed as heading of the sample sheets corresponding to this first calculation
basis In TOTAL...	Second title to remind the basis of the calculation
nuclide_library nubasex	Specify which library will be used, here NUBASEX
output none grammes/thresh=1.0e-7 activity/nucl /thresh=1.0e-3 gamma check=5	Specify the conditions for the printing of the results here the element inventories in grams and the element activities in Curies will be printed if they are larger than 1.0e-7 respectively 1.0e-3 at step time 5
conc zero	The initial concentrations are set to zero
prod file = "nucdat.dat"	The file nucdat.dat, containing data derived from MCNPX-HTAPE3X calculation, will be used as input data file with the element concentrations in gram.atom/sec
calculate logfile = 200EFPD.bup	The results of the calculation will be written in a file called 200EFPD.bup
concen time_step=7	The initial concentrations for the decay calculation are taken at step time number 7 of the previous calculation i.e at 1.73e7=200 days of irradiation

Table 4.2: *Meaning of the terms used in the ORIHET3 input file.*

4.2.2 Element concentrations after irradiation

The results of section 4.1 were used for a depletion calculation to estimate the production of Sn, Zn, Hg and Po 210 after 200 EFPD (Equivalent Full Power Day) of irradiation. This calculation was done with ORIHET3 and we obtained the following inventories for the above mentioned elements, see table 4.3. The results are element concentrations im Grams in the total target mass for the total beam current of 1.74 mA.

Element	^{210}Po	Sn	Zn	Hg
MCNPX-Bertini **Element Concentrations [g]**	0	2.30E-01	5.21E-02	1.90E+01
MCNPX-ISABEL **Element Concentrations [g]**	0	2.40E-01	5.42E-02	1.95E+01
MCNPX-CEM **Element Concentrations [g]**	0	8.33E-02	1.85E-02	2.10E+01

Table 4.3: ^{210}Po, *Sn, Zn, Hg inventories in grams in the PbBi after 200 EFPD.*

One can notice that no ^{210}Po is foreseen with this calculation method. ^{210}Po is formed by activation, i.e by the interaction of the produced neutrons on the target, but ORIHET3 does not allow the simulation of the activation. Thus it was to be expected that the estimated ^{210}Po production would be zero.

The results of table 4.3 were compared to the results obtained by other participants to the benchmark exercise proposed by CEA [47]. Our results are shown in table 4.4 and are given in atoms.

Element	^{210}Po	Sn	Zn	Hg
MCNPX-Bertini	0	1.1670 E+21	4.7988 E+20	5.7041 E+22
MCNPX-ISABEL	0	1.2177 E+21	4.9922 E+20	5.8542 E+22
MCNPX-CEM	0	4.2264 E+20	1.7040 E+20	6.3045 E+22
Mean value of data from 5 reference codes	8.3725 E+21	9.5283 E+20	4.2113 E+20	4.5512 E+22

Table 4.4: ^{210}Po, *Sn, Zn, Hg inventories in atoms in the PbBi after 200 EFPD. Data for comparison coming from calculations performed at PSI, ENEA, CEA, JAERI and taken from [47].*

With these data, one can notice that Bertini and ISABEL models provide results which are in good agreement with the data obtained by the other groups. But there are quite large discrepancies between the data obtained with the CEM model and the results of the other groups. Those groups and the corresponding codes were CEA (SPARTE), PSI (MCNPX), PSI (FLUKA), ENEA (MCNPX), JAERI (NMTC). The discrepancies in % between the MCNPX ^{210}Po, Sn, Zn, Hg estimated amounts and the mean value of the estimations of the other reference codes are given in table 4.5. CEM underestimates the production of Sn and Zn. For Hg, the estimation of CEM is on the contrary quite in good agreement with the other data. We have already observed such a behaviour while validating MCNPX for the *"thin target experiments"*,

Element	^{210}Po	Sn	Zn	Hg
MCNPX-Bertini	-100	+22.48	+13.95	+25.33
MCNPX-ISABEL	-100	+27.80	+18.54	+28.63
MCNPX-CEM	-100	-55.64	-59.54	+38.52

Table 4.5: *Discrepancies in % between the MCNPX ^{210}Po, Sn, Zn, Hg estimated amounts and the mean value of the estimations of the other reference codes. Data for comparison coming from calculations performed at PSI, ENEA, CEA, JAERI and taken from [47].*

see section 3.4 fig. 3.15. In that case, CEM was in good agreement with the experimental data for elements with a charge number Z close to the charge number of the irradiated element (PbBi). Note that this lack of reliability of the CEM model has already been noticed by the scientific community and the development of a new version of this model, called CEM2k, is in progress.

We studied the production of Sn, Zn, and Hg a bit further. One could notice in section 3.4 that the best code for estimating the production cross-sections for 1000 MeV protons was KHSv3p+INCL4. Thus, one can assume that this code would be the best suited for predicting the produced amounts of Sn, Zn, and Hg for 600 MeV protons. To have an idea of what this code would have predicted, we compared the production cross-sections of Sn, Zn, and Hg obtained with MCNPX-Bertini and KHSv3p+INCL4 in section 3.4. We obtained the discrepancies given in table 4.6. For the predicted amounts of Sn and Hg, although the values we obtained with the Bertini model were about 25 % larger than the mean value of the reference code calculations, it is to be expected that the Cugnon code would predict even larger amounts. On the contrary for Zn, it is to be expected that the amounts predicted with the Cugnon code would be in good agreement with the mean value of the reference code calculations.

Element	Sn	Zn	Hg
MCNPX-Bertini [mb]	4.28	6.99	154.97
KHSv3p+INCL4 [mb]	5.88	6.14	195.20
Bertini - INCL4 [%]	-27.2	+13.7	-20.6

Table 4.6: *Discrepancies in % between the MCNPX-Bertini and KHSv3p+INCL4 estimated production cross-sections for Sn, Zn and Hg.*

4.2.3 Decay of elements causing chemical damages in the target

In this section we study the decay Sn, Zn, Hg after 200 EFPD irradiation. The estimation of the decay was performed by using ORIHET3 as explained just before. For these three elements, we obtained the following results, see table 4.7 :

To precise in some more detail the predictions of MCNPX, let us mention that :

- For Sn, MCNPX predicts the generation of isotopes from ^{105}Sn to ^{134}Sn. Among those isotopes, ^{112}Sn, ^{114}Sn to ^{120}Sn, ^{122}Sn, ^{124}Sn are stable. The unstable isotopes are created in relative small amounts and decay rapidly (half-lives in the range of the minute, unless for ^{126}Sn where it is 10^5 years).

- For Zn, MCNPX predicts the generation of isotopes from ^{59}Zn to ^{83}Zn. Among those isotopes, ^{64}Zn, ^{66}Zn, ^{67}Zn, ^{68}Zn, ^{70}Zn are stable, the half life of ^{65}Zn is 244.5 days.

Decay time	MCNPX-Model	Sn	Zn	Hg
0	Bertini	2.30e-01	5.21e-02	1.90e+01
	ISABEL	2.40e-01	5.42e-02	1.95e+01
	CEM	8.33e-02	1.85e-02	2.10e+01
30 min	Bertini	2.30e-01	5.21e-02	1.90e+01
	ISABEL	2.40e-01	5.42e-02	1.95e+01
	CEM	8.33e-02	1.85e-02	2.10e+01
1 h	Bertini	2.30e-01	5.21e-02	1.90e+01
	ISABEL	2.40e-01	5.42e-02	1.95e+01
	CEM	8.33e-02	1.85e-02	2.10e+01
12 h	Bertini	2.30e-01	5.21e-02	1.90e+01
	ISABEL	2.40e-01	5.42e-02	1.95e+01
	CEM	8.33e-02	1.85e-02	2.10e+01
24 h	Bertini	2.30e-01	5.21e-02	1.90e+01
	ISABEL	2.40e-01	5.42e-02	1.95e+01
	CEM	8.33e-02	1.85e-02	2.10e+01
31 d	Bertini	2.29e-01	5.22e-02	1.92e+01
	ISABEL	2.39e-01	5.43e-02	1.96e+01
	CEM	8.30e-02	1.85e-02	2.11e+01
91 d	Bertini	2.27e-01	5.20e-02	1.92e+01
	ISABEL	2.38e-01	5.41e-02	1.96e+01
	CEM	8.25e-02	1.85e-02	2.11e+01
182 d	Bertini	2.25e-01	5.18e-02	1.91e+01
	ISABEL	2.36e-01	5.39e-02	1.96e+01
	CEM	8.20e-02	1.84e-02	2.11e+01
365 d	Bertini	2.23e-01	5.15e-02	1.91e+01
	ISABEL	2.35e-01	5.36e-02	1.96e+01
	CEM	8.16e-02	1.83e-02	2.11e+01
2 y	Bertini	2.22e-01	5.13e-02	1.91e+01
	ISABEL	2.34e-01	5.33e-02	1.96e+01
	CEM	8.14e-02	1.83e-02	2.11e+01
10 y	Bertini	2.22e-01	5.12e-02	1.91e+01
	ISABEL	2.34e-01	5.32e-02	1.96e+01
	CEM	8.13e-02	1.82e-02	2.11e+01

Table 4.7: *Sn, Zn, Hg inventories in grams in the PbBi for decay times after 200 EFPD.*

- For Hg, MCNPX predicts the generation of isotopes from ^{181}Hg to ^{207}Hg. Among those isotopes, ^{196}Hg, ^{198}Hg to ^{202}Hg, ^{204}Hg are stable.

For those three elements, the major amounts are created for the stable isotopes. Therefore it was to be expected that the amounts of Zn, Sn, Hg would not change significantly during 10 years of decay, as confirmed in table 4.7. Whereas the predicted amounts of Sn and Zn seem to be quite low (in the range of 10^{-1} grams respectively 10^{-2} grams, the quantities of Hg are much more significant, about 20 grams. Thus, at least Hg can cause non negligeable chemical reactions in the target material and possibly damage it. In addition, the production of Hg has to be assessed because of its toxicity (in case of ingestion or inhalation) in case of an accident.

4.2.4   Decay of alpha emitters

In the previous sections, we have seen that light particles (n, p, α...) are produced during the spallation process. These particles can take part in other reactions with the nuclei of the target. Thus, the production of nuclei with a heavier mass than the nuclei of the target is possible, alltough the probability is small. In this sense, Polonium may be created. Polonium, especially some isotopes such as ^{208}Po, ^{209}Po and ^{210}Po, has been recognised by the research authorities as responsible for PbBi contamination in the MEGAPIE spallation target [49]. We therefore studied the production of the above mentioned Polonium isotopes.

The Polonium isotopes are created in the MEGAPIE spallation target by the following reactions :

$$^{209}Bi\,(n,\gamma)\,^{210}Bi \to\,^{210}Po \tag{4.4}$$

$$^{209}Bi\,(p,xn)\,^{210-x}Po, \quad with\,x\,=\,1...12 \tag{4.5}$$

$$^{208}Pb\,(\alpha,xn)\,^{212-x}Po, \quad with\,x\,=\,2...14 \tag{4.6}$$
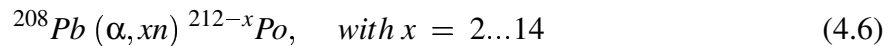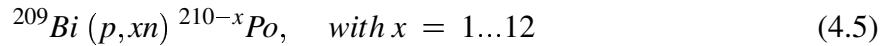
The major isotopes ^{210}Po, ^{209}Po, ^{208}Po produced by these reactions are all alpha emitters. Their half-lives are 138.4 days, 102 years, and 2.9 years respectively. These alpha-emitters could be dangerous for someone who would handle the target. That is one of the reasons why the contamination due to these Polonium isotopes should be assessed before implementing the MEGAPIE target in the SINQ facility.

- **Estimation of ^{208}Po and ^{209}Po :**

As already said, ORIHET3 does not allow us to estimate the production of ^{210}Po because this isotope is mainly created by neutron activation. Nevertheless ORIHET3 allows to simulate the time dependant evolution of ^{208}Po and ^{209}Po. Thus we started with those two isotopes. In table 4.8 and table 4.9, we give their expected activity in the MEGAPIE target after 200 EFPD irradiation and several times of decay.

Decay time	MCNPX-Bertini	MCNPX-ISABEL	MCNPX-CEM
0	2.61e+02	3.75e+02	2.90e+02
30 min	2.61e+02	3.75e+02	2.90e+02
1 h	2.61e+02	3.75e+02	2.90e+02
12 h	2.61e+02	3.75e+02	2.90e+02
24 h	2.61e+02	3.75e+02	2.90e+02
31 d	2.56e+02	3.67e+02	2.84e+02
91 d	2.46e+02	3.53e+02	2.73e+02
182 d	2.32e+02	3.33e+02	2.58e+02
365 d	2.06e+02	2.95e+02	2.29e+02
2 y	1.62e+02	2.32e+02	1.80e+02
10 y	2.39e+01	3.42e+01	2.65e+01

Table 4.8: ^{208}Po *activity in Curies in the PbBi for several times of decay after 200 EFPD.*

Decay time	MCNPX-Bertini	MCNPX-ISABEL	MCNPX-CEM
0	9.12e-01	2.55e-00	3.14e-00
30 min	9.12e-01	2.55e-00	3.14e-00
1 h	9.12e-01	2.55e-00	3.14e-00
12 h	9.12e-01	2.55e-00	3.14e-00
24 h	9.12e-01	2.55e-00	3.14e-00
31 d	9.11e-01	2.55e-00	3.13e-00
91 d	9.10e-01	2.55e-00	3.13e-00
182 d	9.08e-01	2.54e-00	3.13e-00
365 d	9.05e-01	2.54e-00	3.11e-00
2 y	8.99e-01	2.52e-00	3.09e-00
10 y	8.52e-02	2.39e-00	2.93e-00

Table 4.9: ^{209}Po *activity in Curies in the PbBi for several times of decay after 200 EFPD.*

The evolution of the ^{208}Po activity in the central PbBi of the MEGAPIE target is shown on fig. 4.5.

Knowing ^{208}Po and ^{209}Po activities at decay time 0 in tables 4.8 and 4.9, we could calculate the amounts of those two isotopes existing in the target just after 200 EFPD irradiation.

The time dependent evolution of the number of unstable nuclei can be written as :

$$N(t) = N_0 e^{-\lambda t} \tag{4.7}$$

with $\lambda = \frac{ln(2)}{T_{1/2}}$

The number of decays per second A is

$$A = N_0 - N(1sec) = N_0(1 - e^{-\frac{ln(2)}{T_{1/2}(sec)}}) \tag{4.8}$$

So we can calculate the number of atoms of an unstable nucleus N_0 existing before decay :
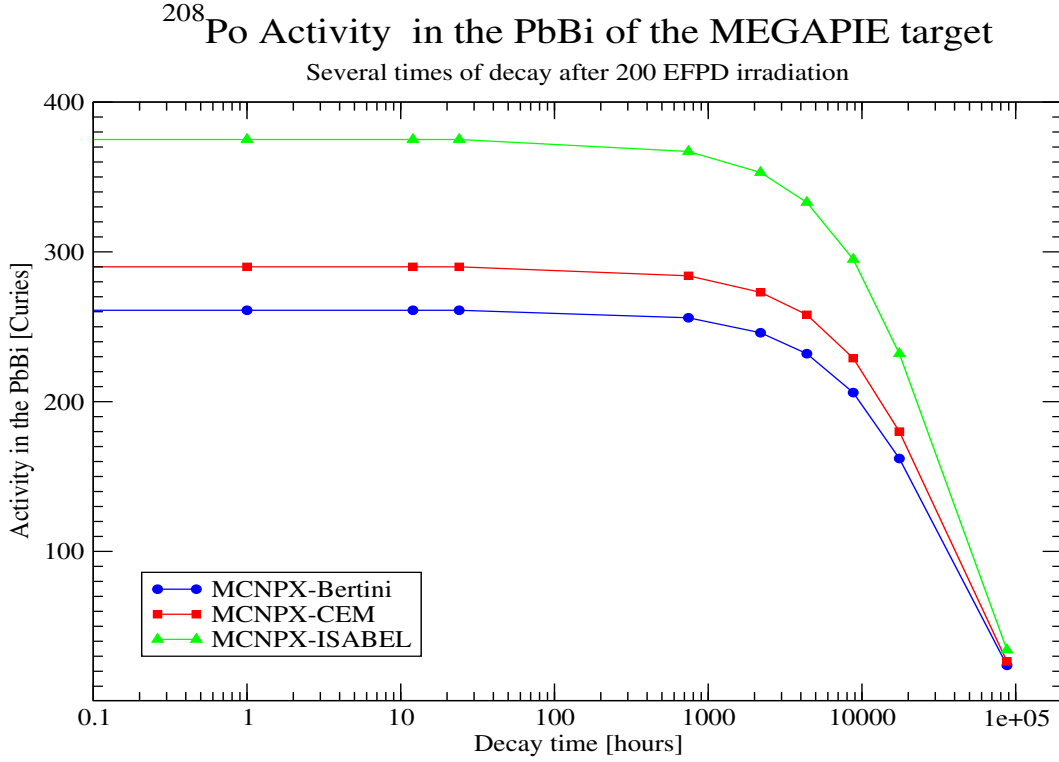
Figure 4.5: *MCNPX estimations of the ^{208}Po Activity (Curies) in the central PbBi of the MEGAPIE target for several decay times after 200 EFPD of irradiation.*

$$N_0 = \frac{A(Bq)}{1 - e^{-\frac{ln(2)}{T_{1/2}(sec)}}} \tag{4.9}$$

and deduce the corresponding amount in grams m_0 :

$$m_0 = m_{atom} \frac{N_0}{N_{avogadro}} \tag{4.10}$$

where m_{atom} is the atomic mass of the considered nuclei, $N_{avogadro} = 6.023 \ 10^{23}$

The respective half-lives are :

$$T_{1/2}(^{208}Po) = 2.9 \ years = 91.4544 \ 10^6 \ sec \tag{4.11}$$

$$T_{1/2}(^{209}Po) = 102 \ years = 3.2167 \ 10^9 \ sec \tag{4.12}$$

To give an example of the calculation, for ^{208}Po, ISABEL predicts $A = 375$ Curies at decay time zero. Thus we have $A = 375 \times 3.7 \ 10^{10}$ Bq.
Thus using equation 4.9 we get $N_0(208) = 1.4843 \ 10^{21}$ atoms.
And then using equation 4.10, we get $m_0(208) = 0.51$ grams.

The results we obtained are given in table 4.10. In this table, we also give as reference data the results obtained by J.C. Klein (see [49]) who calculated, in the scheme of a framework with CEA, the amount of Polonium isotopes generated in the MEGAPIE target.

Element	^{208}Po	^{209}Po
MCNPX-Bertini	0.35	0.044
MCNPX-ISABEL	0.51	0.12
MCNPX-CEM	0.40	0.15
Reference data	0.33	0.17

Table 4.10: *^{208}Po and ^{209}Po mass in grams generated in the PbBi of the MEGAPIE target. Reference Data taken from [49].*

The results of our calculation are well in the range of the results obtained by J.C. Klein, alltough the prediction of the Bertini model for ^{209}Po is quite astonishing. It was not expected that this model would give such a small value. This holds also for the fact that the CEM model seems to agree best with the calculation of J.C. Klein although CEM was the model which gave the less satisfactory results in our validation investigations.

- **Estimation of ^{210}Po :**

^{210}Po is produced according to reaction 4.13 :

$$^{209}Bi\ (n,\gamma)\ ^{210}Bi \rightarrow ^{210}Po \tag{4.13}$$
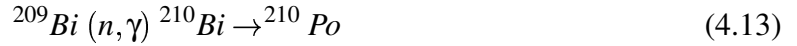
To simplify the notations let us write this as :

$$A\ (n,\gamma)\ B \rightarrow C \tag{4.14}$$

By activation of ^{209}Bi with the neutron flux, two isotopes of Bi may be reached, "normal" ^{210}Bi and metastable ^{210m}Bi. Let us call σ the cross-section for the (n,γ) reaction giving "normal" ^{210}Bi and let us call Φ the neutron flux in the target and λ the decay constant of ^{210}Bi giving ^{210}Po by β decay. Then from equation 4.14, we can write the equations giving the time evolution of ^{209}Bi, ^{210}Bi and ^{210}Po (i.e. A, B, C) and we have :

$$\begin{cases} \frac{dA(t)}{dt} = -\sigma\Phi A(t) \\\\ \frac{dB(t)}{dt} = \sigma\Phi A(t) - \lambda B(t) \\\\ \frac{dC(t)}{dt} = \lambda B(t) \end{cases}$$

We solved this system of differential equations using the following boundary conditions, $A(t=0) = A(0)$, $B(t=0) = 0$ and $C(t=0) = 0$ and we got :

$$\begin{cases} A(t) = A(0)\ e^{(-\sigma\Phi t)} \\\\ B(t) = A(0)\ \frac{\sigma\Phi}{\lambda-\sigma\Phi}\left[e^{(-\sigma\Phi t)} - e^{(-\lambda t)}\right] \\\\ C(t) = A(0)\left[1 - \frac{\lambda}{\lambda-\sigma\Phi}e^{(-\sigma\Phi t)} + \frac{\sigma\Phi}{\lambda-\sigma\Phi}e^{(-\lambda t)}\right] \end{cases}$$

We could then estimate the amounts of ^{210}Po formed in the target. For this purpose, we first needed to calculate Φ and σ in the target according to the energy of the neutrons. This

calculation was performed earlier [51]. Results for Φ and σ_{tot} are estimated in the mesh cells V_{16}, W_{16}, X_{16}, Y_{16} and V_5 to V_{11} (mesh cells as shown in [46] in fig.1.3). The calculated flux as well as the cross-sections were given as one group quantities for all energies below 600 MeV.

We then had to calculate σ, the cross-section for the neutron capture in ^{209}Bi giving ^{210}Bi. Let us remind that two elements may be formed by neutron irradiation of ^{209}Bi : ^{210}Bi (we note the corresponding cross-section σ) and ^{210m}Bi (the metastable nuclei, we note the corresponding cross-section σ_m). With these notations we have $\sigma_{tot} = \sigma + \sigma_m$. Using the data of IEAF-2001 [50], we could calculate the ratio $\frac{\sigma+\sigma_m}{\sigma} = \frac{\sigma_{tot}}{\sigma}$ and we found that this ratio was constant (about 1.478) for energies below 600 keV as shown in fig.4.6. Thus we could calculate σ as $\sigma = \frac{\sigma_{tot}}{1.478}$.

^{209}Bi Activation : Evolution of the cross-sections ratio (S+Sm) / S with the energy

Cross-sections for neutron capture in ^{209}Bi, S for channel giving ^{210}Bi, Sm for channel giving ^{210}Bi^m (metastable)
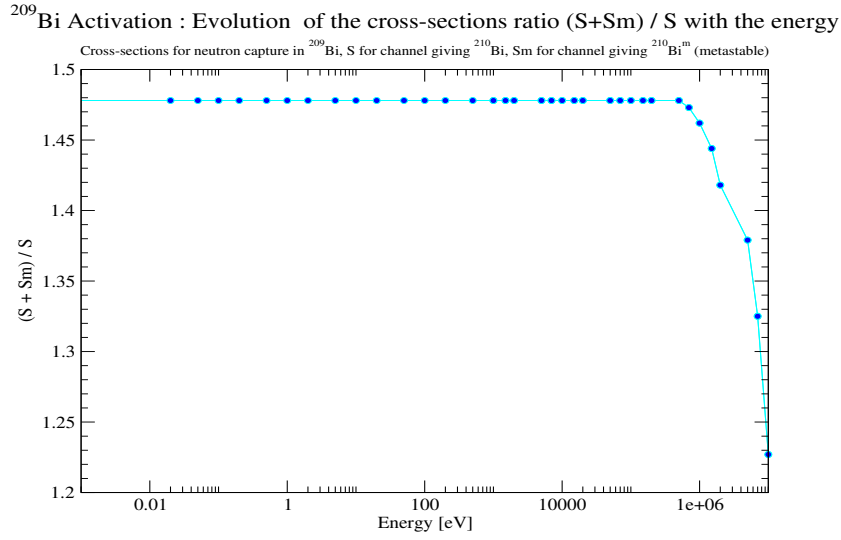
Figure 4.6: *Ratio $\frac{\sigma+\sigma_m}{\sigma}$ as a function of the neutron energy. Data for σ and σ_m taken from [50].*

We then calculated the mass of ^{210}Po created in each mesh cell of the PbBi target and got the following results (see table 4.11).

Mesh cell	σ [mb]	Φ [n.cm^{-2}.s^{-1}]	^{210}Po [g]
V_5	4.5288	5.7864 e+14	0.643
V_6	5.9356	3.5029 e+14	0.510
V_7	8.7296	1.7223 e+14	0.368
V_8	11.1851	9.7635 e+13	0.268
V_9	13.2476	5.7132 e+13	0.182
V_{10}	14.8012	3.4521 e+13	0.125
V_{11}	15.8957	1.2749 e+13	0.130
V_{16} W_{16} X_{16} Y_{16}	mean value for σ 4.9331	mean value for Φ 6.1295 e+14	0.784

Table 4.11: *Estimated σ in mb, Φ in n.cm^{-2}.s^{-1} and the created ^{210}Po mass in grams in the PbBi mesh cells of the MEGAPIE target. Reference data for σ and Φ taken from [51].*

Now we could compare our estimation of the poduced ^{210}Po with the calculated value of J. C. Klein [49] and the data obtained by five reference code calculations [47]. We obtained the results given in table 4.12.

Calculation	Total ^{210}Po [g]
MCNPX this work	3.01
Reference calculation [49]	2.60
Mean value of data from five reference code [47]	2.91 maximum = 3.82 g, miminum = 2.24 g

Table 4.12: *Total ^{210}Po mass in grams created in the PbBi of the MEGAPIE target. Reference data taken from [49] and [47].*

The amount of created ^{210}Po predicted by our calculation is about 3 grams. This result is in the same order of magnitude as the values obtained by J. C. Klein as well as the mean value of the data from five reference codes. For the moment, only a few calculations were done in the field of ^{210}Po production and the available values for the evaluated ^{210}Po amounts are lying between 2 and 4 grams. Special efforts are presently made at IRS-FZK in order to assess more precisely the production of ^{210}Po. For this purpose, the improvement of the description of the time dependence of the neutron irradiation is in progress [52].

4.3   Impact for disposal

As shown by our calculations as well as by the already existing ones (J.C. Klein [49] and MEGAPIE neutronic Benchmark [47]), the amount of Polonium created in the MEGAPIE target is small. The activity due to Polonium is mainly due to ^{208}Po, ^{209}Po, ^{210}Po and is sufficiently small to be considered at contamination level rather than at irradiation level [49].

There are several problems triggered by Polonium as explained in detail in [49]. One of the issues is that Polonium interacts whith LBE to produce intermetallic compounds such as PbPo. In addition radioactive gases, vapours, aerosols or even gaseous compounds such as PoH_2 are formed. In case of a leakage, these elements would be responsible for some activity at the surface and in the environment of the PbBi.

Two main solutions may be distinguished to solve the problem of Polonium contamination. These solutions are presented and discussed in detail in [49]. One solution consists of keeping the Polonium confined in the PbBi in case of an accident. The second solution consists of extracting the Polonium from the PbBi. For this purpose, three methods may be considered :

● the use of chemical elements (cerium, tellurium, selenium) or salts (potassium chloride, lithium chloride) used as extractors to remove Polonium as already done for commercial purposes.

● the use of the so-called *"Vacuum sublimation method"*.

● the use of the so-called *"Alkaline extraction method"*.

Chapter 5

Conclusion

At the Institute for Reactor Safety (IRS) of the Reasearch Center of Karlsruhe, some of the actual activities are focused on the near future developments of Accelerator Driven Systems. In this scope, IRS is participating within the 5th *European Community Framework Program* to MEGAPIE, MUSE and XADS projects. The present work focused on the MEGAPIE project. It aimed at qualifying the application of the available calculation tools, in particular MCNPX, in order to make simulations on the MEGAPIE target for improving the knowledge about the buildup of reaction products in the target.

The first part of the present work allowed us to validate our application of MCNPX. This was done in the scope of the *MCNPX Beta-Testing* activities within which IRS-FZK participates. In this part, special attention was paid on the estimation of parameters related to reaction products created in the spallation target. For the prediction of the residual nuclei production, MCNPX results were compared to reference code results obtained in the scope of a benchmarking exercise. This showed that our MCNPX predictions are well in the range of other reference code predictions. After these encouraging results, we focussed on the experimental validation of the generation of spallation products. For this purpose, we used three experiments, one made in the scope of the SAD project for measuring spallation products activities, the two others carried out for measuring the production cross-sections of the spallation products (one experiment made in the scope of an ISTC project, the other carried out at GSI-Darmstadt). The results we got by simulating these experiments were in quite good agreement with the experimental data and allowed us to validate our application of MCNPX for estimating this sort of parameters. In addition, for the estimation of the production cross-section, we had the opportunity to use the KHSv3p+INCL4 code of the Cugnon group. We could point out that this code was the best suited for estimating cross-sections, although the predictions of MCNPX-ISABEL were already quite good, especially for the nuclei with high mass number.

After validating our application of MCNPX, we investigated predictions for the MEGAPIE spallation target. After defining which parameters were relevant and had to be studied in some detail, we decided to focus on the time dependent behaviour of the target materials especially on the production of elements which may lead to the contamination of the target (Mercury, Polonium...). In particular for Polonium, our calculations showed that a few grams of Polonium may be produced in the spallation target. It showed also that the main isotopes which would be built, are alpha-emitters (^{208}Po, ^{209}Po, ^{210}Po), which would trigger some contamination problems because of their activity. Special efforts were done to estimate the production of ^{210}Po created by neutron activation of ^{209}Bi. We found that about 3 g of ^{210}Po would be produced

in the target. This value is in good aggreement with the predictions of recent calculations (J.C. Klein predicted 2.6 g) [49] and reference code calculations, done for a MEGAPIE neutronic Benchmark, predicted 2.9 g [47]). Solutions have then to be foreseen in order to manage the elements formed in the MEGAPIE target, in particular Polonium. Several methods have already been studied and proposed for this purpose.

Appendix A

Symbols used in chapters 1 and 2

Symbol	Meaning
A	mass number
Z	charge number
σ, σ_i	cross-section
ρ, ρ_i, $\rho(r)$	nucleon density
$\vec{p}$, $\vec{p}_i$	momentum
E, E_i, ε_i	energy
W_{ij}, ω_{ij}, W_i, ω_i	probabilities
v_i	velocity
v_{ij}	relative velocity
λ	wavelength
λ_i	mean free path in medium "i", decay constant
t, t_i	time
S, S_i	separation energy
m, m_i	mass
V	volume
V_i	potential (energy)
r, R	radius
h	Planck's constant 6.6262e-34 J.s
ν_i	branching ratio
g, g_i	number of spin states

Appendix B

MCNPX data for section 3.2

One will find hereafter the results obtained with MCNPX for the problem presented in section 3.2. These data were used for fig 3.4 and they are given in the following unit : number of produced nuclei per source proton over the whole target.

Mass number A	Nuclide production	Absolute error
8	1.99999999E-06	1.99999999E-06
10	1.99999999E-06	1.99999999E-06
11	6.00000021E-06	3.46380011E-06
13	1.99999999E-06	1.99999999E-06
14	1.99999999E-06	1.99999999E-06
15	3.99999999E-06	2.82839983E-06
16	9.99999975E-06	4.47200000E-06
17	3.99999999E-06	2.82839983E-06
18	3.99999999E-06	2.82839983E-06
19	7.99999998E-06	3.99999999E-06
20	6.00000021E-06	3.46440038E-06
21	3.99999999E-06	2.82839983E-06
22	3.99999999E-06	2.82839983E-06
23	9.99999975E-06	4.47200000E-06
24	1.60000000E-05	5.65760001E-06
25	1.80000006E-05	5.99939995E-06
26	1.60000000E-05	5.65760001E-06
27	2.59999997E-05	7.20980006E-06
28	3.79999983E-05	8.71719931E-06
29	4.40000003E-05	9.38080029E-06
30	3.19999999E-05	7.99999998E-06
31	3.40000006E-05	8.24500057E-06
32	4.80000017E-05	9.79680044E-06
33	2.99999992E-05	7.74599994E-06
34	5.40000001E-05	1.03896000E-05
35	6.80000012E-05	1.16620004E-05
36	4.40000003E-05	9.38080029E-06
37	7.40000032E-05	1.21656003E-05
38	7.79999973E-05	1.24877997E-05
39	1.18000004E-04	1.53636011E-05
40	9.00000014E-05	1.34190004E-05
41	1.25999999E-04	1.58759995E-05
42	1.01999998E-04	1.42800000E-05
43	1.06000000E-04	1.45643999E-05
44	1.50000007E-04	1.73250010E-05
45	1.61999997E-04	1.79981998E-05
46	1.44000005E-04	1.69632003E-05
47	1.65999998E-04	1.82267995E-05
48	2.03999996E-04	2.01959992E-05
49	2.47999997E-04	2.22704002E-05
50	2.61999987E-04	2.28987974E-05
51	2.34000006E-04	2.16216013E-05
52	3.14000004E-04	2.50572011E-05
53	3.19999992E-04	2.53119979E-05
54	3.52000003E-04	2.65408016E-05
55	3.87999986E-04	2.78583993E-05

Mass number A	Nuclide production	Absolute error
56	4.40000003E-04	2.96560011E-05
57	3.52000003E-04	2.65408016E-05
58	5.30000019E-04	3.25420006E-05
59	5.55999984E-04	3.33600001E-05
60	5.77999977E-04	3.39863982E-05
61	5.01999981E-04	3.16762016E-05
62	6.07999973E-04	3.48991998E-05
63	6.30000024E-04	3.54690019E-05
64	6.99999975E-04	3.73799994E-05
65	6.12000003E-04	3.50064001E-05
66	7.07999978E-04	3.75948002E-05
67	7.91999977E-04	3.97584008E-05
68	8.75999976E-04	4.18727977E-05
69	8.69999989E-04	4.16729999E-05
70	9.39999998E-04	4.33340028E-05
71	8.64000001E-04	4.15584000E-05
72	9.58000019E-04	4.37806011E-05
73	1.01000001E-03	4.49450017E-05
74	1.04799995E-03	4.57975948E-05
75	9.66000021E-04	4.39530013E-05
76	1.21999998E-03	4.94099986E-05
77	1.13200000E-03	4.75439992E-05
78	1.34399999E-03	5.18784000E-05
79	1.20199996E-03	4.90415987E-05
80	1.32799998E-03	5.16591972E-05
81	1.33000000E-03	5.16040018E-05
82	1.44400005E-03	5.37168016E-05
83	1.33999996E-03	5.17240005E-05
84	1.49800000E-03	5.49765973E-05
85	1.44400005E-03	5.38612039E-05
86	1.59200002E-03	5.65160008E-05
87	1.51400000E-03	5.52609999E-05
88	1.76599994E-03	5.95141973E-05
89	1.53999997E-03	5.57480016E-05
90	1.67799997E-03	5.80588021E-05
91	1.48600002E-03	5.45361981E-05
92	1.64200005E-03	5.73057987E-05
93	1.55799999E-03	5.59321998E-05
94	1.59400003E-03	5.67464012E-05
95	1.48800004E-03	5.47584023E-05
96	1.45200000E-03	5.40143992E-05
97	1.40199997E-03	5.32759987E-05
98	1.46800000E-03	5.43160022E-05
99	1.40800001E-03	5.30816033E-05
100	1.45400001E-03	5.39433968E-05

Mass number A	Nuclide production	Absolute error
101	1.40600000E-03	5.30062025E-05
102	1.51600002E-03	5.50307996E-05
103	1.46399997E-03	5.41679983E-05
104	1.46399997E-03	5.41679983E-05
105	1.29799999E-03	5.08816011E-05
106	1.29599997E-03	5.09327983E-05
107	1.25199999E-03	5.00799979E-05
108	1.29799999E-03	5.08816011E-05
109	1.00799999E-03	4.48560022E-05
110	1.14199996E-03	4.77355970E-05
111	1.09799998E-03	4.68845974E-05
112	1.07400003E-03	4.62894022E-05
113	9.56000003E-04	4.36892005E-05
114	1.04400003E-03	4.57271999E-05
115	7.74000015E-04	3.93191985E-05
116	8.37999978E-04	4.09782006E-05
117	8.18000000E-04	4.04092025E-05
118	7.83999974E-04	3.95919997E-05
119	6.98000018E-04	3.73430012E-05
120	7.50000007E-04	3.87000000E-05
121	6.96000003E-04	3.73055991E-05
122	6.63999992E-04	3.64535990E-05
123	6.14000019E-04	3.50594019E-05
124	5.61999972E-04	3.35513978E-05
125	5.00000024E-04	3.16000005E-05
126	5.20000001E-04	3.22400010E-05
127	4.95999993E-04	3.14960016E-05
128	4.02000005E-04	2.83410009E-05
129	4.36000002E-04	2.95171994E-05
130	4.11999994E-04	2.87164003E-05
131	3.52000003E-04	2.65408016E-05
132	3.61999992E-04	2.68965996E-05
133	3.31999996E-04	2.57632000E-05
134	3.48000001E-04	2.63784004E-05
135	2.65999988E-04	2.30621990E-05
136	2.60000001E-04	2.28019999E-05
137	2.50000012E-04	2.23500010E-05
138	2.36000007E-04	2.17356010E-05
139	2.55999999E-04	2.26304001E-05
140	2.03999996E-04	2.01959992E-05
141	1.74000001E-04	1.86527996E-05
142	2.18000001E-04	2.08843994E-05
143	1.82000003E-04	1.90736009E-05
144	1.99999995E-04	1.99999995E-05
145	1.93999993E-04	1.96909987E-05

Mass number A	Nuclide production	Absolute error
146	2.05999997E-04	2.02909996E-05
147	2.32000006E-04	2.15296004E-05
148	3.27999995E-04	2.56168005E-05
149	3.22000007E-04	2.53735998E-05
150	3.26000008E-04	2.55258001E-05
151	3.57999990E-04	2.67425985E-05
152	4.83999989E-04	3.11211988E-05
153	4.72000014E-04	3.07272021E-05
154	6.22000021E-04	3.52673997E-05
155	7.42000004E-04	3.85097992E-05
156	9.45999986E-04	4.35160000E-05
157	8.39999993E-04	4.09919994E-05
158	1.17199996E-03	4.84035954E-05
159	1.17800001E-03	4.85336022E-05
160	1.64200005E-03	5.73057987E-05
161	1.88400003E-03	6.14184028E-05
162	2.21799989E-03	6.65399930E-05
163	2.50800001E-03	7.07256040E-05
164	3.02399998E-03	7.77167952E-05
165	3.26199993E-03	8.05714008E-05
166	3.65599990E-03	8.55503968E-05
167	4.12799977E-03	9.08159927E-05
168	4.49599978E-03	9.48655943E-05
169	4.84000007E-03	9.82520069E-05
170	5.54999989E-03	1.05449995E-04
171	6.18600007E-03	1.11347996E-04
172	6.53199991E-03	1.14310002E-04
173	8.02200008E-03	1.26747589E-04
174	8.57200008E-03	1.31151595E-04
175	9.80199967E-03	1.40168588E-04
176	1.11060003E-02	1.48820400E-04
177	1.15900002E-02	1.51829008E-04
178	1.26219997E-02	1.59037198E-04
179	1.48059996E-02	1.71749591E-04
180	1.57619994E-02	1.76534391E-04
181	1.61019992E-02	1.78732182E-04
182	1.80680007E-02	1.89714003E-04
183	2.09420007E-02	2.03137417E-04
184	1.98160000E-02	1.98159993E-04
185	2.17320006E-02	2.08627214E-04
186	2.37900000E-02	2.16489003E-04
187	2.44740006E-02	2.20265996E-04
188	2.55779997E-02	2.25086391E-04
189	2.37080008E-02	2.18113608E-04
190	2.70680003E-02	2.32784805E-04

Mass number A	Nuclide production	Absolute error
191	2.69440003E-02	2.31718412E-04
192	2.85299998E-02	2.36798995E-04
193	3.29059996E-02	2.56666797E-04
194	3.81679982E-02	2.74809572E-04
195	4.25340012E-02	2.89231219E-04
196	5.40239997E-02	3.29546398E-04
197	5.81220016E-02	3.42919811E-04
198	7.18979985E-02	3.81059392E-04
199	8.04940015E-02	4.02470003E-04
200	0.105076000	4.62334399E-04
201	0.122475997	5.02151612E-04
202	0.169661999	5.93817036E-04
203	0.207846001	6.44322601E-04
204	0.319110006	8.29686003E-04
205	0.424834013	9.34634823E-04
206	0.676127970	1.21703034E-03
207	0.387825996	8.91999807E-04

Table B.1: *MCNPX data for fig 3.4 : nuclide production given in number of produced nuclei per source proton over the whole target.*

Appendix C

MCNPX data for section 3.3

One will find hereafter the results obtained with MCNPX for the problem presented in section 3.3. The data are given in the following unit : activity in Bq per proton per second.

Distance from target front [cm]	Activity [Bq/proton*sec]	Absolute error [Bq/proton*sec]
0	3.49333328E-13	8.01370621E-14
0.7	5.33193010E-13	9.90139367E-14
1.3	6.25122838E-13	1.07208567E-13
1.9	4.59649083E-13	9.19298207E-14
2.5	6.43508792E-13	1.08752986E-13
6.8	5.88350874E-13	1.04020437E-13
11.7	4.96421047E-13	9.55114080E-14
16.7	4.96421047E-13	9.55114080E-14
21.5	4.96421047E-13	9.55114080E-14
25.5	1.83859641E-13	5.81364180E-14
28.6	3.30947373E-13	7.80042941E-14
28.7	3.12561419E-13	7.57961470E-14
28.8	4.04491219E-13	8.62375289E-14
28.9	6.43508792E-13	1.08752986E-13
29.0	6.80280702E-13	1.11838151E-13
29.1	6.98666656E-13	1.13323725E-13
29.2	1.04800001E-12	1.38755205E-13
29.3	1.17670175E-12	1.47087719E-13
29.4	1.45249112E-12	1.63405246E-13
29.5	1.67312279E-12	1.75343274E-13
29.6	9.56070184E-13	1.32606925E-13
29.7	8.64140356E-13	1.26078076E-13
29.8	4.59649083E-13	9.19298207E-14
29.9	2.57403501E-13	6.88039578E-14
30.0	1.10315796E-13	4.50309074E-14
30.1	3.67719296E-14	2.60014297E-14
30.2	9.19298182E-29	9.19298182E-29
30.3	1.83859648E-14	1.83859648E-14
30.4	1.83859648E-14	1.83859648E-14
30.5	1.83859648E-14	1.83859648E-14
30.6	9.19298182E-29	9.19298182E-29

Table C.1: *Data for fig 3.6.*

Distance from target front [cm]	Activity [Bq/proton*sec]	Absolute error [Bq/proton*sec]
0	9.02456115E-13	2.01789188E-13
0.7	1.17319294E-12	2.30063147E-13
1.3	9.02456115E-13	2.01789188E-13
1.9	1.12807019E-12	2.25614029E-13
2.5	1.44392983E-12	2.55286786E-13
6.8	9.47578929E-13	2.06761718E-13
11.7	7.67087728E-13	1.86018789E-13
16.7	6.31719286E-13	1.68858566E-13
21.5	4.96350899E-13	1.49649783E-13
25.5	3.60982457E-13	1.27643393E-13
28.6	8.12210542E-13	1.91438025E-13
28.7	8.12210542E-13	1.91438025E-13
28.8	5.86596472E-13	1.62663204E-13
28.9	9.02456115E-13	2.01789188E-13
29.0	7.67087728E-13	1.86018789E-13
29.1	4.96350899E-13	1.49649783E-13
29.2	1.21831581E-12	2.34403968E-13
29.3	1.62442108E-12	2.70791012E-13
29.4	1.39880696E-12	2.51225744E-13
29.5	2.70736840E-12	3.49521247E-13
29.6	2.52687715E-12	3.37590795E-13
29.7	2.30126313E-12	3.22176828E-13
29.8	8.12210542E-13	1.91438025E-13
29.9	4.06105271E-13	1.35354876E-13
30.0	2.25614026E-28	2.25614026E-28
30.1	4.51228071E-14	4.51228071E-14
30.2	2.25614026E-28	2.25614026E-28
30.3	2.25614026E-28	2.25614026E-28
30.4	2.25614026E-28	2.25614026E-28
30.5	2.25614026E-28	2.25614026E-28
30.6	2.25614026E-28	2.25614026E-28

Table C.2: *Data for fig 3.7.*

Appendix D

MCNPX data for section 3.4

One will find hereafter the results obtained with MCNPX-Bertini for the problem presented in section 3.4. The data are production cross sections and are given in mb.

Mass number A	Production cross section [mb]	Absolute error [mb]
1.000000E+00	0.000000E+00	0.000000E+00
2.000000E+00	0.000000E+00	0.000000E+00
3.000000E+00	0.000000E+00	0.000000E+00
4.000000E+00	0.000000E+00	0.000000E+00
5.000000E+00	0.000000E+00	0.000000E+00
6.000000E+00	4.073323E-02	2.880247E-02
7.000000E+00	2.036668E-02	2.036668E-02
8.000000E+00	2.036668E-02	2.036668E-02
9.000000E+00	0.000000E+00	0.000000E+00
1.000000E+01	0.000000E+00	0.000000E+00
1.100000E+01	2.036668E-02	2.036668E-02
1.200000E+01	0.000000E+00	0.000000E+00
1.300000E+01	2.036668E-02	2.036668E-02
1.400000E+01	2.036668E-02	2.036668E-02
1.500000E+01	0.000000E+00	0.000000E+00
1.600000E+01	2.036668E-02	2.036668E-02
1.700000E+01	2.036668E-02	2.036668E-02
1.800000E+01	0.000000E+00	0.000000E+00
1.900000E+01	0.000000E+00	0.000000E+00
2.000000E+01	6.110003E-02	3.527612E-02
2.100000E+01	6.110003E-02	3.527612E-02
2.200000E+01	2.036668E-02	2.036668E-02
2.300000E+01	8.146670E-02	4.073335E-02
2.400000E+01	1.222001E-01	4.988799E-02
2.500000E+01	1.425667E-01	5.388112E-02
2.600000E+01	6.109991E-02	3.527582E-02
2.700000E+01	8.146659E-02	4.073310E-02
2.800000E+01	6.109991E-02	3.527582E-02
2.900000E+01	1.425666E-01	5.388295E-02
3.000000E+01	2.647666E-01	7.343654E-02
3.100000E+01	2.036667E-01	6.440917E-02
3.200000E+01	3.258668E-01	8.146090E-02
3.300000E+01	3.462329E-01	8.396691E-02
3.400000E+01	2.240333E-01	6.754603E-02
3.500000E+01	2.443999E-01	7.054635E-02
3.600000E+01	3.665999E-01	8.640128E-02
3.700000E+01	4.277002E-01	9.333045E-02
3.800000E+01	3.665999E-01	8.640338E-02
3.900000E+01	3.666000E-01	8.641016E-02
4.000000E+01	3.462333E-01	8.396667E-02
4.100000E+01	5.091668E-01	1.018325E-01
4.200000E+01	5.498997E-01	1.058300E-01
4.300000E+01	7.331999E-01	1.221827E-01
4.400000E+01	6.313664E-01	1.133968E-01
4.500000E+01	5.906330E-01	1.096689E-01

Mass number A	Production cross section [mb]	Absolute error [mb]
4.600000E+01	1.038700E+00	1.454469E-01
4.700000E+01	8.553998E-01	1.319902E-01
4.800000E+01	1.201635E+00	1.564313E-01
4.900000E+01	1.140533E+00	1.523986E-01
5.000000E+01	1.242366E+00	1.590559E-01
5.100000E+01	1.181267E+00	1.551004E-01
5.200000E+01	1.344201E+00	1.654585E-01
5.300000E+01	1.262733E+00	1.603562E-01
5.400000E+01	1.670066E+00	1.844303E-01
5.500000E+01	1.568232E+00	1.786738E-01
5.600000E+01	1.975566E+00	2.006012E-01
5.700000E+01	1.710799E+00	1.866353E-01
5.800000E+01	1.894101E+00	1.964049E-01
5.900000E+01	1.384933E+00	1.679462E-01
6.000000E+01	2.016300E+00	2.026471E-01
6.100000E+01	1.934832E+00	1.985015E-01
6.200000E+01	2.464366E+00	2.240019E-01
6.300000E+01	2.444000E+00	2.230610E-01
6.400000E+01	2.871702E+00	2.418057E-01
6.500000E+01	2.586566E+00	2.295263E-01
6.600000E+01	2.749501E+00	2.366033E-01
6.700000E+01	2.729135E+00	2.357377E-01
6.800000E+01	2.688400E+00	2.339555E-01
6.900000E+01	3.319764E+00	2.600339E-01
7.000000E+01	3.116099E+00	2.518447E-01
7.100000E+01	3.156831E+00	2.535530E-01
7.200000E+01	3.238302E+00	2.567826E-01
7.300000E+01	3.604901E+00	2.709335E-01
7.400000E+01	3.482698E+00	2.662631E-01
7.500000E+01	3.401236E+00	2.631444E-01
7.600000E+01	3.991866E+00	2.850989E-01
7.700000E+01	3.543800E+00	2.686126E-01
7.800000E+01	3.849299E+00	2.799979E-01
7.900000E+01	3.788202E+00	2.791598E-01
8.000000E+01	4.032599E+00	2.893797E-01
8.100000E+01	4.215900E+00	2.929828E-01
8.200000E+01	4.073333E+00	2.893991E-01
8.300000E+01	4.134433E+00	2.901699E-01
8.400000E+01	3.747470E+00	2.762478E-01
8.500000E+01	3.788201E+00	2.806858E-01
8.600000E+01	4.256630E+00	2.957451E-01
8.700000E+01	3.828934E+00	2.806816E-01
8.800000E+01	4.317733E+00	2.965224E-01
8.900000E+01	3.767834E+00	2.769666E-01
9.000000E+01	4.501034E+00	3.026834E-01

Mass number A	Production cross section [mb]	Absolute error [mb]
9.100000E+01	3.706735E+00	2.761868E-01
9.200000E+01	4.114067E+00	2.893903E-01
9.300000E+01	2.729132E+00	2.357579E-01
9.400000E+01	3.564169E+00	2.694280E-01
9.500000E+01	3.503066E+00	2.670804E-01
9.600000E+01	3.340133E+00	2.608203E-01
9.700000E+01	3.584536E+00	2.701609E-01
9.800000E+01	3.604901E+00	2.709546E-01
9.900000E+01	3.401235E+00	2.632166E-01
1.000000E+02	3.238298E+00	2.567855E-01
1.010000E+02	2.810601E+00	2.392753E-01
1.020000E+02	2.953167E+00	2.452519E-01
1.030000E+02	2.830968E+00	2.400841E-01
1.040000E+02	3.238299E+00	2.568066E-01
1.050000E+02	2.769868E+00	2.375164E-01
1.060000E+02	2.668035E+00	2.331043E-01
1.070000E+02	2.301433E+00	2.164974E-01
1.080000E+02	2.281067E+00	2.154839E-01
1.090000E+02	2.077401E+00	2.056812E-01
1.100000E+02	1.873734E+00	1.953376E-01
1.110000E+02	2.036664E+00	2.036557E-01
1.120000E+02	2.097766E+00	2.066928E-01
1.130000E+02	1.751534E+00	1.888732E-01
1.140000E+02	1.853367E+00	1.942866E-01
1.150000E+02	1.914468E+00	1.974499E-01
1.160000E+02	1.995932E+00	2.015927E-01
1.170000E+02	1.384933E+00	1.679355E-01
1.180000E+02	1.731166E+00	1.877612E-01
1.190000E+02	1.344200E+00	1.654497E-01
1.200000E+02	1.222001E+00	1.577589E-01
1.210000E+02	1.649700E+00	1.832843E-01
1.220000E+02	1.181266E+00	1.550989E-01
1.230000E+02	1.079435E+00	1.482686E-01
1.240000E+02	1.038700E+00	1.454310E-01
1.250000E+02	1.018333E+00	1.440033E-01
1.260000E+02	8.961332E-01	1.350771E-01
1.270000E+02	1.059065E+00	1.468542E-01
1.280000E+02	9.368678E-01	1.381367E-01
1.290000E+02	9.979678E-01	1.425630E-01
1.300000E+02	1.323833E+00	1.641843E-01
1.310000E+02	1.221999E+00	1.577514E-01
1.320000E+02	1.018334E+00	1.440096E-01
1.330000E+02	1.201633E+00	1.564314E-01
1.340000E+02	1.507133E+00	1.752091E-01
1.350000E+02	1.670067E+00	1.844189E-01

Mass number A	Production cross section [mb]	Absolute error [mb]
1.360000E+02	2.179233E+00	2.106803E-01
1.370000E+02	1.670065E+00	1.844153E-01
1.380000E+02	2.647667E+00	2.322297E-01
1.390000E+02	2.729131E+00	2.357153E-01
1.400000E+02	3.340133E+00	2.607461E-01
1.410000E+02	3.503069E+00	2.671063E-01
1.420000E+02	4.276997E+00	2.950593E-01
1.430000E+02	3.808568E+00	2.784806E-01
1.440000E+02	4.317734E+00	2.964851E-01
1.450000E+02	4.908363E+00	3.160217E-01
1.460000E+02	5.865601E+00	3.455099E-01
1.470000E+02	5.458267E+00	3.333111E-01
1.480000E+02	6.395133E+00	3.607641E-01
1.490000E+02	6.945034E+00	3.759594E-01
1.500000E+02	7.759701E+00	3.972819E-01
1.510000E+02	7.515312E+00	3.909889E-01
1.520000E+02	8.492912E+00	4.156820E-01
1.530000E+02	9.327923E+00	4.356325E-01
1.540000E+02	1.038700E+01	4.596851E-01
1.550000E+02	1.044809E+01	4.611761E-01
1.560000E+02	1.234222E+01	5.010155E-01
1.570000E+02	1.148682E+01	4.831879E-01
1.580000E+02	1.315686E+01	5.174733E-01
1.590000E+02	1.372713E+01	5.283410E-01
1.600000E+02	1.533610E+01	5.583409E-01
1.610000E+02	1.482692E+01	5.491706E-01
1.620000E+02	1.625259E+01	5.748943E-01
1.630000E+02	1.727093E+01	5.926419E-01
1.640000E+02	1.877807E+01	6.177933E-01
1.650000E+02	1.957239E+01	6.306338E-01
1.660000E+02	2.040741E+01	6.443584E-01
1.670000E+02	1.896138E+01	6.204075E-01
1.680000E+02	2.177196E+01	6.651093E-01
1.690000E+02	2.156829E+01	6.621245E-01
1.700000E+02	2.285141E+01	6.817837E-01
1.710000E+02	2.470477E+01	7.081473E-01
1.720000E+02	2.317727E+01	6.858439E-01
1.730000E+02	2.680251E+01	7.381086E-01
1.740000E+02	2.627299E+01	7.307750E-01
1.750000E+02	2.830968E+01	7.586194E-01
1.760000E+02	3.026490E+01	7.839370E-01
1.770000E+02	3.093699E+01	7.920856E-01
1.780000E+02	2.961312E+01	7.756243E-01
1.790000E+02	3.321806E+01	8.207374E-01
1.800000E+02	3.350317E+01	8.246667E-01
1.810000E+02	3.138501E+01	7.983609E-01
1.820000E+02	3.183312E+01	8.039217E-01

Mass number A	Production cross section [mb]	Absolute error [mb]
1.830000E+02	3.661925E+01	8.607324E-01
1.840000E+02	3.358463E+01	8.256508E-01
1.850000E+02	3.256631E+01	8.126371E-01
1.860000E+02	3.232193E+01	8.092521E-01
1.870000E+02	3.309583E+01	8.197009E-01
1.880000E+02	3.362537E+01	8.255590E-01
1.890000E+02	2.928726E+01	7.713348E-01
1.900000E+02	3.081477E+01	7.912087E-01
1.910000E+02	2.833001E+01	7.591031E-01
1.920000E+02	2.775978E+01	7.506766E-01
1.930000E+02	2.904288E+01	7.681963E-01
1.940000E+02	3.079441E+01	7.909909E-01
1.950000E+02	3.146652E+01	7.990860E-01
1.960000E+02	3.505103E+01	8.434978E-01
1.970000E+02	3.224043E+01	8.094776E-01
1.980000E+02	3.403268E+01	8.309857E-01
1.990000E+02	3.397159E+01	8.305554E-01
2.000000E+02	3.486770E+01	8.411410E-01
2.010000E+02	3.466408E+01	8.387814E-01
2.020000E+02	3.551948E+01	8.493329E-01
2.030000E+02	3.611008E+01	8.561776E-01
2.040000E+02	4.142580E+01	9.165288E-01
2.050000E+02	4.613049E+01	9.660647E-01
2.060000E+02	5.759703E+01	1.077918E+00
2.070000E+02	1.311206E+02	1.615681E+00
2.080000E+02	1.257662E+03	3.898317E+00
2.090000E+02	0.000000E+00	0.000000E+00
2.100000E+02	0.000000E+00	0.000000E+00
2.110000E+02	0.000000E+00	0.000000E+00
2.120000E+02	0.000000E+00	0.000000E+00
2.130000E+02	0.000000E+00	0.000000E+00
2.140000E+02	0.000000E+00	0.000000E+00
2.150000E+02	0.000000E+00	0.000000E+00

Table D.1: *MCNPX data with Bertini model for fig 3.11 to fig 3.13.*

Bibliography

[1] The European Technical Working Group on ADS, *A European Roadmap for Developing Accelerator Driven Systems (ADS) for Nuclear Waste Incineration*, ENEA, ISBN 88-8286-008-6, April 2001, revised May 10th 2001.

[2] *http://itumagill.fzk.de/ADS*

[3] *http://itumagill.fzk.de/ADS/publications.html*

[4] *http://hikwww4.fzk.de/irs/anlagensicherheit_und_systemsimulation/reactor_physics*

[5] *http://inrwww.fzk.de*

[6] J. Taieb, thesis, *Etude de la production de noyaux résiduels d'évaporation issus de la réaction de spallation de l'uranium-238 par des protons à 1 Gev*, IPN-CNRS Orsay, Oct. 2000.

[7] *http://www-dsm.cea.fr/Dossiers/Spallation*

[8] C. D. Bowman et. al., *Nuclear Energy Generation and Waste Transmutation Using an Accelerator-Driven Intense Thermal Neutron Source* Nuclear Instruments and Methods **A320**, 336-367 (1992).

[9] C. D. Bowman, *Accelerator-Driven Systems in Nuclear Energy: Role and Technical Approach*, Report ADNA/97-013, October 14, 1997.

[10] C. Rubbia et al., Report CERN/AT/95-44(ET), September 1995.

[11] C. Rubbia et al., Report CERN/AT/95-53(ET), December 1995.

[12] *http://aaa.lanl.gov*

[13] *Les annales de la physique : Production d'énergie nucléaire et traitement des déchets*, Vol.**25** Nr.2, 93-113 (2000).

[14] *Les annales de la physique : Production d'énergie nucléaire et traitement des déchets*, Vol.**25** Nr.2, 113-152 (2000).

[15] N. Metropolis, Phys. Rev. **110**, 185 (1958).

[16] N. Metropolis, Phys. Rev. **110**, 204 (1958).

[17] R. Serber, Phys.Rev. **72 N 11**, 1114 (1947).

[18] H.W. Bertini, Phys.Rev. **131**,1801 (1963).

[19] H.W. Bertini, Phys.Rev. **188**,1711 (1969).

[20] Y. Yariv, Z. Fränkel, Phys.Rev.C **20**, 2227 (1979).

[21] Y. Yariv, Z. Fränkel, Phys.Rev.C **24**, 488 (1981).

[22] K. Chen et al., Phys.Rev **166**, 949 (1968).

[23] J. Cugnon, Nucl.Phys.A **389**, 191c (1982).

[24] J. Cugnon, M.-C. Lemaire, Nucl.Phys.A **489**, 781 (1988).

[25] J. Cugnon, Nucl.Phys.A **462**, 751 (1987).

[26] A. Boudard, J. Cugnon, S. Leray, C. Volant, *Intranuclear Cascade for a comprehensive description of spallation reaction data*, December 3, 2001.

[27] A. R. Junghans et al., Nucl.Phys.A **629**, 635 (1998).

[28] V.F. Weisskopf, Phys.Rev **52**, 295 (1937).

[29] V.F. Weisskopf, D.H. Ewing, Phys.Rev **57**, 472 (1939).

[30] N. Bohr, J.A. Wheeler, Phys.Rev **56**, 426 (1939).

[31] V. S. Barashenkov et al., Sov. Phys. Usp **16**, 31, 1973.

[32] R. Prael, H. Lichtenstein, *User Guide to LCS : the LAHET Code System*, Los Alamos National Laboratory, report LA-UR-89-3014, Revised (September 15, 1989).

[33] Judith F. Briesmeiter, Editor, *MCNP-A General Monte Carlo N-Particle Transport Code*, LA-12625-M Version 4B, UC705 and UC700, March 1997.

[34] L. S. Waters, Editor, *MCNPX user's manual*, TPO-E83-G-UG-X-00001, Revision 0, November 14, 1999

[35] H. Grady Hughes, R. Prael, R. Little, *The LAHET/MCNP code merger*, Los Alamos National Laboratory, research note XTM-RN (U) 97-012, April 22, 1997.

[36] *OECD thick target benchmark for lead and tungsten*, Editors D. Filges, P. Nagel, R. D. Neef, report NSC/DOC(95)2, (1995)

[37] *Spallation Neutron Production Measurements*, M.S Zucker et al., *Proceedings of the Second International Conference on Accelerator-Driven Transmutation Technologies and Applications*, 527, June 3-7, 1996, Kalmar, Sweden.

[38] T. Enqvist et al., Nucl.Phys.A **686**, 481-524 (2001).

[39] *Private communication*, J. Cugnon, A. Boudard, K. -H. Schmidt, January 7, 2002.

[40] ISTC Project 2267, http://www.tech-db.ru/istc/db/projects.nsf/prjn/2267.

[41] W. Pohorecki et al., Faculty of Nuclear Physics and Techniques, Cracow, Poland; A. Polanski, Joint Institute of Nuclear Research, Dubna, Russia, *Measurements of production and distribution of radionuclides in the spallation target*, PHYSOR 2002.

[42] F. Atchinson, H. Schaal, *ORIHET3-Version1.12, A guide for users*, May 6, 2002.

[43] *Private communication, E-mail*, F. Atchinson, Paul Scherrer Institute Villingen, May 23-24, 2002.

[44] *http://www.pnl.gov/atw*

[45] *http://asq.web.psi.ch/ASQ/facilities/SINQSYSTEMS.html*

[46] Y. Poitevin, R. Enderlé, E. Lehmann, *Specifications for a Neutronic Benchmark on the MEGAPIE Spallation Target*, CEA Report, DMT/SERMA/LCA/RT/00-2862/A, December 14, 2000.

[47] R. Enderlé et al. *Compilation of results of the Neutronic Benchmark on the MEGAPIE Spallation Target*, CEA Report, DM2S/SERMA/LCA/RT/01-XX/A, October 9, 2001.

[48] *Accelerator driven systems : Energy generation and transmutation of nuclear waste.*, Status Report, Editor W. Gudowski, IAEA-TECDOC-985, 156, November 1997.

[49] P. Trabuc, *The problem of Polonium contamination in the MEGAPIE spallation target*, CEA Technical Note, DRN-DER-NT-STR-LCEP-2001/009a, October 25, 2001.

[50] *Intermediate Energy Activation File*, Yu. A. Korovin, A. Yu. Konobeyev, P.E. Pereslavtsev, Institue of Nuclear Power Engineering, Obninsk, Russia ; U. Fischer, U. von Möllendorff, Institute for Reactorsafety, Research Center Karlsruhe, Germany; Nov. 2001.

[51] I. Broeders, *Private communication, E-mail*, Juli 23, 2002.

[52] C. Broeders, *Private communication*, Juli 2002.